Report of Leakage Assessment

Deliverable number 1.1

Rolf B. Pedersen[1], Tamara Baumberger[1], Christian Berndt[3], Ann E. Blomberg[1,2], Stefan Bünz[4], Andy Chadwick[6], Holger Class[5], Melanie Darcis[5], Bernd Flemisch[5], Sam Holloway[6], Jens Karstens[3], Karin Landschulze[1], Alexandros Tasianas[4], Ingunn H. Thorseth[1], James C. White[6]

1 – University of Bergen (UiB), Norway
2 – University of Oslo (UiO), Norway
3 –GEOMAR Helmholtz Centre for Ocean Research Kiel (Geomar), Germany
4 – University of Tromsø (UiT), Norway
5 – University of Stuttgart (UStutt), Germany
6 – British Geological Survey (BGS), UK

FOREWORD

This report of leakage assessment constitutes the first of four Deliverables from WP 1 of the ECO2 project. The full title of this Deliverable report is "D1.1: Report of leakage assessment and identification of fluid leakage scenarios at industrial storage sites for implementation in fluid flow modeling". This report is the collaborative work of ECO2 partners at the University of Bergen, the University of Tromsø, the GEOMAR Helmholtz Centre for Ocean Research Kiel, the University of Stuttgart and the British Geological Survey.

This Deliverable (D1.1) report analyses and evaluates possible leakage scenarios at the Sleipner and Snøhvit industrial storage sites and builds on the milestone report (MS 12) on the geological models for the overburden structure. With both this Deliverable (D1.1) and the Milestone report (MS 12), WP 1 provides the full basis for the simulations of fluid and gas flow from the caprock through the overburden of storage sites as part of Task 1.3.

The main part of the work was conducted at the University of Bergen and the GEOMAR Helmholtz Centre for Ocean Research Kiel, who were working on Sleipner, and at the University of Tromsø, who was working on Snøhvit. The University of Stuttgart implemented the leakage scenarios into the geological models at both storage sites and ran a number of flow models in order to test the suitability of the leakage scenarios in their simulations. The British Geological Survey contributed results from a study on detection thresholds of CO2 by means of seismic data that will be integrated with and provide constraints for the modeling work at a later stage of the project.

This report is divided into four parts. Part I and II present the leakage assessment for the Sleipner and Snøhvit CO2 storage sites. Part III presents the implementation of the leakage scenarios into the geological models and part IV the initial result on detection thresholds of CO2 in the overburden. Each section has its own table of contents.

Deliverable Report (D1.1), content list:

We acknowledge the support by the European Commission under the Framework Seven Programme, ECO2 project (project number 265847). We also acknowledge Statoil, Lundin Petroleum and the Norwegian Petroleum Directorate for providing seismic data and the DISKOS Petrobank for providing access to well log data.

EXECUTIVE SUMMARY

One of the major objectives of the ECO2 project is to assess the risks associated with the storage of CO2 below the seabed. Within this frame, work package 1 investigates the sedimentary cover at currently active and potential storage sites using novel geophysical baseline studies (Task 1), monitoring (Task 2) and modeling (Task 3) techniques in order to better understand CO2 migration mechanisms and its spatial and temporal evolution. A proper risk assessment of CO2 storage hinges on a thorough understanding of the geological evolution of an area and a sound comprehension of subsurface anomalies associated with the flow of fluids and their governing geological controls. To this end, WP 1 has analyzed a wealth of seafloor imaging and seismic data from the industrial storage sites at Sleipner and Snøhvit on the Norwegian Margin. In addition to conventional seafloor and seismic data, several novel high-resolution acquisition technologies have been used during offshore expeditions in 2011 and 2012, and their data integrated into this study. A solid background on the geological development and the stratigraphic framework has been presented in the Milestone report (MS 12) on the "Geological models of the industrial storage sites". That MS 12 report also included an interpretation of subsurface structure and structures related to the presence of fluids and possible fluid pathways on the basis of conventional 3D seismic data. In this Deliverable report (D1.1), this interpretation is expanded by integrating several additional high-resolution data sets. The data revealed a number of fluid-flow features, as for example gas chimneys, pipes, shallow gas accumulations, leaking faults, fractures along the seafloor as well as gas hydrates. Each of these structures or set of structures has been evaluated with respect to their occurrence, distribution, origin and as a means for providing a potential pathway for CO2 if it would leak out of the storage formation. On the basis of this evaluation and the assumptions that paleo fluid-flow structures may be reactivated by CO2 injection and that the caprock of the storage formation may breach, a number of potential leakage scenarios have been formulated for both the Sleipner and Snøhvit CO2 storage sites. The leakage scenarios largely include leakage along a chimney (blow-out structure) or along a fault but are adapted to the specific geological background at each storage site and hence, depending on its exact subsurface location and context may yield a complex migration pathway for CO2 from the storage formation to the seafloor. Initial modeling work shows that the leakage scenarios can be successfully implemented into the simulations of fluid flow. Within WP 1, this modeling work will be integrated with seismic modeling work on detection thresholds of CO2 in the overburden in order to develop simulation-assisted monitoring strategies for seabed and sub-seabed leakage detection of CO2. Within ECO2, the modeling of leakage scenarios provides important constraints on flux rates at the seafloor interface for associated activities in other work packages.

PART I

Report of leakage assessment and identification of fluid leakage scenarios at the Sleipner CO_2 storage site (UiB and GEOMAR)

Report of leakage assessment and identification of fluid leakage scenarios at the Sleipner CO$_2$ storage site (UiB and GEOMAR)

Content

1 Introduction to the Sleipner CO_2 storage site

The Sleipner storage site in the North Sea was the world´s first demonstration of CO_2 capture and underground storage in a saline aquifer about 800 m beneath the seafloor. Injections of CO2 started in 1996, and since then 1 million tons CO_2 per year have been injected. Carbon dioxide is stored in the Utsira Formation, which is a highly elongated sand reservoir, extending for more than 400 km from north to south and between 50 and 100 km from east to west. The thickness of the sand layer varies from around 200 to more than 300 m in certain areas. The Utsira Formation has a good storage quality with respect to porosity, permeability, sealing capacity and storage capacity. It is estimated that the Utsira Formation is capable of storing 600 billion tons of CO_2. 3D seismic monitoring of the CO_2 injection into the Utsira Formation shows that there is no leakage of CO_2 into other horizons.

2 Geological background of the Sleipner region

Sleipner is located in the central part of the North Sea, which is a sedimentary basin formed in Late Jurassic to Early Cretaceous periods from a failed rift system (Brooks and Glennie, 1987). In the syn- and post-rift phases large quantities of sediments have been deposited under marine conditions. The Nordland formation consists of the sandy Utsira formation and the overlying Nordland shales, which were deposited after the Middle Miocene epoch. In the Pleistocene epoch, the North Sea area was highly affected by glaciations causing pronounced erosion and reworking of the surface sediments in the North Sea basin (Sejrup, 2000). The remnants of ice stream activity can still be identified as iceberg plough marks and streamlined bedforms (Graham et al., 2007) as well as tunnel valleys, which are related to the retreat of ice sheets (Kristensen et al., 2008; Lonergan et al., 2006).

The Utsira formation is a saline aquifer mainly composed of sand but intersected by layers of shale (Audigane, 2007) It has a thickness of ~250 m – 300m in the Sleipner area (*Figure 1*) and is a target area for CO_2 storage. The Utsira formation is overlain by a thin (~5 m) shale drape separating the unit from an overlying sand layer, which we refer to as the Sand wedge. These sandy units are overlain by Nordland shales, which act as a seal for the stored CO_2. Laboratory measurements by Harrington et al. (2009) revealed intrinsic permeability of 4×10^{-7} D perpendicular and 10^{-6} D parallel to the bedding demonstrating that the Nordland shales act as an effective capillary seal for the CO_2 under estimated and current storage conditions. The uppermost 40 m of the Pliocene section have a higher sand content as the background (Figure 1). The Sand wedge above the main Utsira sand body, the Top Utsira itself, and the Top Pliocene are the most important stratigraphic boundaries for the following fluid flow analyses.

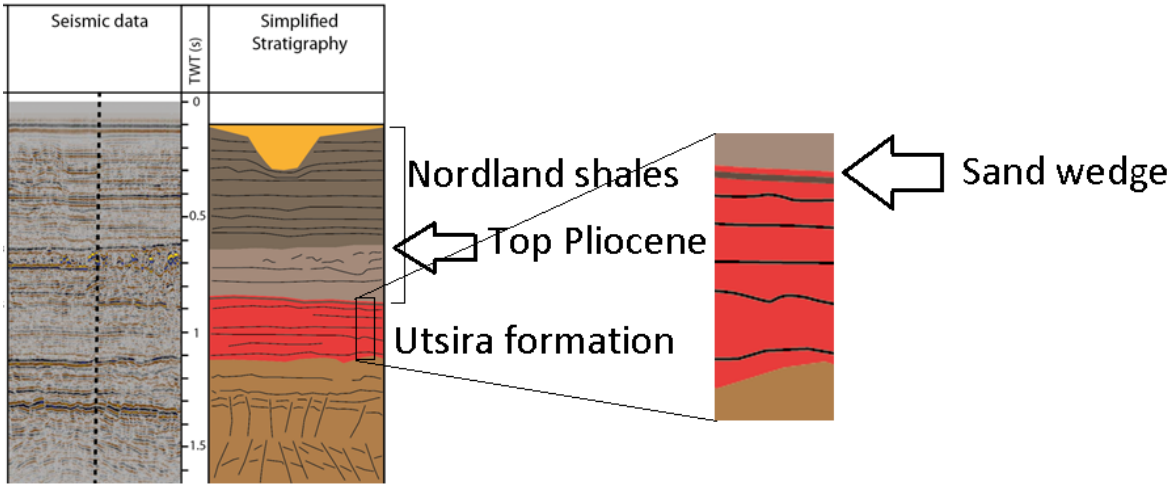

Figure 1: Simplified stratigraphy of the North Sea around the Sleipner CO_2 project.

A more detailed description on the stratigraphy and the parameter estimation for porosity and permeability of the geological structures can be found in the Geological Model Report (MS12).

3 Active seafloor fluid flow at Sleipner and surrounding area (UiB)

3.1 Leaking wells

About 30 wells are present in block 15/9, most of which are abandoned. Three abandoned wells (15/9-11, 15/9-13 and 15/9-16) located in the vicinity of the Sleipner CO_2-storage site, were visited by the research vessel G.O. Sars during expeditions in June 2011 and 2012. Bubble plumes rising up in the water column were detected at all three sites using hull-mounted echo sounder systems. Remotely operated vehicle (ROV) operations were used to observe and sample the gas leakages at the seafloor. Visual observations confirmed bubbles rising from the seafloor into the water column at the abandoned well sites (Figure 2). Where bubbles were emanating from the seafloor, growing microbial mats were observed. To get some information about the chemical composition of the rising bubbles, gas samples were taken using a sampling cylinder connected to gas-tight sampling bottles. Sub-samples were taken for shore-based analyses of total gas content by gas chromatography and isotopic carbon compositions. At the three abandoned wells that were sampled, CH_4 contents of between 99.0 and 99.3 % were determined. Only traces of CO_2 were seen. A corresponding CH_4 carbon isotope composition of -75.5 ± 0.6 ‰ and C1/C2+C3 ratios >1000 point to a biogenic carbon source of the detected CH_4.

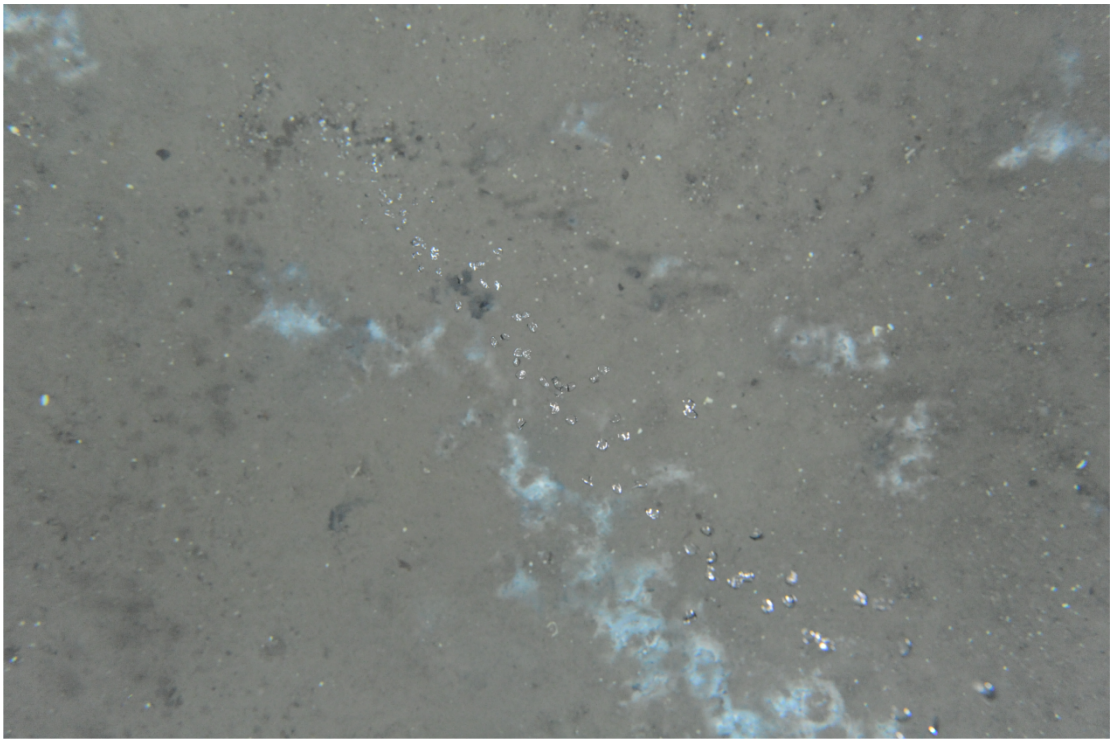

Figure 2: Gas bubbles rising from the seafloor above an abandoned well. The growth of microbial mats is visible in the same areas as where bubbles are exiting from the seafloor. (Picture taken by the University of Bergen)

3.2 Discovery of active seepage in block 16/4

To reveal potential seafloor leakage sites, UiB has been using an autonomous underwater vehicle (AUV) equipped with a high-resolution interferometric synthetic aperture sonar system (HiSAS). The HISAS is capable of synthetic aperture sonar (SAS) imaging of the seafloor with a resolution 2x2 cm under optimal conditions. The HISAS frequency range is approximately 60 to 120 kHz, with a bandwidth of 30-50 kHz.

During a UiB-led cruise in June 2011, a seafloor seepage structure was discovered 25 km north of Sleipner using this advanced technology. In 2012, the structure, which is located in block 16/4 was revisited by UiB, and then later during GEOMAR and NOC-lead cruises. The structure was then traced further to the west, and sediments, seepage fluids and biota were sampled. Fluid flux measurements were also carried out using benthic lander systems.

3.2.1 Surface expressions

The structure - named the Hugin Fracture - has a total length of at least 3 km. The maximum width of the feature was found to be 10 m (*Figure 3*). The surface expression of the structure changes along the strikes and it is characterized by: 1) linear; 2) en echelon; and 3) branching segments. The detailed SAS imaging of the fracture revealed areas with dark patches, which are regions on the seafloor with lower backscatter values than their surroundings. During subsequent ROV operations, some of these patches were later visually identified as areas covered with bacterial mats (*Figure 6*). The lower backscatter probably reflects different sediment properties or fluid saturation.

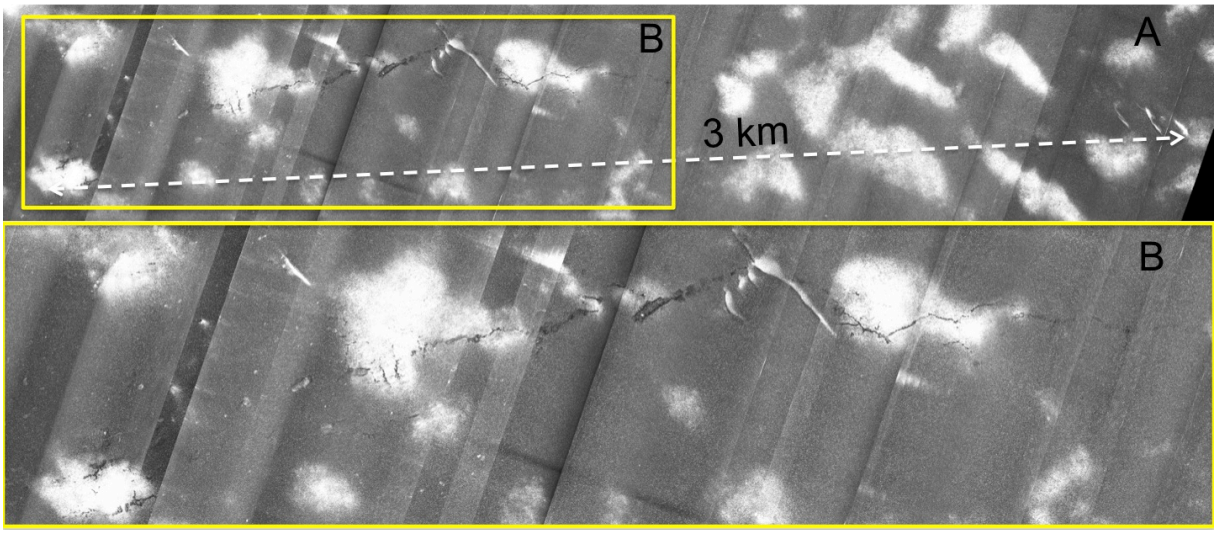

Figure 3: Entire extent of the fracture area (A) including a close-up view of the western area (B). The eastern part does not show the same characteristic fracture-like pattern as the western part, but rather a sequence of dark regions and circular structures.

Ring-structures, typically are 5-10 meters across, are common along the fracture system. Multiple and composite ring structures locally form semi-linear rows that some places extend from the tip of the fracture-like features. In other places they occur as more isolated structures.

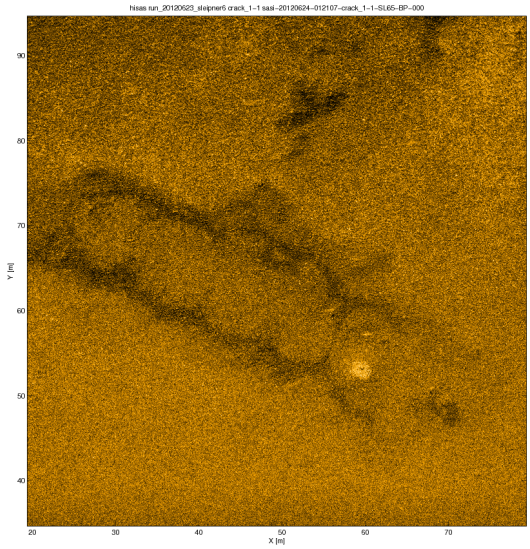

Figure 4: SAS reflectivity image showing how a segment in the central part of the Hugin Fracture is made up of composite ring structures. The darker regions are at least partially covered by bacterial mats. This was verified using a ROV. The circular bright spot represents a region of about 3 m in diameter with about 10 times higher reflectivity than the surrounding. This feature, apparently, consists of carbonate crust that has formed as a result of the seepage.

In addition to seafloor imaging, the HISAS system is also capable of high-resolution bathymetric mapping based on interferometry. The micro-bathymetry acquired using the HISAS system demonstrates that sub-meter scale elevation changes are present along the seepage feature.

Semi-linear en-echelon structures exhibit sub-meter scale vertical movement across the fractures. Linear segments are uplifted by a few tens of centimeters relative to the surrounding seafloor, and are also characterized by a small central depression. Several of the ring structures display such an elevation along the edge of the ring, as well as a depression in the centre.

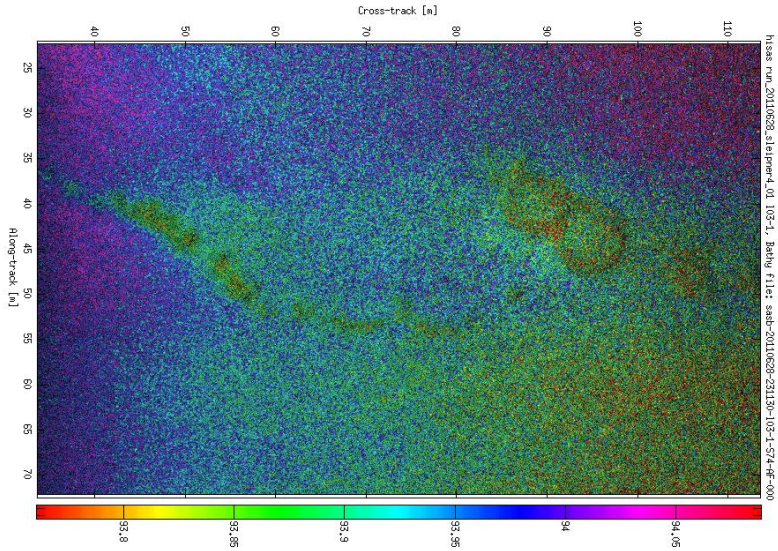

Figure 5: Example image of two ring structures. The image is a synthetic aperture sonar (SAS) reflectivity image, with colour-coded bathymetry. The diameters of the two rings are about 4-5m, and they are elevated by about 10 to 15 cm compared to the surrounding seafloor.

Bacterial mats, signalling active fluid flow, occur along different parts of the structure. High resolution, near seafloor ROV imaging of the bacterial mats revealed that the mats typically are thin and scattered - consistent with relative low fluid flow rates. AUV based photo-imaging of parts of the structure has provided an overview of the mat distribution in some areas. This shows that the bacterial mats - and thereby active seepage – predominantly are associated with ring structures and some of the linear fracture segments. Along the en echelon oriented fractures, bacterial mats have not yet been observed. Bacterial mats have not been observed at the western part of the fracture either suggesting that active seepage at a rate necessary to sustain bacterial mats presently does not occur in this part of the Hugin Fracture.

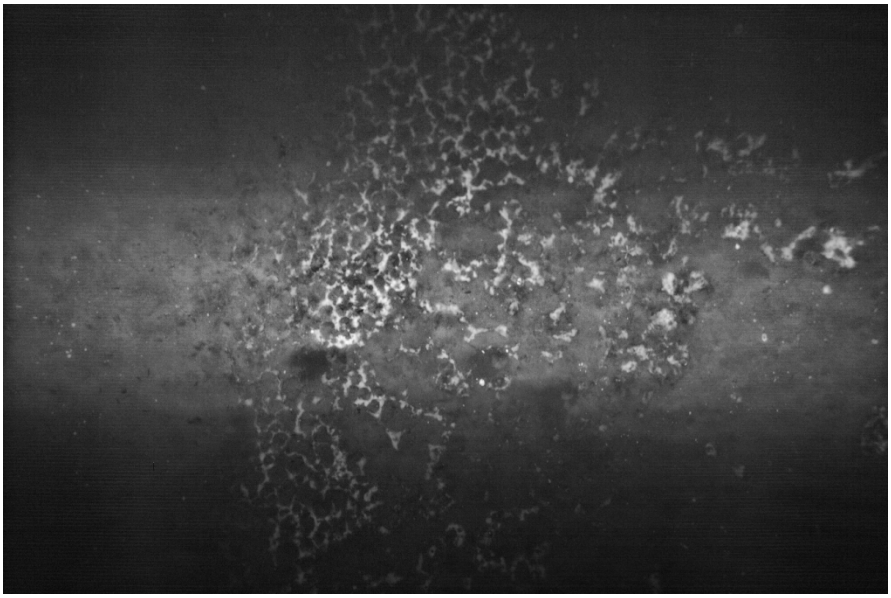

Figure 6: Image of the bacterial mats obtained by using an optical camera mounted on the AUV.

3.2.2 Composition of seepage fluids from pore water analyses

Sediment pore waters have been analysed at several sites to assess the composition of the fluids that are seeping from the fracture system. The pore fluids were extracted from sediment push cores taken at seepage sites, as well as in the background sediments. The pore fluids were extracted from the sediments using Rhizon samplers, and then analysed for major element composition using photometric methods, ion chromatography (IC) and inductively coupled plasma optical emission spectrometry (ICP-OES). The results (Figure 7) show that the Na, Cl and Mg contents of the fracture pore fluids are 10 - 15 % lower compared to background pore fluid concentrations. Thus, a fluid distinct from seawater is seeping along the structure.

To assess if the seepage fluids stem from the Utsira Formation, the pore fluid compositions are been compared with compositional characteristics of the Utsira formation water. The formation water is characterized by high Li (15 times background seawater concentration), high B (3 times background seawater concentration), Na contents similar to background seawater and 40 % lower Mg concentrations than in background seawater. Another striking difference between the Utsira formation water and background seawater is a sulphate concentration of only 10 µmol/l in the formation water (background seawater concentrations are about 52 mmol/l). The composition of the pore fluids at seepage sites along the fracture is thus, distinctly different from the formation water of the Utsira formation water. This is shown by lower concentrations of Na, Li and B than would be derived through a seawater-formation water mixture. Instead the major element composition of the fracture pore fluids points towards a fresh water input.

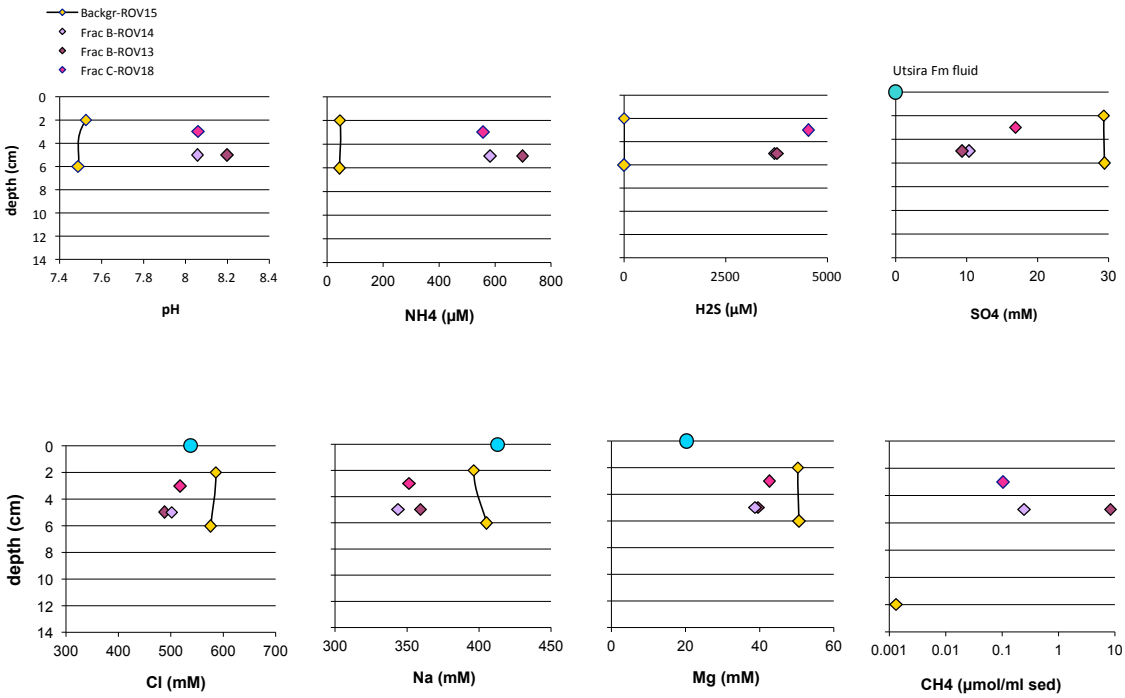

Figure 7: Fluid composition of the fracture pore fluids, background sediment pore fluids (yellow) and the Utsira Formation water (blue).

The fracture pore fluid compositions are also characterized by elevated methane, ammonium and hydrogen sulphide contents compared to the background seawater. The presence of these volatiles is likely caused by subsurface bacterial activity. Carbon isotope investigations confirm a biological source of the detected methane. However, the presence of ethane (CH_4/C_2H_6 of 126) indicates a small input of a thermogenic carbon to these fluids.

3.2.3 Subsurface imaging - Ship-based sub bottom profiling

To document the shallow subsurface expression of the fracture system, subsurface imaging was carried out both in 2011 and 2012 using a hull mounted parametric sub bottom profiler (Topas, Kongsberg Maritime). During the 2012 UiB cruise, the central parts of the fracture system were imaged systematically and the sediments and the structure were then imaged to a depth of around 30 m (*Figure 8*). The Topas imaging revealed that an upper sequence of stratified sediments overly more massive units. This is interpreted to represent Holocene stratified sediments overlying quaternary moraine. At several crossings, the Topas data show sub-meter scale vertical movements along the fracture, which is consistent with the micro-bathymetry. Subsurface, vertical structures are observed below the seafloor seepage features and these extend downwards to the maximum penetration depth of the acoustic profiler, which here was around 30 metres. Across the structures the layering is locally displaced by up to 30 cm (*Figure 9*). Associated with the structures are small bright spots that may reflect gas accumulations.

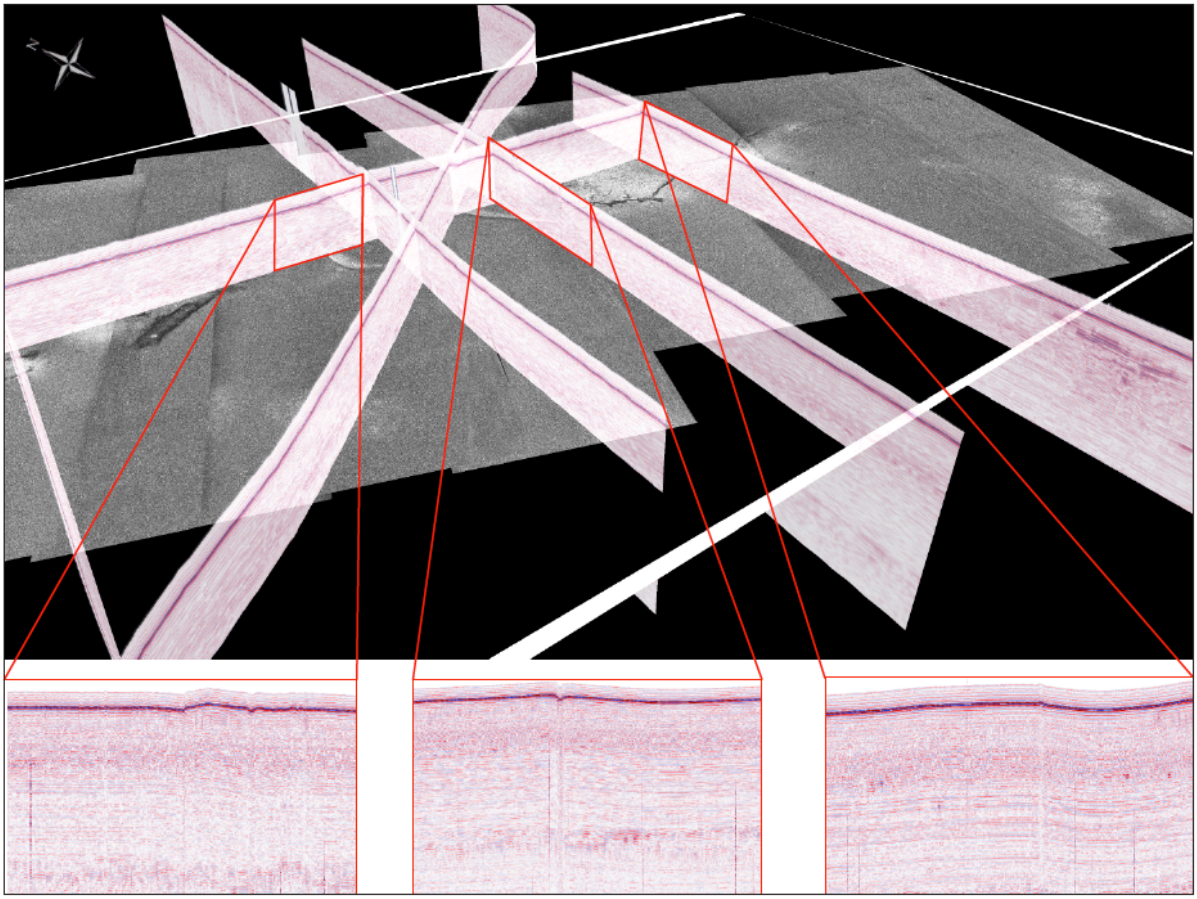

Figure 8: Subsurface acoustic profiles superimposed on a SAS image of the central parts of the Hugin Fracture. The profiles show the disturbances at the seafloor and the vertical structures below that extend to the penetration depth of the TOPAS profiler (here around 40 m).

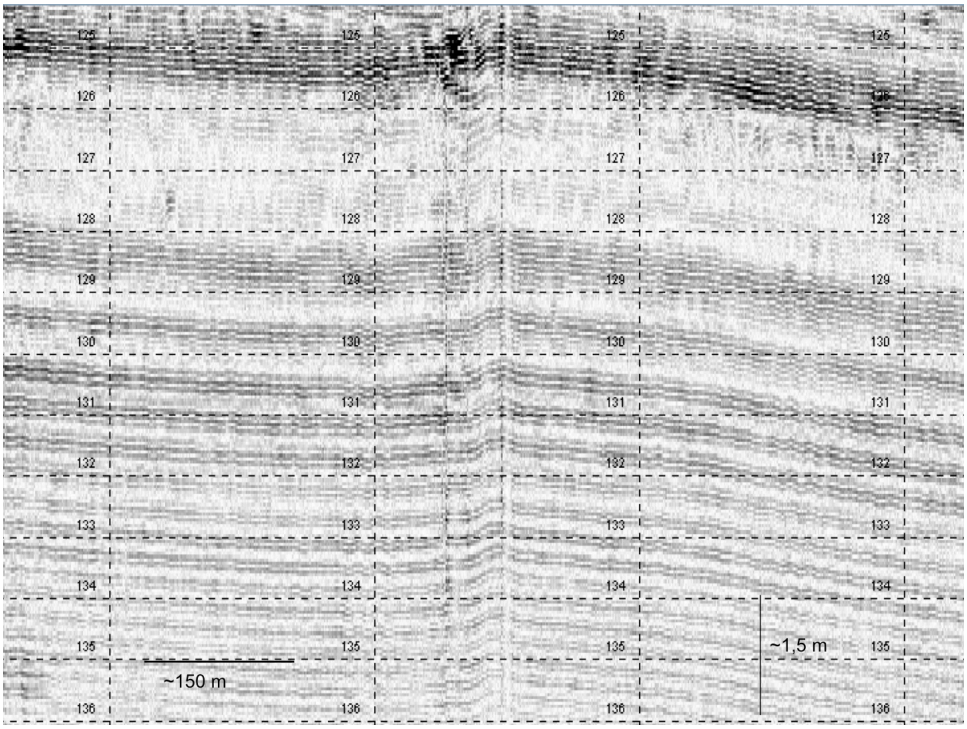

Figure 9: The sub bottom profiling data show up to up to 0.3 m of vertical displacements of sediment layers along some of the vertical fracture systems.

3.2.4 Acquisition of shallow seismic data acquired using a mini streamer

In 2012, UiB also collected mini-streamer seismic data across and around the Hugin Fracture. The aim of this data acquisition was to get high-resolution shallow seismic data from the sea-floor to 100-200 m below the sea floor, in an attempt to link the surface features to deeper structures. Seismic data acquisition was accomplished on a total of 28 lines covering the extent of the fracture, as visible on the sonar data, and also extending further to the west. Most of the seismic lines are parallel 2-km lines running North-South with a spacing of 50 m between lines. Four long 2D lines were also obtained: two 7-km North-South lines crossing the fracture and two 4.275-km East-West lines parallel to the structure. The survey outline is indicated in Figure 10.

We used a single 90 inch^3 airgun from Bolt, model 1900, with an operating pressure of 138 bar and towed it at approx. 4 m depth. Shot interval was 12 s at 5 knots ship speed, which corresponds to approximately 25 m distance between each shot. The receiver unit was a 200 m long mini-streamer with 8 hydrophone groups with 6.25 m spacing on the 43,75m long active part of the streamer. The streamer was towed just below the surface and had no birds or other depth control mechanisms. Because of the shallow water depth, only 80-90 m in the study area, the offset between airgun and first receiver on the streamer was chosen to be 60m, except during the first part of the survey where an offset of 100 m was used (see the cruise log for details of each line).

The data seismic image quality is limited due to the short streamer length. More importantly, 4 out of 8 receivers were heavily affected by noise and do not appear to be recording the signal properly. Attempts have been made to correct this in post-processing, but this has not been possible since no useful information seems to have been recorded by these sensors. In addition,

the shot distance of 25 m was too long. During the cruise we tried to reduce the shot distance to 12.5 m without success. The signal-to-noise ratio on the final seismic image is poor as a result.

Still, preliminary results show acceptable quality seismic data in the upper 50-150 m. After initial processing of the data (sorting, split to 2D lines, NMO-correction, TVG, removal of bad receiver channels, filtering, predictive deconvolution, Radon demultiple), we are able to distinguish a buried channel structure. The channel-like structure is seen from 150 ms to 270 ms corresponding to approx. 25-175m below seafloor. The width of the structure is approx. 3.2 km. The fracture is situated above the southern flank of the channel. More details can be found in the processing report.

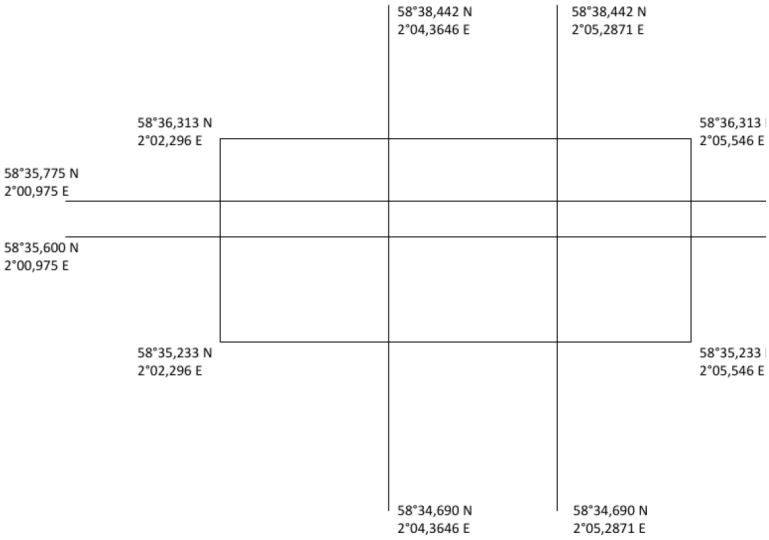

Figure 10: General outline of the seismic survey with coordinates, indicating four long lines and a rectangular area with parallel short lines running North-South.

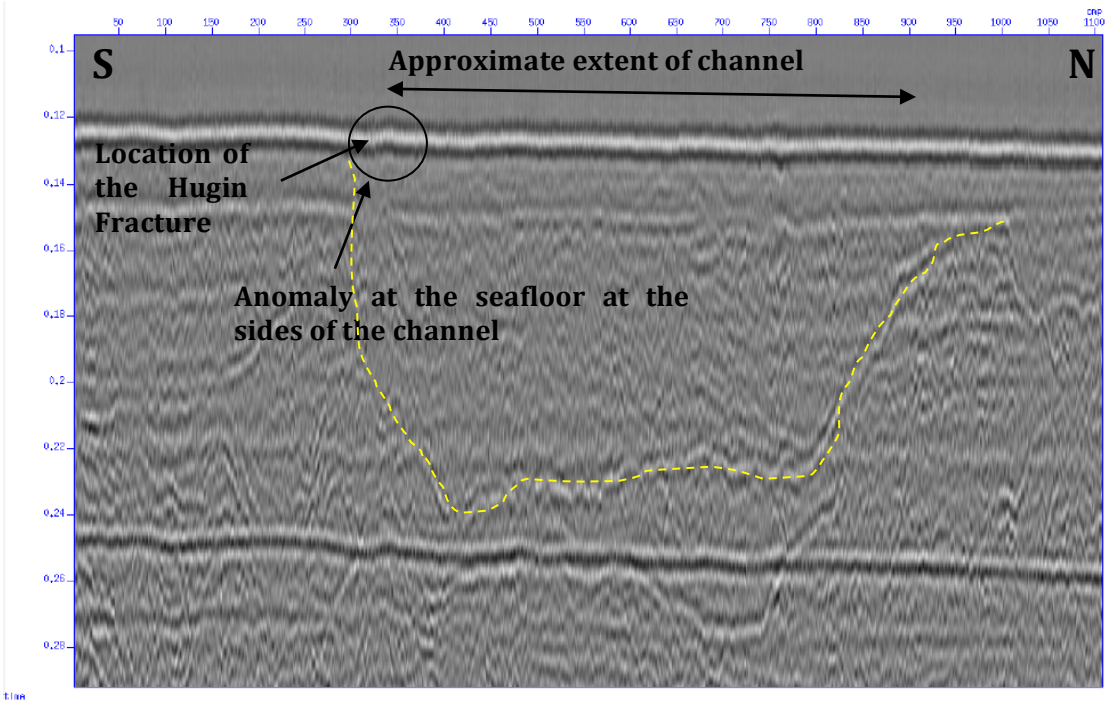

Figure 11: Seismic profile detail of the channel structure described in the text. The strong black line in the lower part is a seafloor multiple.

3.2.5 Formation of the Hugin Fracture

The active seafloor seepage discovered in block 16/4 is clearly linked to a large, km-scale fracture-like structure. The interpretation of the structure as a fracture is based on: 1) the branching nature of the structure; 2) the presence of en echelon segments; and 3) sub-meter scale vertical displacement of both the seabed and of subsurface layering along the structure. Associated with the fracture system there are micro-bathymetric feature with slopes of 5-10%. In an area with seabed erosion and sediment transport, as signalled by sand ripples and shell hashes, the presence of such features suggests that these small seafloor features must have formed relatively recently.

The development of such a fracture system on the seafloor implies that the mechanical properties of the upper sediments layers are such that permit brittle failure. At Sleipner, very high undrained shear strengths (up to 180 kN/m2) have been measured in the clay-rich sediments that are present from five meters below the seafloor and downwards (Sejrup et al. 1987). It seems likely that the formation of the Hugin Fracture is somehow related to brittle failure of such very stiff sediments.

At least three formation mechanisms seems possible: 1) the fracture system is related to neotectonism, and represents the surface expression of a deep seated fault system that recently has been activated; 2) the fracture system results from differential compaction; and 3) the fracture system results from fluid overpressure.

In the 3D seismic data no deep-seated fault system is apparent below the fracture, and it seems therefore unlikely that the fracturing is related to reactivation of deeper fault systems. On the contrary, the seismic data show that the structure is located above the boundary of a channel-like feature that is present about 40 m below the surface. This subsurface feature may represent

a shallow fluvial channel that formed during glaciation/deglaciation. A structural connection between the seafloor seepage structure and a fluvial channel is supported by the pore water chemistry at the seepage site. This shows a dilution of seawater compositions by fresher water that could stem from a subsurface fluvial water reservoir. Formation of the fracture as a result of differential compaction at the edge of a subsurface fluvial channel seems as a possible formation mechanism. In addition, we are also looking into whether fluid overpressure or production of water from the Utsira Formation may have triggered the fracturing.

The Hugin Fracture demonstrates that the clay-rich and impermeable sediments that represent the uppermost seal of the Utsira Formation may be broken as a result of brittle failure and the formation of km-scale fracture systems. The fracturing of this impermeable top layer may connect permeable fluvial channels to the seafloor. The presence in the fluids of hydrocarbons (ethane) that generally are linked to thermogenic processes indicates that this shallow fluid flow system may be connected to deeper channels for fluid flow.

4 Subsurface pathways for fluid flow - 3D seismic data

4.1 Seismic chimneys and bright spots (GEOMAR)

Our 3D seismic analysis comprises the industrial 3D seismic cubes ES9401R99 and ST98M3 (Figure 12), which is a merged compilation of different 3D seismic data sets (ST98M11, MC3D, NH9302, TQ3D, SG9501M, ES9401, and UP96). The analysis included the interpretation of seismic sections and different seismic attributes (e.g. Similarity and Chimney Cube).

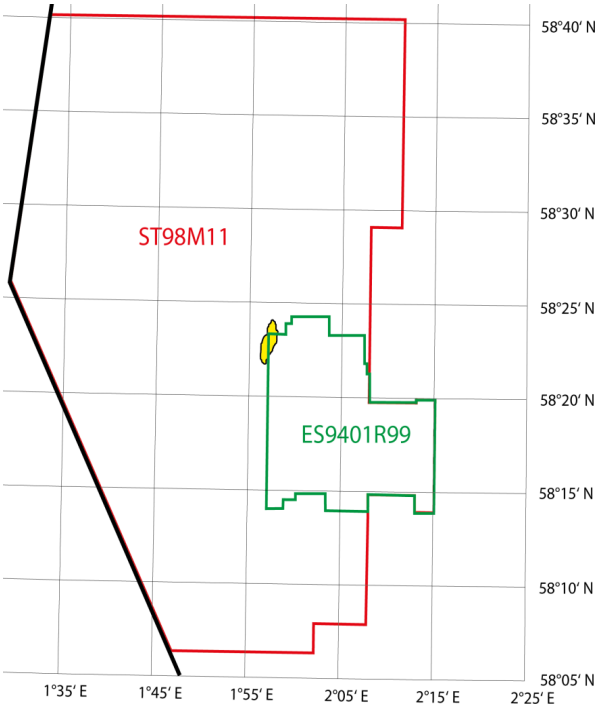

Figure 12: Base map showing extents of the 3D seismic cubes (green and red) and the location of the CO2 plume (yellow)

We were able to identify numerous geological features in the seismic data, such as tunnel valleys, iceberg plough marks, sediment mobilizations and polygonal faults (Figure 13). While these features may have an influence on the pathway of leaking CO_2, we were focusing our analysis on the seismic anomalies that indicate active or paleo vertical fluid flow. Therefore, our main targets have been **seismic chimneys** and **bright spots**. A more detailed compilation can be found in the Geological Model Report (MS12).

Seismic chimneys are vertically oriented, fluid-flow associated seismic anomalies. They are characterized by an increase or decrease in the seismic amplitude. Seismic chimneys are interpreted as hydro-fractured low-permeable shales (Arntsen et al., 2007). The observed seismic chimneys vary in their seismic appearance and are interpreted as overpressure induced fluid pathways through low permeable cap rocks (*Figure 14*). We were able to identify more than 50 chimneys in the study area. Their diameter varies from 50 to 1400 m and some root as deep as the Utsira formation (or even deeper).

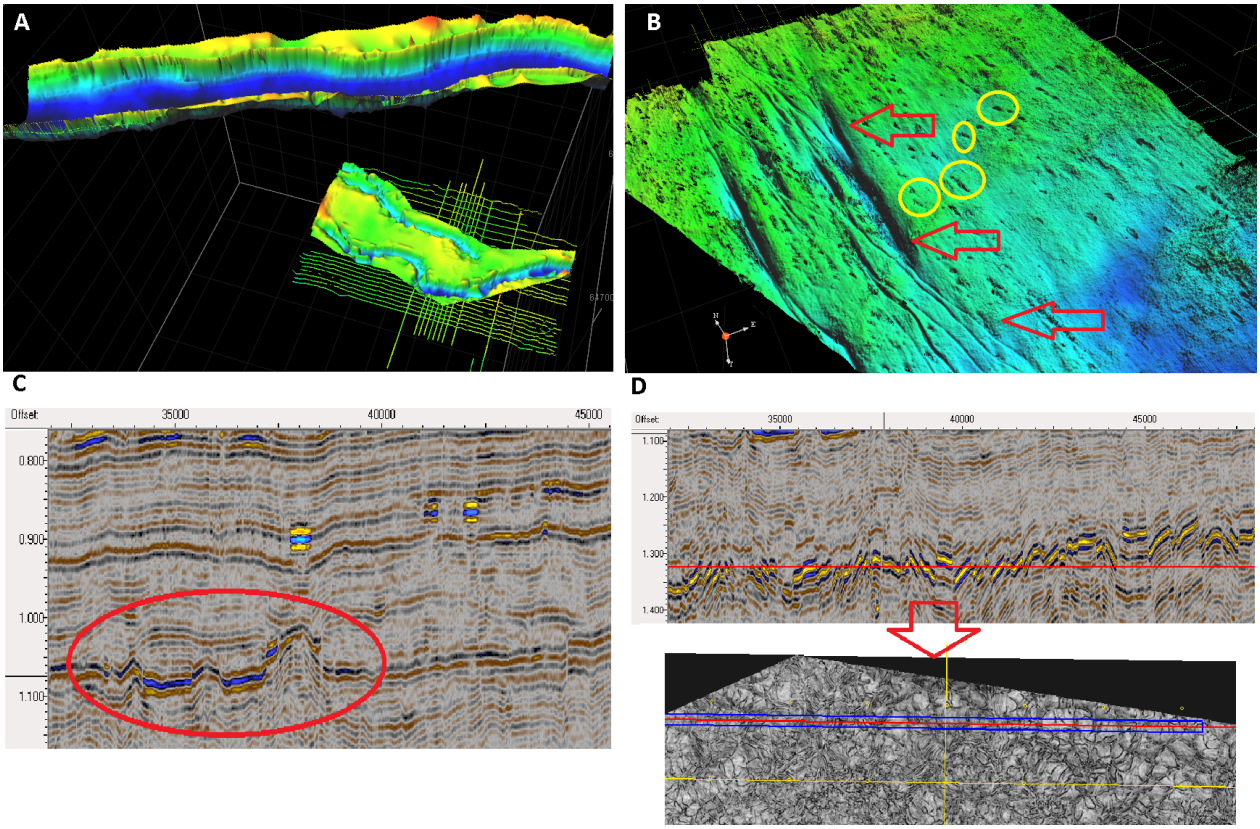

Figure 13: Geological features; A: Tunnel valleys; B: Iceberg plough marks; C: Sediment mobilization; D: Polygonal faults

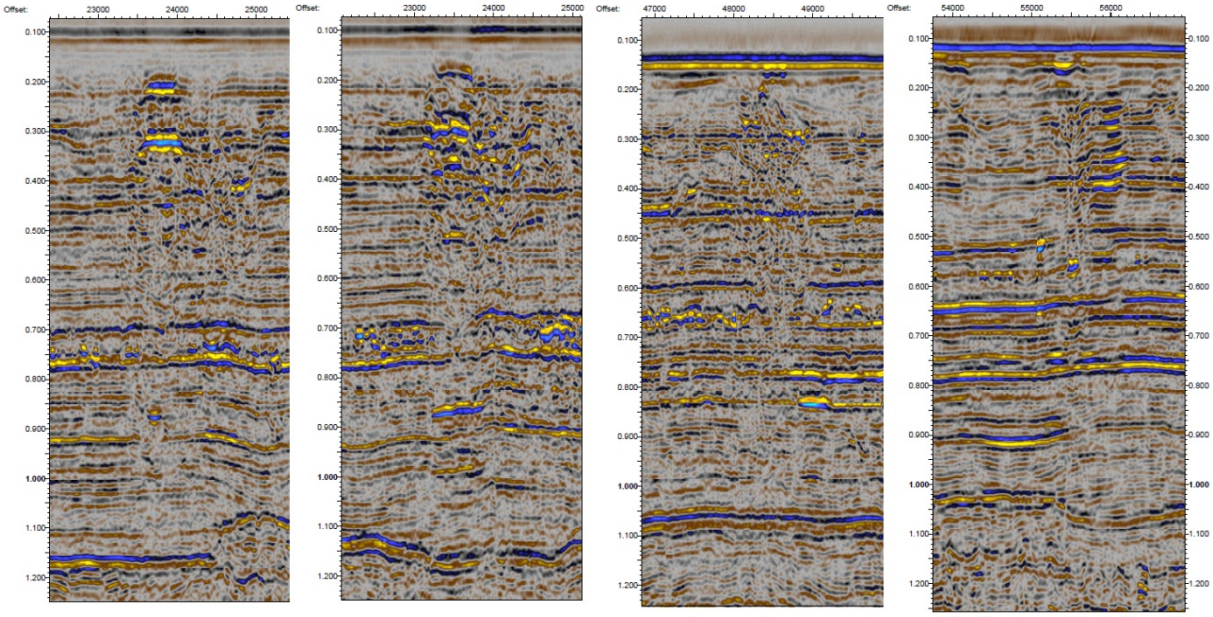

Figure 14: Seismic chimneys with different seismic appearance

Bright spots are high amplitude anomalies, which indicate an abrupt and strong change in the acoustic properties of the underground. Bright spots with a reversed polarity are a strong indicator for gas in the pore space. Therefore, we will refer to those high amplitude reverse polarity anomalies as gas pockets.

The top of the Utsira formation, the Sand wedge and the top Pliocene are the three stratigraphic levels containing gas pockets (*Figure 14*). The three gas hosting layers are at least partly connected (*Figure 15*) indicating that gas has migrated from deeper to more shallow units through chimneys.

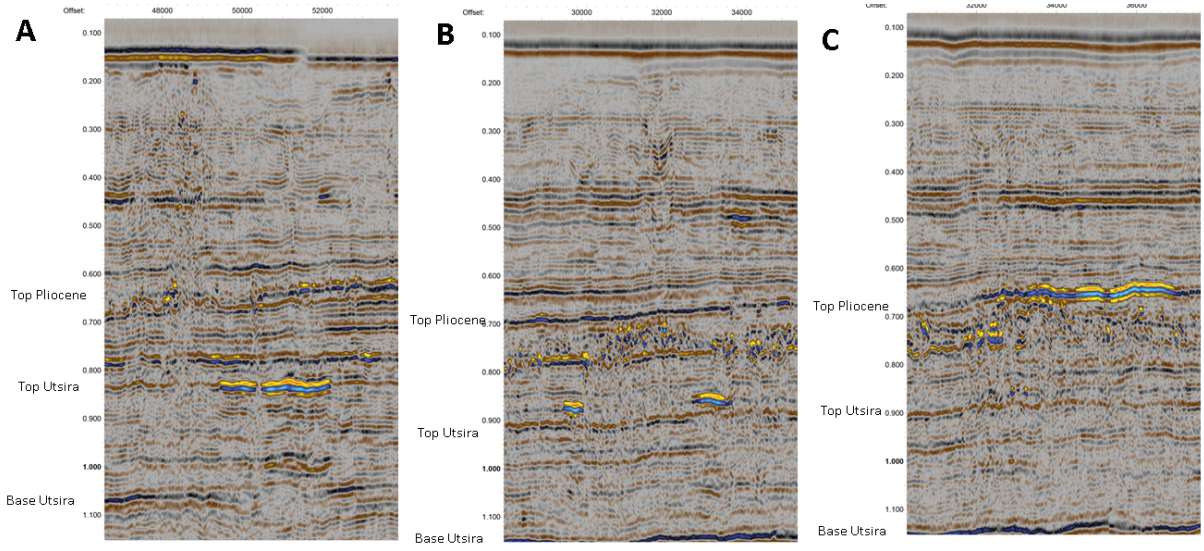

Figure 15: Bright spots: A) Top Utsira; B) Sand wedge; C) Top Pliocene

An overview about the spatial distribution of seismic chimneys and bright spots in relation to the location of the CO_2 plume is given in *Figure 16*.

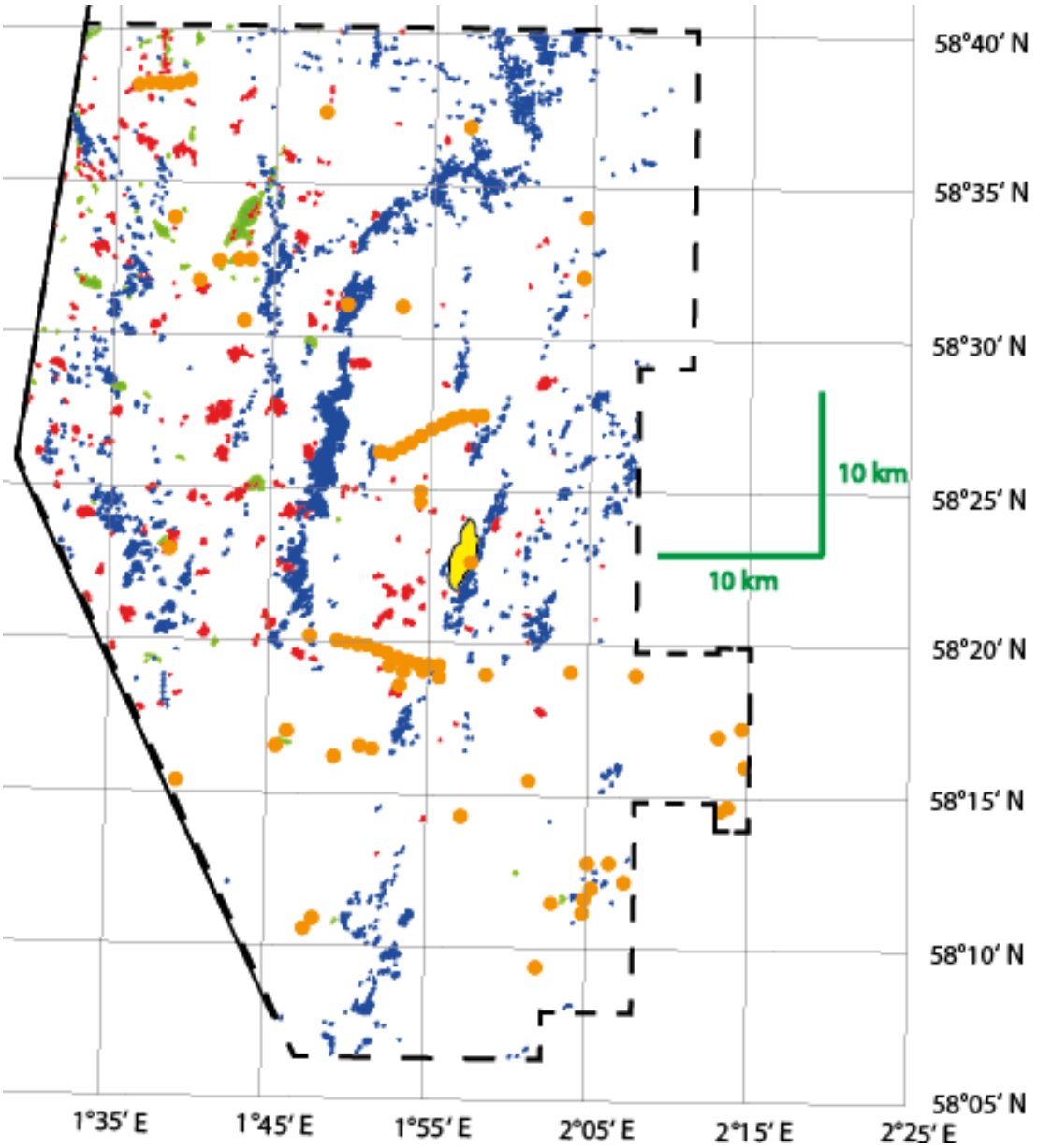

Figure 16: Spatial distribution of fluid flow features at Sleipner: CO_2 plume (yellow), seismic chimneys (orange), bright spots beneath top Utsira (green), bright spots in the Sand wedge (red), bright spots beneath top Pliocene (blue)

4.2 Glacifluvial channels (UiB)

Glacifluvial sand channels represent potential pathways for lateral fluid flow. UiB recently gained access to an additional 3D seismic dataset that covers the Hugin Fracture area. The Norwegian Petroleum Directorate and Lundin Petroleum provided access to the data set, which is a near-offset stack merged of four different surveys covering an area of almost 3000 km^2 (Figure 17). The spacing of the bins has been set to 25m x 25m although the surveys used have a grid spacing of 12.5m x 12.5m and 25m x 12.5m The seismic data have been collected at

different times spanning a period from 1995 to 2008. This 3D seismic cube (LN09M02) has a higher resolution than the ST98M3 cube provided by Statoil to the ECO2 project.
These data are now being studied to document potential links between the Hugin Fracture and deeper structures that may serve as fluid pathways. For that purpose, a sub-cube of the data was chosen for analysis and interpretation. This cube covers a rectangular area of about 940 km^2 around the fracture location (Figure 17). Our data interpretation is so far restricted to time slice observations and an initial variance analysis.

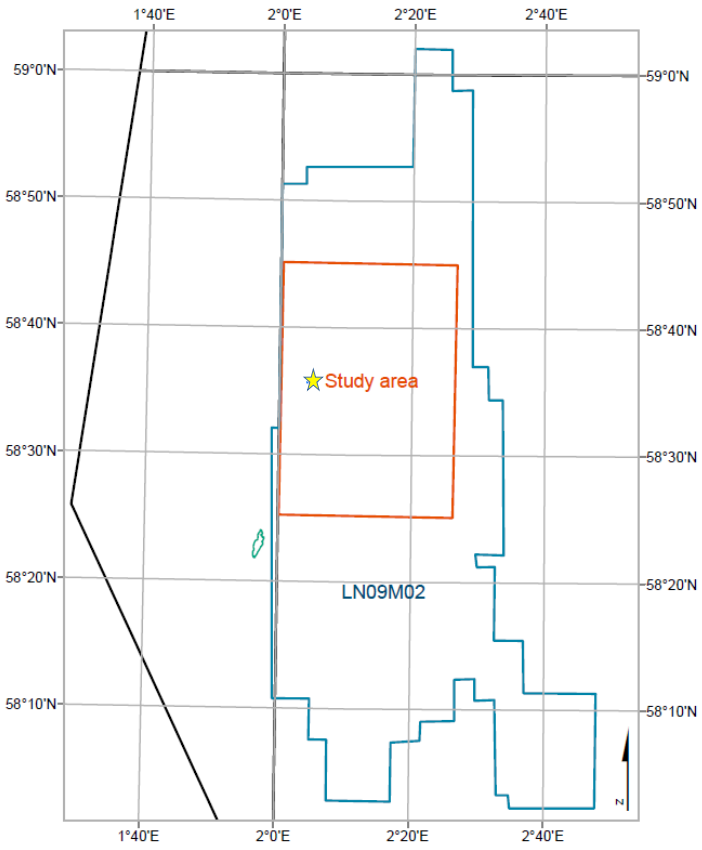

Figure 17: Location and extent of the 3D seismic cube LN09M02 (blue line) and the subset used for interpretation (red line). The CO_2 plume from 2008 (green line) and the fracture location (star) are also indicated. The black line shows the border between Norwegian and British sector in the North Sea.

The 3D seismic data show that the Hugin Fracture appears to be situated above the margin of a shallow channel structure, which is consistent with our interpretation of the 2D mini streamer data (Figures 18 and 19). A variance cube was calculated in order to highlight the channel structures in the area. With this we observe distinct channel structures already at the very shallow level of 192 ms, which corresponds to a depth of about 50 m below the seafloor (*Figure 20*). These channels have a width of about 100 to 850 m and do not cross over the whole area but rather seem to fade and die out laterally.

At a depth of 276 ms, corresponding to about 140 m below the seafloor, a new set of channels is observed. Whereas the shallowest observable channel is oriented NE-SW, the deeper channels are larger and longer and have predominantly a NE-SW and E-W orientation. The channels are

190 m to 1750 m wide and several seem to continue outside of the study area (*Figure 21*). Channels structures can be tracked down to a depth of at least 484 ms, which is around the expected depth of the top Pliocene that occurs about 85 m above the top of the Utsira Formation in this area.

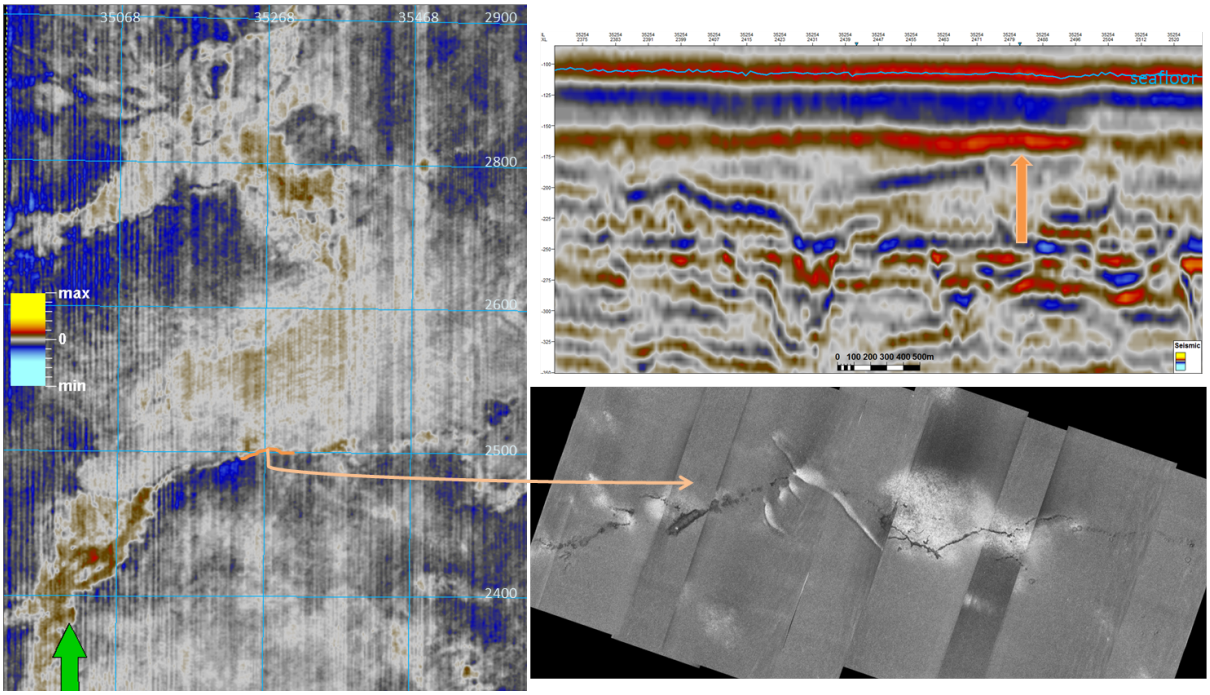

Figure 18: 3D seismic data compilation about the Hugin-Fracture which is located at a border of a glacial channel. The time slice shows that the Hugin-Fracture is evident at shallow depths (about 40m).

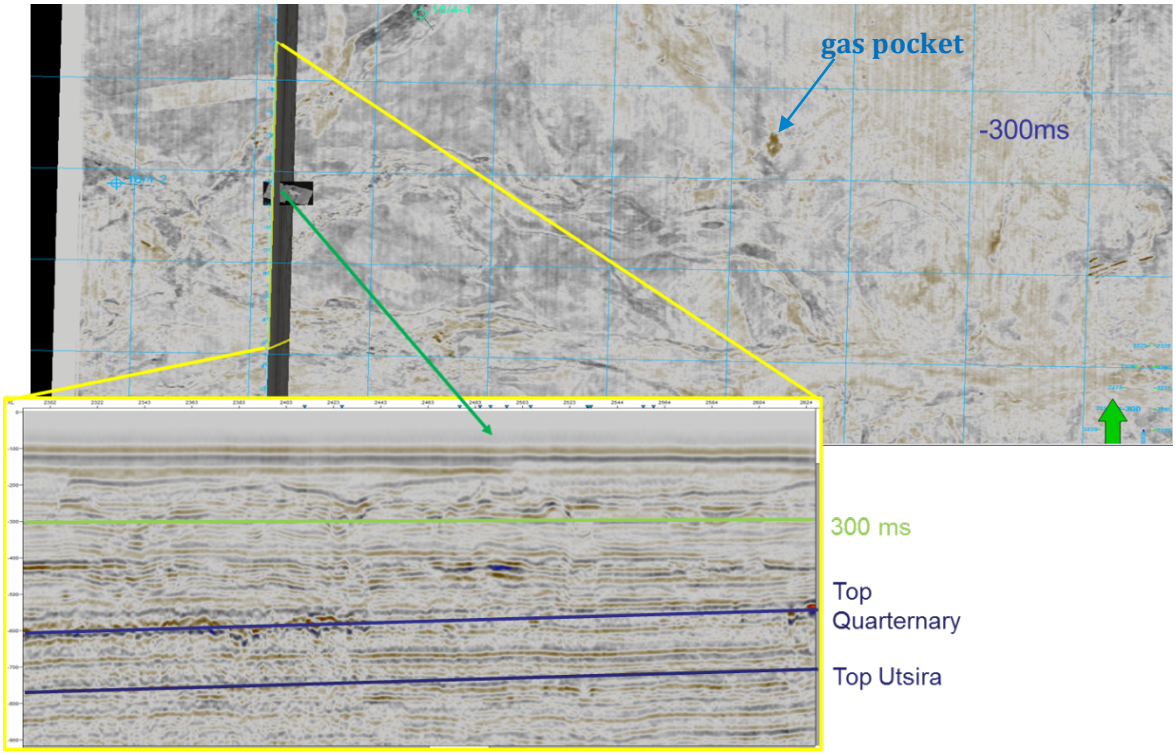

Figure 19: Time slice (300ms) of the LN09M02 3D seismic data in the upper part with clear signs of channels in the whole area. Small black rectangular HiSAS picture indicates the position of the seafloor fracture. Lower part shows a seismic line crossing the fracture. There seem to be many different disturbances, some consistent with channels and seismic pipes.

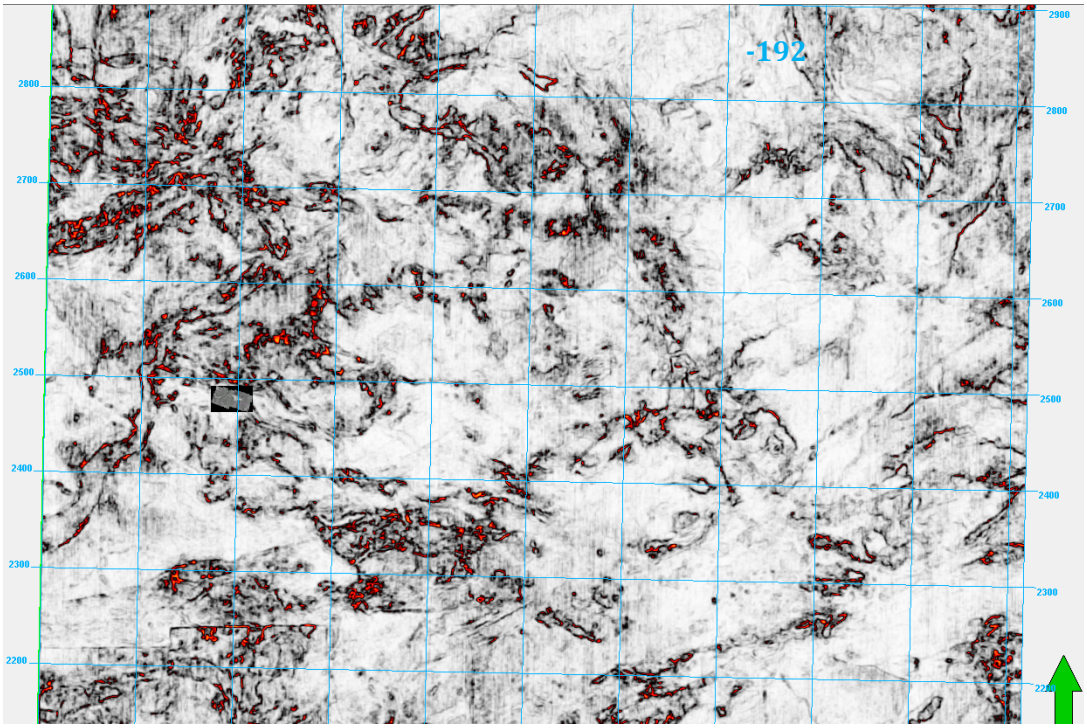

Figure 20: Time slice at -192 ms of the variance cube calculated in order to highlight channel structures. In the western part clear channels are visible where in the vicinity of the fracture (black/white HiSAS image) and to the North. Channel widths vary from 100 m to 850 m.

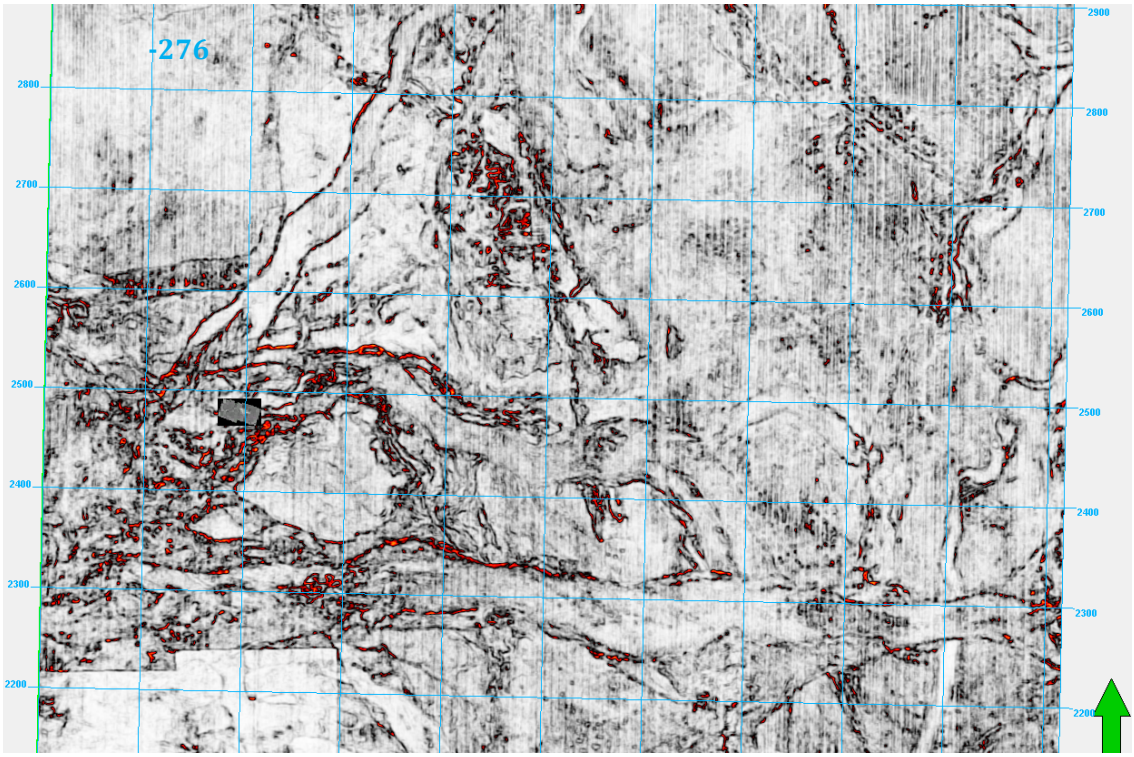

Figure 21: Time slice at -276 ms of the calculated variance cube. Another set of channels with different orientation and extent can be seen. The channels cross the whole area and their widths vary from 190 m to 1750 m.

5 Assessment of potential leakage scenarios in the Sleipner area

5.1 Pre-existing fluid flow system

The 3D seismic analysis revealed a complex and diverse network of fluid flow between different stratigraphic layers (*Figure 22*). We were able to identify chimneys, some of which may be traced deeper than the Utsira formation, while most of the large chimneys root in the Utsira formation or above. There are examples of large chimneys that root in the direct vicinity of large gas pockets and for smaller chimneys, which connect gas pockets in different stratigraphic layers (*Figure 23A*). In summary, the Sleipner area is highly affected by paleo fluid flow. The fluid flow is charged from some deeper source and may be linked to deeper hydrocarbon systems. We identified more than 50 seismic chimneys, which are an indicator for hydro-fractures, and therefore we can conclude that the Nordland shales have been fractured in the past.

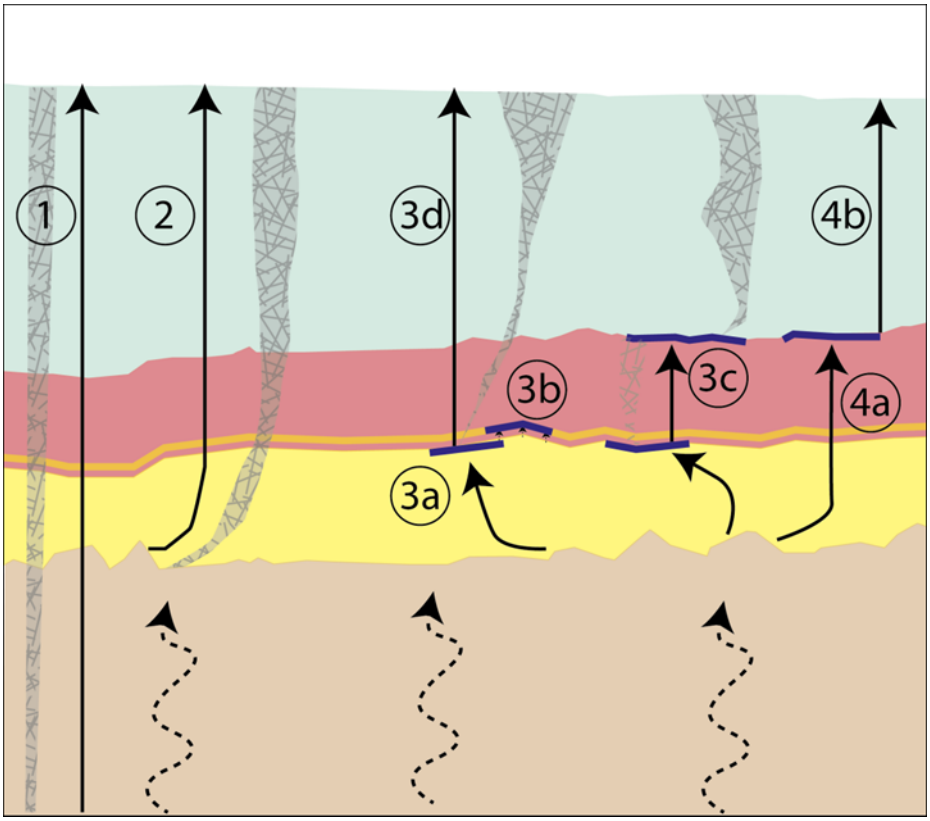

Figure 22: Overview of fluid flow features from 3D seismic interpretation: 1) Chimneys, which are traceable down to deep hydrocarbon reservoirs; 2) Chimneys rooting at the base of the Utsira Formation; 3a) Gas accumulation at the top of the Utsira Formation; 3b) Gas accumulation in the Sand wedge; 3c) Chimneys, which connect gas accumulations at the top of the Utsira Formation and the overburden; 4a) Gas accumulations beneath the Top Pliocene; 4) Chimneys rooting at the top Pliocene

Based on our observations, we develop different scenarios for CO_2 leakage at Sleipner or comparable storage sites. The leakage scenarios presented here are purely hypothetical and as such, have to be considered carefully. They are based upon our fluid flow analysis and on the assumption that paleo fluid flow structures may be reactivated by CO_2 injection.

5.1.1 Blowout

The first potential scenario is the creation of a CO_2 blow out (*Figure 23*). Such a process may be comparable to the Tordis incident in 2008. The Tordis incident occurred as the result of waste water injection in a thin sand formation (which was originally mistakenly believed to be an Utsira-like Formation; Eidvin et al., 2009). After a period of 5.5 months of injection accompanied with a constant formation pressure increase, the 900 m thick overburden fractured and water discharged in a blowout process for 16 to 77 days (Løseth et al., 2011). The usage of a sand formation as a storage formation with the Nordland group acting as caprock mean that that the risk of a blowout event could be a potential leakage scenario for Sleipner. But there are important differences between Sleipner and Tordis. Well sidewall cores revealed that the used sand formation at Tordis is significantly worse in quality and thinner than the Utsira formation at Sleipner (Eidvin et al., 2009).

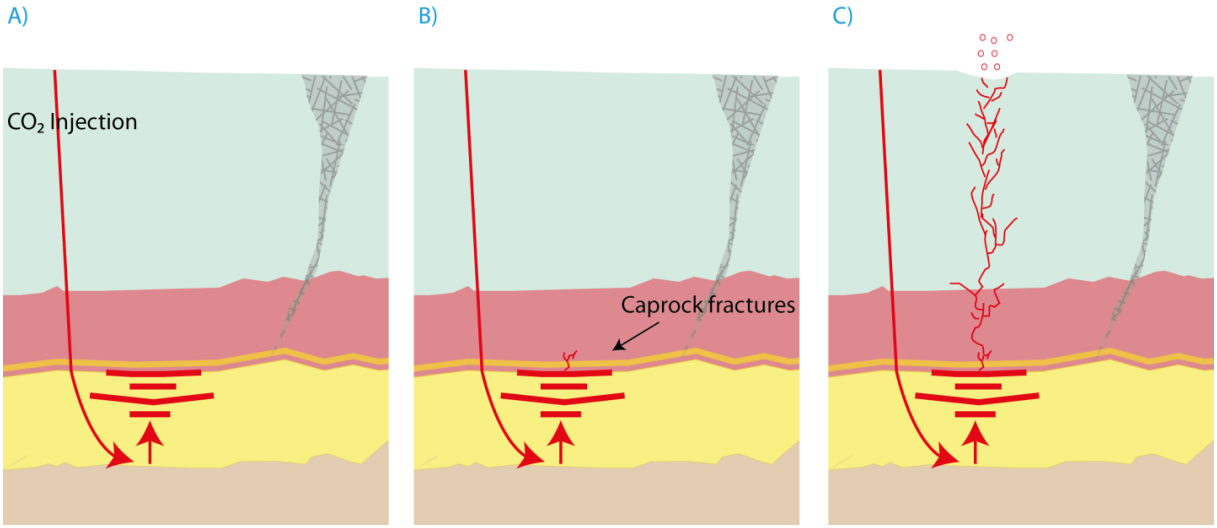

Figure 23: Creation of a blowout by CO_2 injection: A) CO_2 is injected in the Utsira Formation and builds up an overpressure, B) The caprock breaks by hydrofracturing; C) Hydrofractures break the entire caprock and reach the seafloor creating a blowout

It enabled a build-up of high overpressures necessary to hydrofracture the impermeable seal and thereby creating a blowout. Seismic chimneys may represent the natural equivalent of blowouts (Cathles et al., 2010; Løseth et al., 2011). Therefore, the presence of large chimney structures is an indicator that comparable processes have taken place in the study area in the past. However, it has to be pointed out that such a connection is highly speculative.

Since the development of high overpressure is an important precondition, such a blowout can be prevented by prohibiting too high pressures. Because the pore pressure within the Utsira Formation is monitored and no significant overpressure build-up is recorded, the risk of a blowout appears rather unlikely. Nevertheless, blowouts are one of the most important leakage scenarios for CCS in general and might be very important for other storage sites. At the moment, the model building efforts for Sleipner do not include the injection induced fracturing of the caprock scenario (compare with Geological Model Report (MS12)).

5.1.2 CO_2 escape through chimneys

More than 50 major chimneys can be identified in the study area. Some of them are rooting as deep as the Utsira formation. Such features are interpreted as hydro-fractured low-permeable shales (Arntsen et al., 2007). Assuming that the fractures are still high permeable conduits, the escape of CO_2 through these structures is a plausible scenario (*Figure 24*).

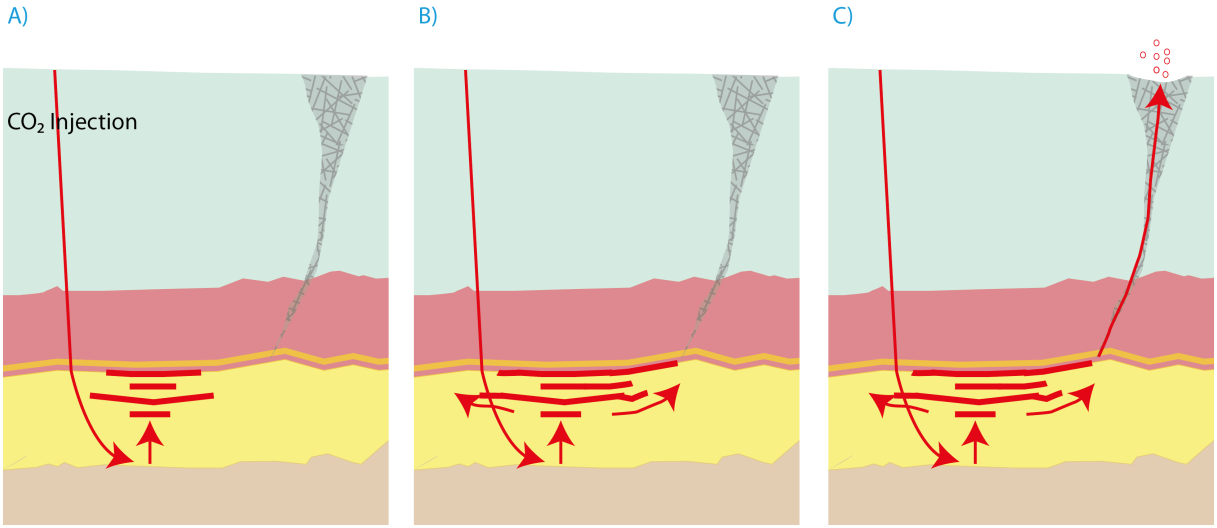

Figure 24: Leakage of CO_2 through pre-existing chimney structures: A) CO_2 is injected in the Utsira Formation; B) CO_2 reaches areas affected by chimneys A) CO_2 is injected in the Utsira Formation; C) CO_2 travels along the chimney structures through the overburden to the seafloor

The permeability of seismic chimneys is not well constrained yet and may even vary with the age of such structures due to self-sealing cementation processes. However, especially in low permeable rocks such as shales, the influence of fracture induced permeability is high and relates to the spacing, length and orientation of the fractures (Guiterrez et al., 2000). Fractures change the permeability of sediments permanently because even fractures that are defined as closed due to changes in the stress regime continue to have much higher permeability values in their matrix (Guiterrez et al., 2000) Further investigations and literature studies are necessary to assess the fracture permeability of the seismic chimneys and thereby assess the likelihood of CO2 leakage via these features. Our future fluid flow simulation will focus on this scenario (compare with Geological Model Report (MS12)). However, the CO_2 has not reached the areas affected by chimneys so far and may not reach it in the coming years. Therefore escape of CO_2 via chimneys is not expected in the near future, but may be an important long-term leakage scenario.

5.1.3 Formation water discharge via chimneys

Assuming high chimney permeability, the discharge of formation water through these structures appears to be a probable scenario. In this case, the pressure build-up caused by the injection of CO_2 would be reduced by the discharge of displaced formation water (*Figure 25*). Such a flow would lead to an uplift of the water column in the affected sediments rather than to a turbulent focused flow. We will try to address this scenario with a multi-phase fluid flow simulation (compare with Geological Model Report (MS12)). Further, we will try to investigate, if a discharge of formation water through chimney structures may prevent the build-up of high overpressures and thus, chimneys may act as “overpressure valves”.

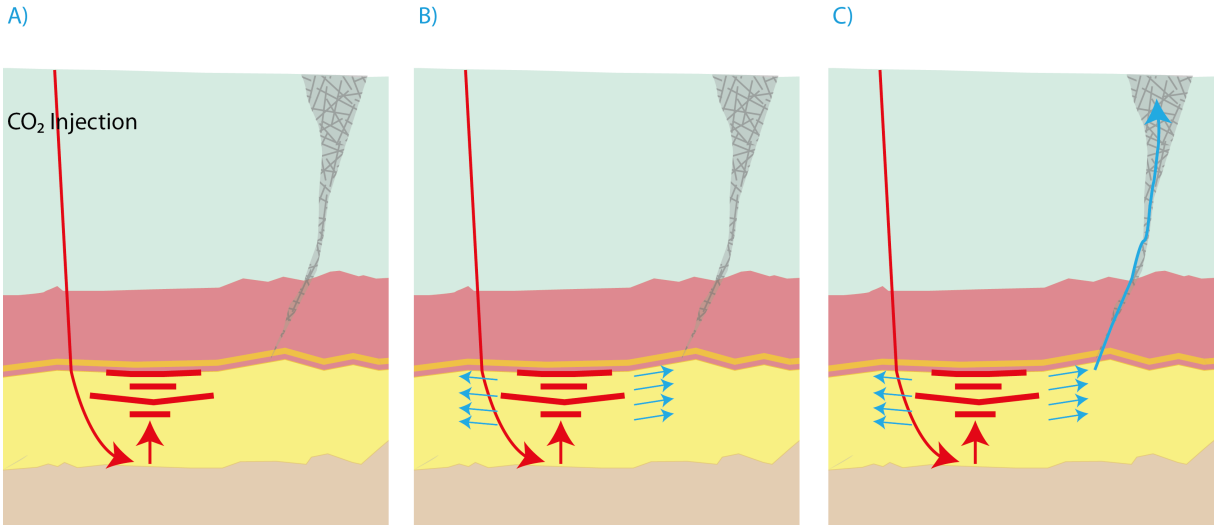

Figure 25: Leakage of formation water through pre-existing chimney structures: A) CO_2 is injected in the Utsira Formation; B) Formation water gets displaced by CO_2; C) Formation water travels along the chimney structures through the overburden to the seafloor

Since no CO_2 would leave the storage formation, it is arguable if this scenario is actually describing leakage. However, as methane, which is present in the pore space and fractures of a chimney structure, may be activated and ascend with upward flow of the formation water, this scenario may have an impact on marine ecosystems.

5.2 Abandoned wells

Abandoned wells have been identified as likely leakage pathways for underground CO_2 storage [e.g. Scherer et al., 2005; Brandvoll et al., 2009]. In the Sleipner area, numerous abandoned wells drive through the Utsira Formation and thus break through the natural sealing layers. This results in possible pathways for fluid and volatiles to migrate from deep geological formations up to the seafloor. Therefore, a leakage assessment of abandoned wells is vital.

During expeditions led by the Centre for Geobiology (UiB), methane leakage was detected from all three abandoned wells visited (see chapter 3.1). Even though no CO_2 was detected, the confirmed leakage of biogenic CH_4 at the abandoned wells clearly demonstrate the possibility of gases rising from or along abandoned wells through the sediments into the water column.

Well 15/9-13 is located only about 450 m from the rim of the CO_2-storage plume (2008 extent, see *Figure 26*). If an east-west migration of the stored CO_2 occurs, then well 15/9-13 would be the first to be reached by the migrating CO_2. Because the wells are cutting through the Utsira Formation and because bubble rise was already detected above these abandoned wells, fluid leakage along the abandoned wells appears as a relevant leakage scenario. Even though multiple post-injection marine seismic surveys of the CO_2-plume were conducted, it is difficult to assess the vertical and horizontal migration through the reservoir (Boait et al., 2012). Thus, it remains unclear, when or if the CO_2-plume will reach the abandoned wells.

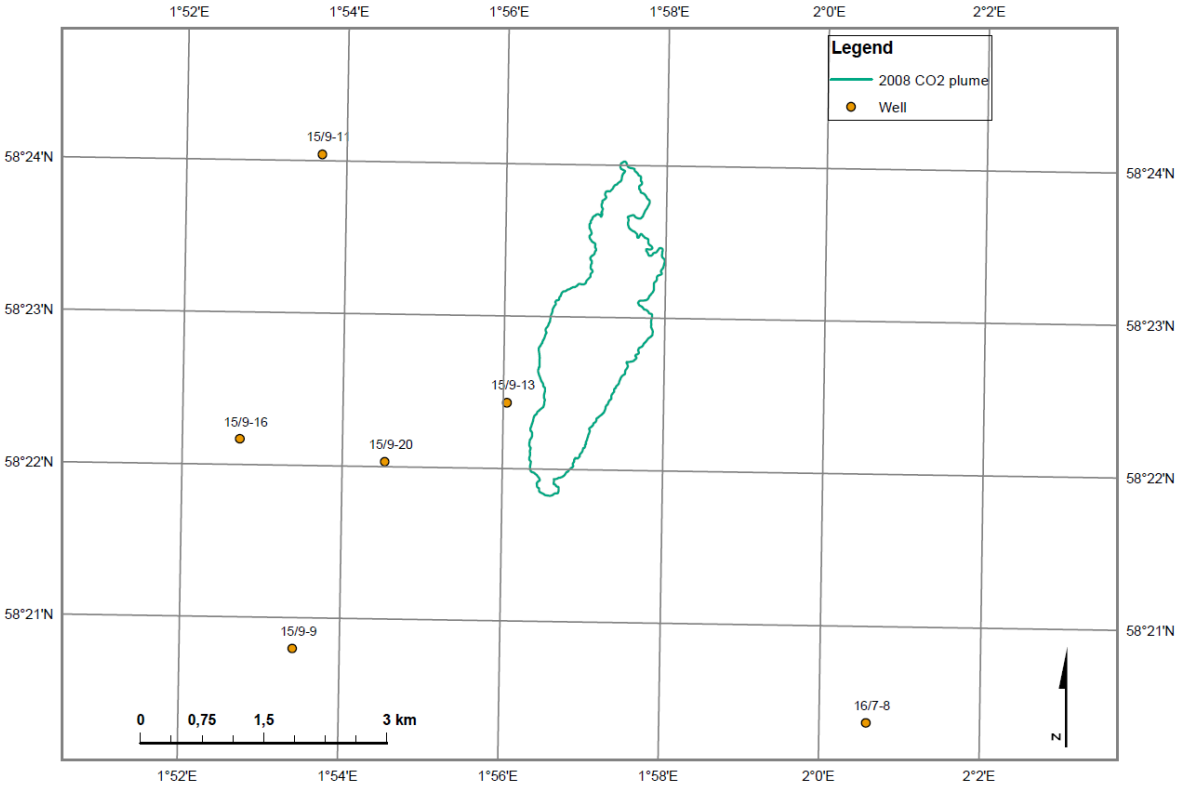

Figure 26: Extent of the Sleipner CO2 plume in 2008 and closest wells. The closest well is 15/9-13, situated about 450m west from the plume and with visible bubbles rising from it at the seafloor.

5.3 Leakage through interconnected pathways involving permeable fluvial channels

The discovery of the Hugin Fracture demonstrates that the uppermost, clay-rich, impermeable seal of the Utsira Formation is broken along a several km long structure. In a leakage assessment perspective, the following observations are of particular importance:

1) The Hugin Fracture seems to follow the margin of a subsurface channel structure.
2) The seep fluids that are emanating appear to stem from a subsurface fresh water reservoir, pointing towards the channel structure being of glacifluvial/fluvial origin.
3) Traces of ethane, which is most likely of thermogenic origin, suggest that the seep fluids include components that ultimately originate from below the Utsira Formation.

Our results this far suggest that the Hugin Fracture is somehow linked to a subsurface fluvial channel. The 3D seismic data from the area shows that fluvial channels/tunnel valleys are abundant above the top Pliocene. This is consistent with a number of previous studies showing that in the North Sea, a complex pattern of filled tunnel valleys have been formed sub-glacially by melt water during deglaciations of the last few full-glacial periods (Huuse & Lykke- Andersen 2000; Praeg 2003; Fichler et al., 2005; Lonergan et al., 2006). The tunnels may reach several tens of kilometres in length, can be several hundred metres deep and up to five km wide, and the sediment infill of the tunnels is mainly silt and sand (Kristensen et al., 2008). Such channels are accordingly potential pathways for lateral fluid flow.

The Hugin Fracture seems to have formed as a result of brittle failure of very stiff and clay-rich Quaternary sediments that are present in this region. The brittle failure may have been caused by differential compaction along the margin of a shallow fluvial channel structure. The

abundance of channel structures in the North Sea, and the spatial and a possible causal link between a shallow channel and the fracture, suggest that such seafloor fractures may be a common feature in this region. It is therefore possible that the top sediment seal may be broken by many similar fracture systems, and that these may provide pathways for fluid flow from the shallow permeable fluvial channels to the seafloor.

Analyses of the 3D seismic data from the Sleipner area show that the lower seal of the Utsira Formation is penetrated by chimney structures. Along such chimneys, fluids may migrate from the Utsira Formation into the fluvial channels that are common above the top Pliocene. If these channels then are permeable, and if they somehow are interconnected, then they could form channel ways for linked lateral and vertical fluid flow. The fluvial channel structures may be vertically connected in several ways: 1) through overlapping and intersecting each other; 2) through pipe structures; 3) through small fractures and faults formed by differential compaction; and possibly 4) as a result of injection induced hydrofracturing of thin shale layers that separate permeable channels.

We therefore also propose a leakage scenario involving vertical and lateral fluid flow through pathways of pipe structures, interconnected fluvial channels and shallow fracture systems that break the top sediment seal (*Figure 27*). This leakage scenario will be further investigated by more detailed analyses of the 3D seismic data and by numeric modelling.

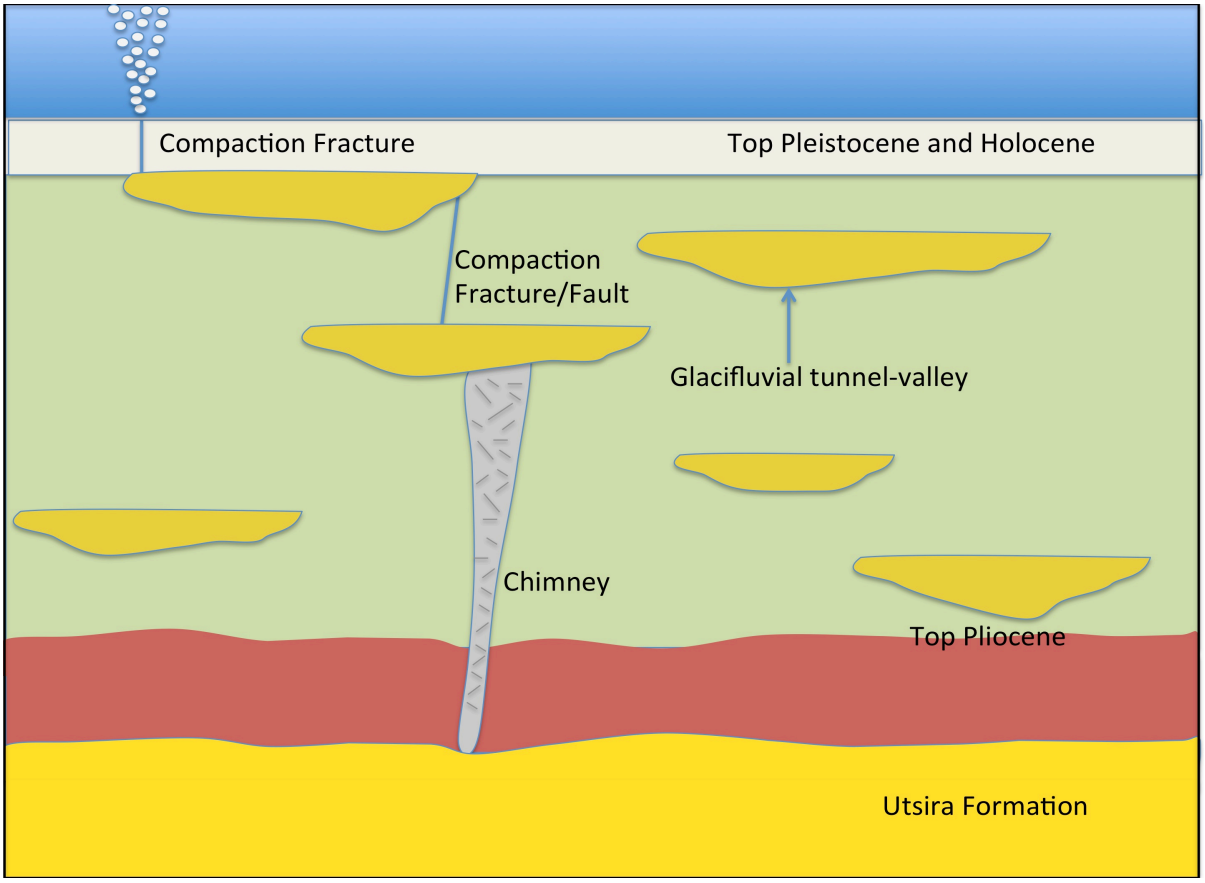

Figure 27: Leakage of CO_2 or formation water through an interconnected network involving chimney structures, fluvial channels, and fractures/faults. Fractures through the top sediment layer, chimneys and fluvial channels are observed at the seafloor and in the seismic data respectively. Interconnection of channels into a permeable network is hypothetical.

6 Summary

As part of WP1, we studied the integrity of the sedimentary cover to the Utsira Formation at the Sleipner CO_2 storage site and in adjacent areas. Using both well-proven and novel technology, we searched for active seabed fluid flow systems during several ECO2 cruises to the area. In addition, we specifically analysed 3D seismic data that was provided by industry, to identify subsurface fluid flow features.

As a result, we documented active seafloor fluid flow at several abandoned wells in block 15/9. Seabed fluid flow was also discovered along a 3 km-long fracture system (the Hugin Fracture) located 25 km to the north of the CO_2 storage site, in block 16/4. In addition, more than 50 major vertical chimneys were identified in the study area, some of which are rooted in the Utsira Formation.

Methane was identified leaking from the three abandoned wells visited in block 15/9. This demonstrates that a pathway for vertical fluid flow exists close to the current CO_2 storage site. In particular, well 15/9-13, which is located only 450 m to the west of the current CO_2 plume, would be the first abandoned well to be reached if the plume is capable of migrating further westwards. The methane emanating from well 15/9-13 is of biogenic origin and probably has a relatively shallow source. Nevertheless, future precautionary measures should include monitoring the gas flow from this well. Such monitoring would also help to document if the gas flow is affected by the injection activity and if there is a connection between the Utsira Formation and the seafloor via this well.

The discovery of the Hugin Fracture demonstrates that the uppermost, clay-rich, impermeable seal of the Utsira Formation is broken along a several km long structure. Our results thus far suggest that this fracture feature is linked to a subsurface fluvial channel. In this region, fluvial channels are common, located from 50 metres below the seafloor to 100 metres above the Utsira Formation. If these channels are somehow inter-connected, they represent a pathway for fluid flow from deeper structures under the seafloor to the surface. The documentation of vertical pipe structures that are rooted in the Utsira Formation shows that the lower seal also may be broken in many places and that fluid flow from the Utsira Formation into the overburden may occur.

We therefore propose leakage scenarios that involve the flow of CO2 or formation water from the Utsira Formation to the surface along pre-existing chimney structures, or through inter-connected fluvial channels that eventually vent to seafloor through fracture systems that break the top sediment seal.

Taking into account the high abundance of fluvial channels and chimney structures, as well as the discovery of a several km-long fracture that breaks the top seal - a feature that may well be common in this area - we conclude that the possibility of fluid flow from the Utsira Formation to the seafloor cannot be excluded. Thus, a more extensive survey and study of the area are considered necessary.

7 References

Arntsen, B., Wensaas, L., Løseth, H., and Hermanrud, C. (2007), Seismic modeling of gas chimneys, Geophysics, 72 (5): 251 – 259

Audigane, P., Gaus, I., Czernichowski-Lauriol, I., Pruess, K. and Xu, T. (2007), Two-dimensional reactive transport modeling of CO2 injection in a saline aquifer at the Sleipner site, North Sea. American Journal of Science, 307(7): 974-1008.

Boait, F. C., N. J. White, M. J. Bickle, R. A. Chadwick, J. A. Neufeld, H. E. Huppert (2012), Spatial and temporal evolution of injected CO_2 at the Sleipner Field, North Sea, *Journal of Geophysical Research*, 117, B03309.

Brandvoll, Ø., O. Regnault, I. A. Munz, I.K. Iden, H. Johansen (2009), Fluid-solid interations related to subsurface storage of CO_2 Experimental tests of well cement, *Energy Procedia*, 1, 3367 – 3374.

Brooks, J. and Glennie, 1988, K. W. (eds) Petroleum Geology of. North West Europe. Graham & Trotman, London, 43-48. BERTRAM, G. T. AND MILTON, N. 1988.

Cathles, L., Su, Z., and Chen, D. (2010), The physics of gas chimney and pockmark formation, with implications for assessment of seafloor hazards and gas sequestration: Marine and Petroleum Geology.

Eidvin, T., Øverland, J. A. (2009), Faulty Geology halts project. Norwegian Continental Shelf, No. 2-2011: 34-36.

Fichler, C., et al. (2005), North Sea Quaternary morphology from seismic and magnetic data: indications for gas hydrates during glaciation?, *Petroleum Geoscience* 11(4), 331-337.

Graham, A.G.C., Lonergan, L. and Stoker, M.S. (2007), Evidence for Late Pleistocene ice stream activity in the Witch Ground Basin, central North Sea, from 3D seismic reflection data. Quaternary Science Reviews, 26(5–6): 627-643.

Gutierrez, M., Øino, L.E. and Nygård, R. (2000), Stress-dependent permeability of a de-mineralised fracture in shale. Marine and Petroleum Geology, 17(8): 895-907.

Harrington, J.F. et al., 2009; Laboratory Study of Gas and Water Flow in the Nordland Shale, Sleipner, North Sea; AAPG Special Volumes, Pages 521 – 543.

Huuse, M., and H. Lykke-Anderse, (2000), Overdeepened Quaternary valleys in the eastern Danish North Sea: morphology and origin, *Quaternary Science Reviews 19.12*, 1233-1253.

Kristensen, T.B., Piotrowski, J.A., Huuse, M., Clausen, O.R. and Hamberg, L., (2008), Time-transgressive tunnel valley formation indicated by infill sediment structure, North Sea – the role of glaciohydraulic supercooling. Earth Surface Processes and Landforms, 33(4): 546-559.

Lonergan, L., Maidment, S.C.R. and Collier, J.S. (2006), Pleistocene subglacial tunnel valleys in the central North Sea basin: 3-D morphology and evolution. Journal of Quaternary Science, 21(8): 891-903.

Løseth, H., Wensaas, L., Arntsen, B., and Hanken, N. (2011), 1000 m long gas blow-out pipes: Marine and Petroleum.

Scherer, G.W., M.A. Celia, J-H. Prevost, S. Bachu, R. Bruant, A. Duguid, R. Fuller, S.E. Gasda, M. Radonjic, W. Vichit-Vadakan (2005), Leakage of CO_2 through abandoned wells: Role of corrosion of cement. In: S.M. Benson (ed), *Carbon dioxide capture for storage in deep geological formations – results from the CO_2 capture project, Elsevier*: Vol 2, 827-848.

Praeg, D. (2003), Seismic imaging of mid-Pleistocene tunnel-valleys in the North Sea Basin—high resolution from low frequencies, *Journal of Applied Geophysics,* 53(4), 273-298.

PART II

Report of leakage assessment and identification of fluid leakage scenarios at the Snøhvit CO_2 storage site (UiT)

Report of leakage assessment and identification of fluid leakage scenarios at the Snøhvit storage site (UiT)

Content

1 Introduction

The Snøhvit hydrocarbon reservoir and CO2 storage site has been opened in 2007. The oil produced from Snøhvit is the first offshore oil field to be produced without offshore installations. Gas production has started in 2007 and CO2 capture, using amine technology, started in 2008. Statoil is the operator of the CO2 storage from Snøhvit. It is located offshore northern Norway in the SW Barents Sea about 150 km from the coastline.

CO2 is removed from the gas stream and piped 150 km back to the field for injection into an offshore deep saline formation. The main CO2 storage formation is the Saline Tubaen Sandstone Formation reservoirs at 2600 meters depth and as of recent changes, the lower part of the Stø Formation. Around 700,000 tonnes of carbon dioxide per year will be stored in this way. A monitoring program has also been set-up to investigate the behavior of CO2 underground.

2 Geological background

The ENE-WSW oriented HFB, located in the south western Barents Sea, was probably established in the Late Carboniferous (Gabrielsen et al., 1990), with important subsidence events in the Triassic and Early Cretaceous, and with the main basin development phases taking place however during the Mid to Upper Jurassic times (Linjordet and Olsen, 1992).

The Snøhvit field is located in the HFB and is about 130 km off the coast of Finnmark (Fig. 1a). The HFB contains approximately 5000 m of strata above the basement (Linjordet et al., 1992). At Snøhvit, in the Lower Jurassic, the Tubaen Formation (TbF), is an important reservoir where CO_2 has been injected into since 2008 (Maldal and Tappel, 2004). The Stø Formation (SF) is the main reservoir rock in the HFB, of Pliensbach-Bajocian age, consisting of vertically stacked units of the lower to the upper beach slope deposits (Worsley et al., 1988). CO2 storage was changed from the Tubaen Fm to the gas producing Stø Fm in March 2011 (Maldal and Tappel, 2004). For a more detailed description of the geological background and lithostratigraphy of the area see the Geological models report (MS12) compiled by WP1 in October 2012.

3 Data, methodology, modeling

A conventional 3D seismic data set (ST0306) provided by Statoil ASA was used in this study. The 3D seismic data covers a large part of the HFB (see section 3 in the Geological models report MS12 on Snøhvit). The cube ST0306 covers the Snøhvit and Albatross fields, (water depth from -511 to -369 ms TWT). We also used two P-Cable high resolution cubes (water depth from -468 to -425 ms TWT) located within the Snøhvit field as shown in figure 1b. The P-Cable system consists of up to 12 streamers towed parallel behind the ship. Streamers with hydrophones are 25 m long and contain 8 channels each.

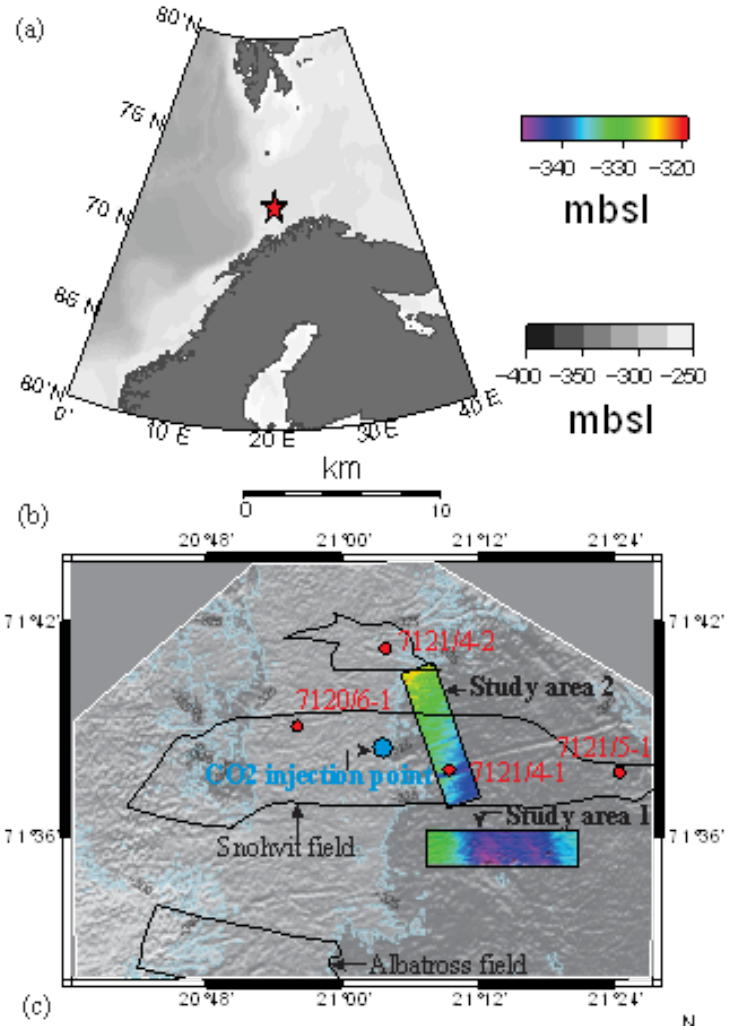

Figure 1: a) Location map of the Snøhvit field b) Location of the 2 P-Cable surveys (colored seafloor bathymetry).

4 3D seismic observations (and interpretations)

The storage formation and overburden at Snøhvit contain sediments as old as the Late Jurassic. In this report, Observations and interpretations of the 3D seismic data are briefly summarized. For a more comprehensive interpretation of fluid flow indicators, structure and stratigraphy, we refer to section 4 in the Geological models report (MS12).

The main areas of fluid flow, derived from interpretation of the geophysical data, are indicated by black circles (CM1-2 and AM1) (fig. 2, 3). These areas are characterized by a vertical zone that is chaotic and acoustically masked and are interpreted as large gas chimneys. These gas chimney structures (CM1-2 in fig.2) have been identified to be of special interest when it comes to modeling gas leakage. Their presence has been interpreted as hydrocarbon leakage pathways, promoted by a connected fracture network penetrating the reservoir's cap rock (Arntsen et al. 2007; Ligtenberg 2005; Meldahl et al. 2001). Due to past fluid migration the gas saturation within the overburden is increased, which leads to an

enhanced relative permeability for the gas phase. Additionally their porosity tends to be relatively high, which in turn increases the rock's permeability.

The Tertiary Torsk Formation (TF) (fig. 3, 4, 5) above the Snøhvit field is characterized by numerous high amplitude bright spots and enhanced reflectors (fig. 3, 5). Some shallow high-amplitude reflections show reverse polarity with respect to the seafloor indicating presence of gas as for example the bright spot on top of a large acoustic masking zone, which is located at around 650 ms TWT. (fig. 5C). Evidence that gas has accumulated in the upper parts of the overburden can also be seen by the acoustic anomalies present along the Upper Regional Unconformity (URU) reflector, (fig. 3B, 3D, 3E, 3F, 5C). For more details on the shallow gas accumulations at Snøhvit see section 4.2.2 in the Geological models report (MS12).

Throughout the subsurface we observe 3 major fault orientations in the area: E/W, NE/SW and NW/SE (fig. 2B). In the dataset we also observe major deep-seated faults (fig. 3) with high-amplitude anomalies often being situated above them (fig. 3B, 3E, 3F). Major faults are mainly normal faults with varying lateral extension, fault orientation and fault throw (fig.3). Faults with offsets into the Cretaceous and Tertiary generally show an E/W direction (figs 2, 3). Faults with offset until the Late Jurassic show a larger variety in directions than the faults with large offsets, which are active until the Tertiary (fig.2). Block faulting is common due to the parallel or nearly parallel strike and dip directions of some of the faults (fig.2, 3). The structural basis for the Snøhvit reservoir is defined by 2 major horst structures bounded by E/W trending faults, (fig. 2, 3).

We observe that all gas chimneys and areas of acoustic masking develop in areas that contain faults of such orientation, ie a NW/SE orientation, (faults drawn in red in fig. 2, 3), that have been active mainly in the Jurassic (fig. 2, 3). Each gas chimney also varies in extent throughout the sedimentary strata being smaller further up in the shallow parts (fig. 6). We also observe the existence of normal faults developing under normal pockmarks Np1-3 (fig. 4).

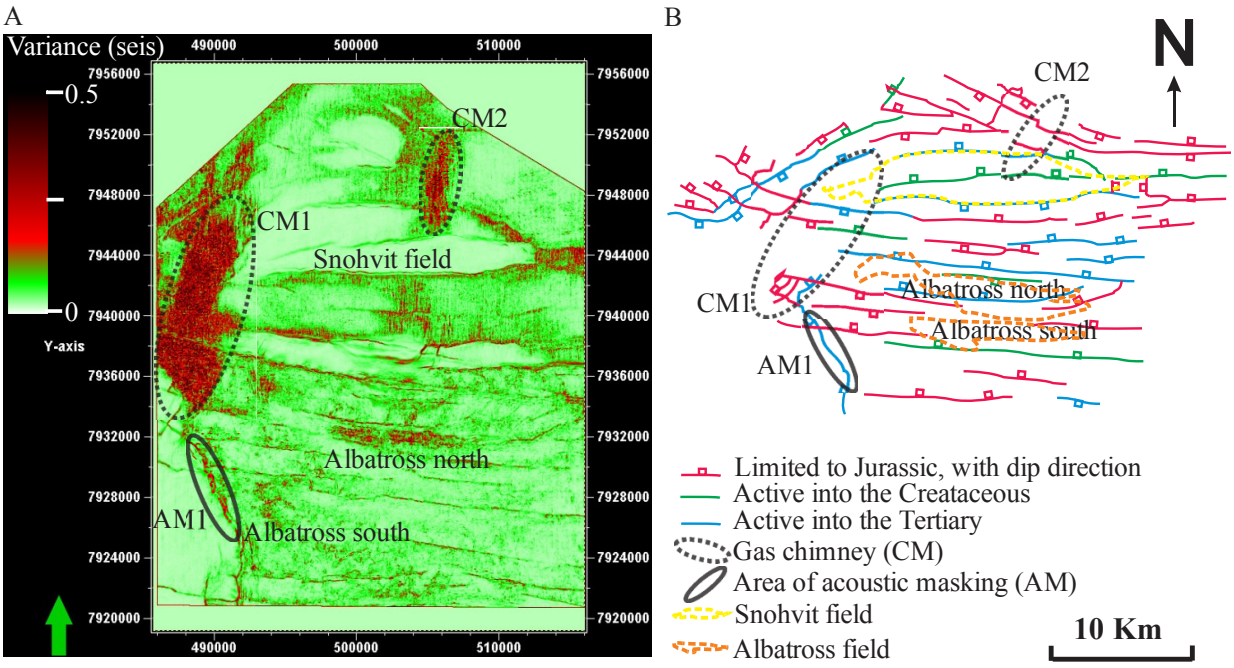

Figure 2: A) Variance map at-1912ms depth (near the top of the reservoir level), B) Pattern of large scale faulting derived from fault positions in the Fuglen formation. Pattern is based on 3D seismic dip map and seismic section interpretations. Faults limited to the Jurassic (red colored) will be called Jurassic faults and faults active into Cretaceous (green colored) and into the Tertiary (blue colored) will be called Cretaceous and Tertiary faults respectively.

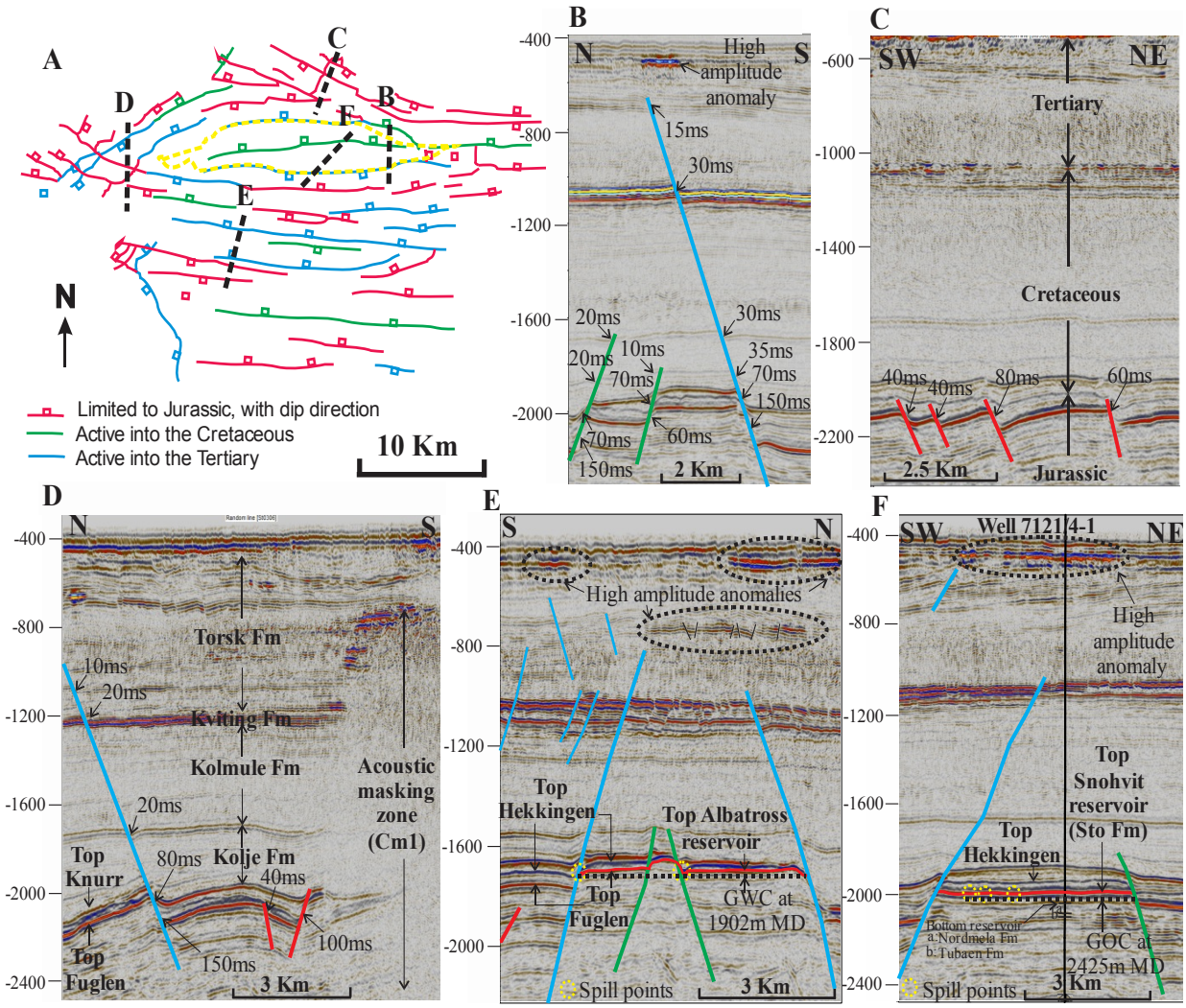

Figure 3: A) Pattern of large scale faulting in the area, Cross sections through B) Cretaceous and Tertiary faults, C) Jurassic faults, D) various faults and CM1. Association of faults and spill points at E) Albatross and F) Snøhvit reservoirs.

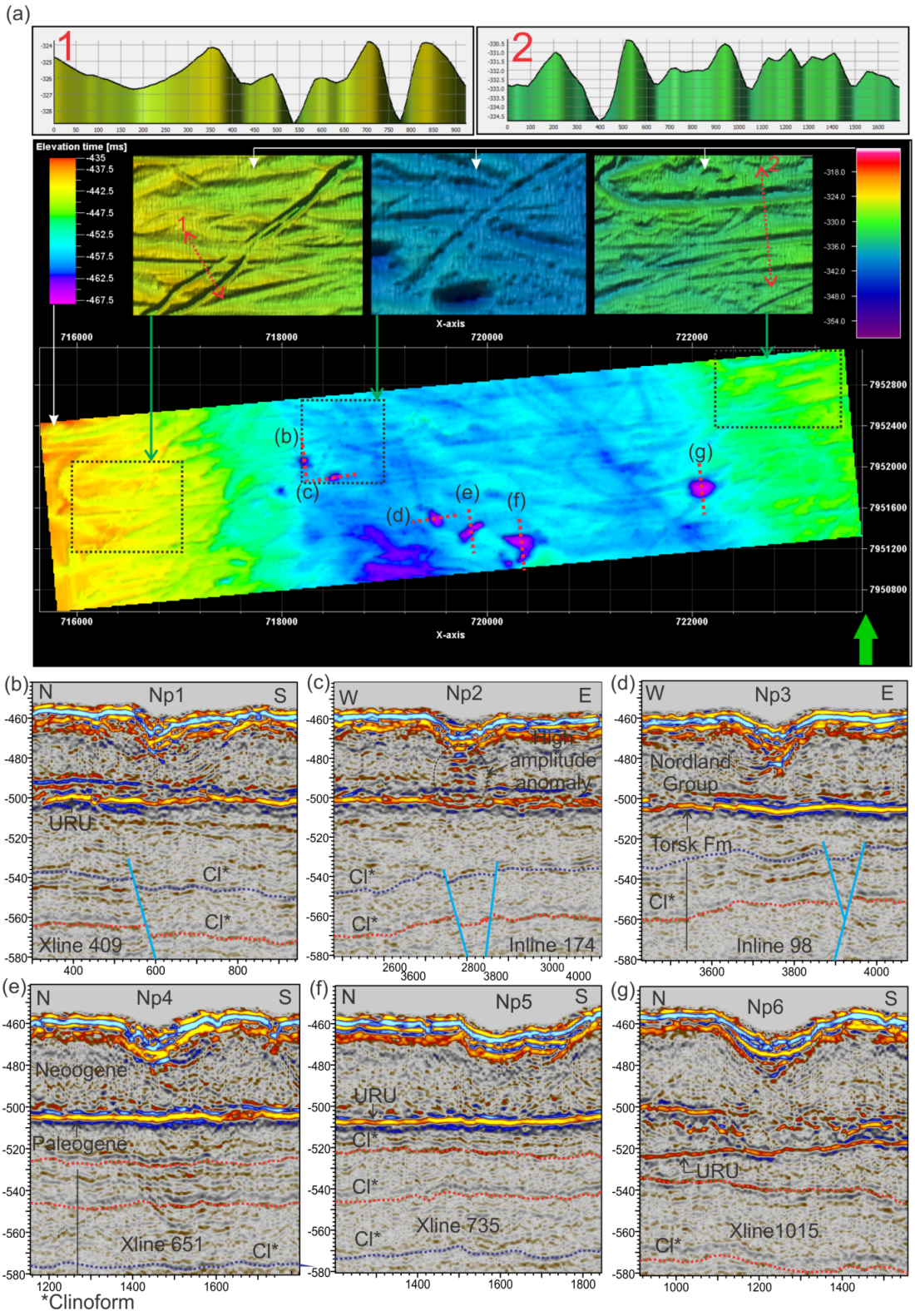

Figure 4: Normal Pockmark characterization through a) A seabed surface map from the 1st P-Cable high resolution seismic data showing location and extent of normal pockmarks (Np's) and ploughmarks on the seafloor, with associated cross sections 1 and 2 showing the ploughmarks in greater detail. Seismic lines illustrating the form and the underlying stratigraphy of the following normal pockmarks from the 1st P -Cable study area: b) Np1, c) Np2, d) Np3, e) Np4, f) Np5 and g) Np6.

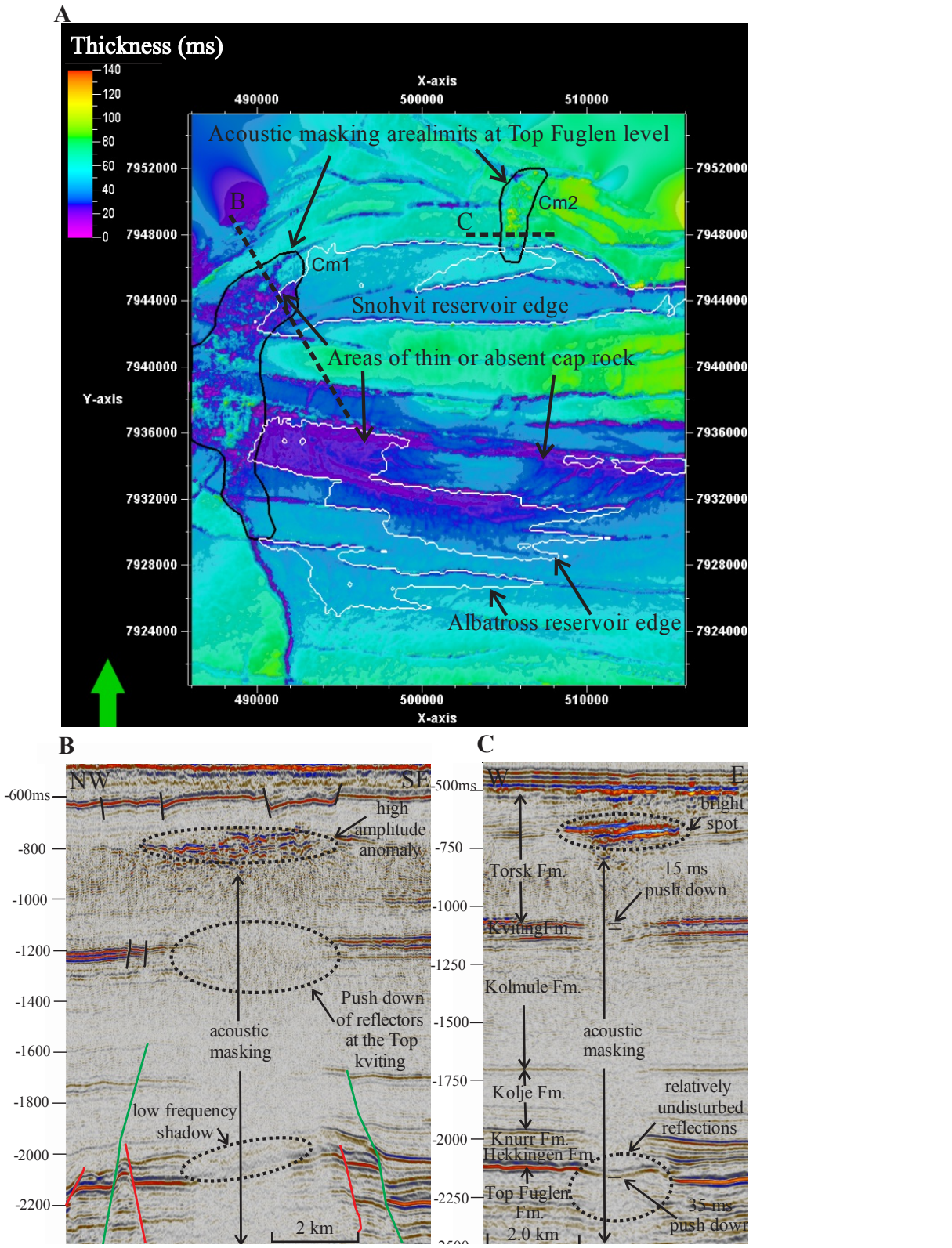

Figure 5: A) Spatial relationship between the reservoirs, cap rock distribution through a thickness map of the Hekkingen Fm and the gas chimneys, and seismic examples of B) CM1 and C) CM2 gas chimneys.

The first of the two high-resolution P-Cable data sets were acquired in the area of the main seafloor installation at Snøhvit (Figure 1). This area is characterized by hundreds of small pockmarks (Fig. 4). The pockmarks are widely distributed along the seabed in a depth of approximately 340 m (Fig. 4). The seabed is characterized by 2 classes of pockmarks, which can be referred to as "normal" and "unit" pockmarks (Judd and Hovland, 2007) (fig. 4). The second P-Cable cube partly covers a large gas chimney in the subsurface. The main objective here is to better understand the development of these large gas chimneys and their upper termination. For more details on the interpretation of the P-Cable data at Snøhvit see section 4.3 in the Geological models report (MS12).

5 Leakage assessment

5.1 Pre-existing fluid flow system

The total or partial absence of cap rock in certain areas (fig. 5A), the existence of spill points in the trap, near or at faults (fig. 3E, 3F) and the observation that faults have also been responsible for displacing the sealing lithologies (fig. 3, 5), suggests that fluid migration has occurred through the seal in the past. Leakage is observed in shallow strata suggesting a close relationship between faults and fluid flow in the area as fluid flow features above major deep-seated faults were also observed (fig. 4) (Vadakkepuliyambatta et al., 2013). The upward migration of fluids leads to accumulation in the shallow subsurface, (fig. 3, 4).

Faults that have a NW/SE orientation, (faults drawn in red in fig. 2, 3) and are located approximately perpendicular to the horizontal extensional stress direction were probably not sealing (Linjordet and Olsen, 1992). These NW/SE orientated faults played a role in the vertical migration of fluids during the Jurassic. Fluid migration through the NW/SE oriented faults (fig. 2) could have taken place through micro-fracturing or molecular diffusion (fig. 7). Such faults can act as valves for the transport of fluids along the fault plane(fig. 7C) (Sibson, 2000). The existence of normal faults developing under Np1-3 (fig. 4) could also suggest that large pockmarks have been formed by fluid flow through such discontinuities such as faults.

We observed spill points at the crossing points between faults and the GWC (fig. 3E, 6), suggesting that leakage could have taken place at these specific locations. The failure of deep-seated faults to effectively seal the trapped hydrocarbons has led to fluid reaching shallow strata such as the URU (fig. 3B). These faults have been reactivated, younger than the Jurassic and Cretaceous ones and pass through the reservoir (fig. 3B, 3D, 3E, 3F) allowing for gas pockets to be associated with them in the overlying sediments. Leakage could have also started through major faults and spread to the minor faults of the Kviting and Torsk Fms (fig. 3E) and of the URU in shallower strata (fig. 3D, 3E, 3F, 5B).

Glaciations affected the SW Barents Sea and led to considerable uplift, associated with erosion and isostatic rebound from deglaciation (Riis and Fjeldskaar, 1992). The actual onset of deglaciation is estimated at around 15ka, when a distinct meltwater event is recorded (Landvik et al., 1998). Erosion, removal of overburden and later uplift led to the reactivation and opening of many pre-existing faults and creation of fluid flow pathways (Nøttvedt et al., 1988). Spill points located near faults or at the intersection of faults and the GWC (fig. 3E,

3F, 6) and the existence of high amplitude anomalies directly above these faults, at the Torsk Fm and URU levels (Figs. 3, 4, 5) indicates that these later may have acted as fluid flow pathways.

The spill point corresponds also to the point where the gas and pressure gradients meet at a certain depth; a depth at which gas spills and which corresponds to the GWC, at 1902 m MD in the albatross field (fig. 3E, 7D). Fluids that leaked, through the spills points, could have led to the emplacement and development of the gas chimneys in the area (fig. 6, 7). Fluid has leaked out of the reservoir in the past by spilling across the spill points (fig. 6) and into the chimneys. In CM1, spill points have fed fluid from the southeastern part of the gas chimney and in CM2 from the southern part of the gas chimney.

The chimney pore space can be saturated by gas and the gas moves through it without major resistance, (figure 7). The upward migrating chimney displaces water sideways and through permeable pathways such as microfractures or fractures (fig. 7), creates water saturated areas. Gas then moved both vertically and laterally, which might explain the observed variability of the gas chimney extent with depth (fig. 6), and the variability of amplitude anomalies at its upper termination (Figs 3, 5)

Transport of gas from the reservoir through the caprock can also take place via a connected fracture framework followed by diffusion. Once passed the caprock the gas can diffuse further upwards through the overburden (fig. 7B, 7C).

5.2 Leakage possibility in the future

Before denudation and during maximum burial (fig. 7A), where pressure and temperature are the highest (Pmax and Tmax) (Nyland et al., 1992), hydrocarbon generation is at its maximum and reservoir filling occurs (fig. 7A) (Linjordet and Olsen, 1992). Gas expansion and pressure increase, due to erosion and uplift (fig. 7B), could have caused reactivation of large-scale fault systems such as those through the early Tertiary (fig. 7C). This dominant driving force could have led to the fracturing of otherwise impermeable rocks and conduction of fluids in the past. Depressurization as a result of erosion translates into gas expansion. This gas expansion and resulting tilting of the reservoir towards the center of the glacial sheet also led to a fluid leakage at the spill point of the reservoir in the past (fig. 7) (Kjemperud and Fjeldskaar, 1992).

From the above chain of events that took place in the past we can conclude that it would probably need another glaciation, and consequent erosion and uplift and other ensuing effects, to stimulate another period of fluid leakage.

The caprock at Snøhvit (the Hekkingen Fm) is composed of shale layers and the permeability of shale is often in the nanoDarcy scale or may be even lower (Fjaer et al, 2008). We would expect such an impermeable cap rock to have an effect on the CO2 plume, not allowing it to develop in the overburden. If some CO2 does get to leak through the cap rock today and if some of the faults can be considered as leaking today, then there is a potential for the CO2 to use these fluid flow pathways and reach very shallow depths near the seabed as it has done in the past.

When the crust is subject to erosion related compressive stress the most likely site for reservoir leakage, through the seal, would not be by hydrofracturing but actually through faults (Løtveit et al., 2012). In reality however we don't expect such an event to occur in the future, therefore the potential for leakage is minimal. Also the faults at the Snøhvit reservoir level do not extend all the way from the reservoir to the seabed thus reducing the risk of CO2 reaching the seabed directly.

Gas accumulations above gas chimneys may also have been trapped by gas hydrates. Such gas build ups are found below the present gas hydrate stability field or Gas Hydrate Stability Zone (GHSZ) (Chand et al., 2008). These gas hydrates, if they remain frozen, can provide an additional sealing effect to any migrating fluids thus reducing the risk of CO2 reaching the seabed. The URU finally, being an erosional surface, constitutes a lithological transition to dense, less permeable glacigenic sediments and can also act as a barrier to fluid flow (fig, 3, 5). This suggests that even if CO2 does reach the URU, which is highly unlikely, it might be trapped at the URU reflector and not continue further upwards and reach the seabed.

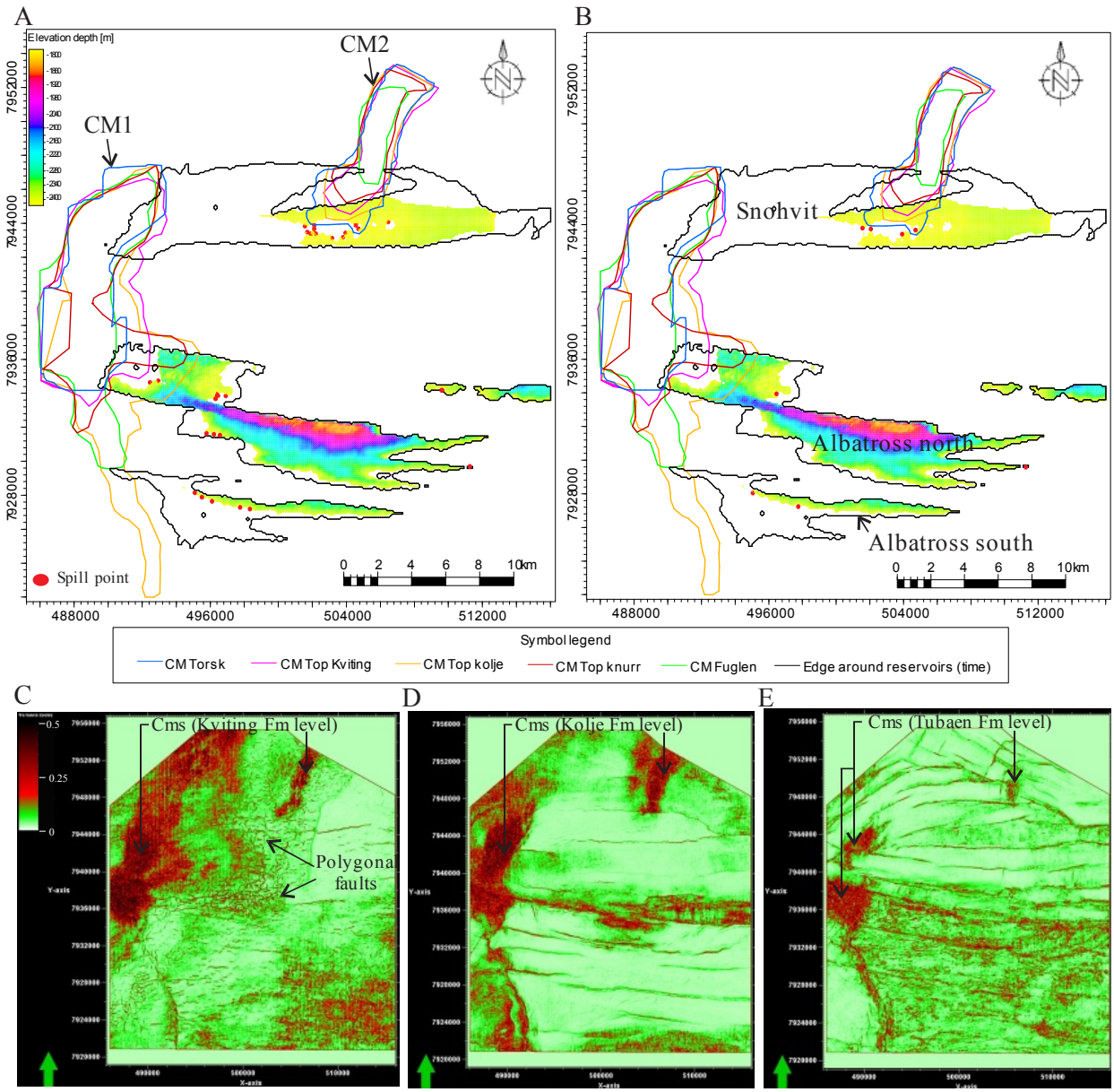

Figure 6: Gas chimney variability with depth for both CM1 and CM2 and spill point location (red dots) using A) a 2m interval, B) a 1m interval. Variance maps at C) -1080ms depth (Kviting Fm) D) -1670ms (Kolje Fm) and E) at -2100ms (Tubaen Fm).

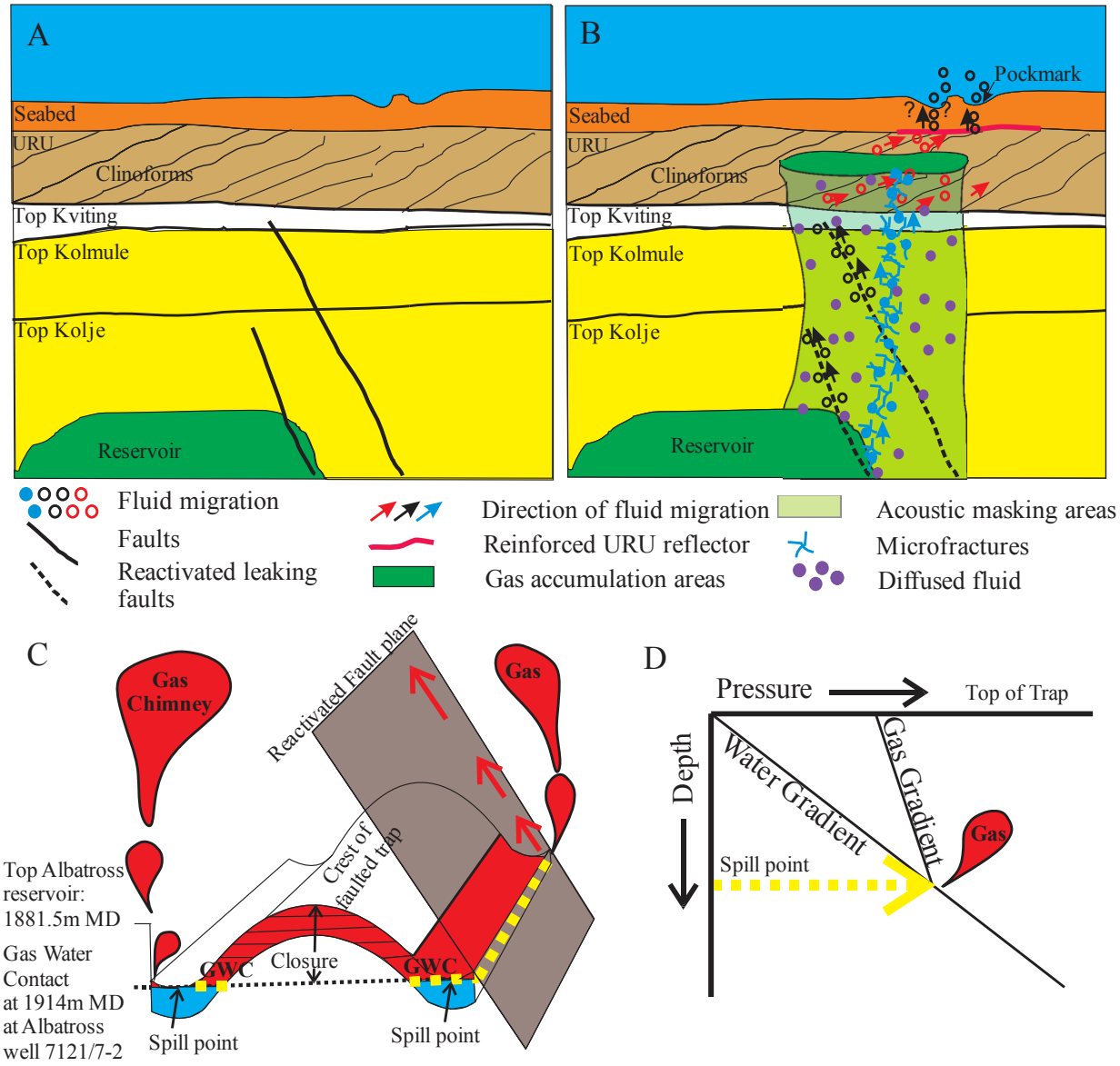

Figure 7: Model of leakage along gas chimneys and faults A) before denudation and B) after denudation. C) Chimney formation mechanism through leakage at the spill point and fluid leakage along reactivated faults D) Pressure-depth diagram explaining how gas can reach the spill point

6 Leakage scenarios

CO2 from the Tubåen Formation (Fm) can partially leak upwards to the Hekkingen Fm or less deep formations via faults and gas chimneys. If leaking CO2 reaches the Top Kviting Fm it can continue migrating upwards via pipe structures, faults, gas chimneys or the clinoforms of the Torsk Fm and accumulate under the Upper Regional Unconformity (URU). The presence of pockmarks at the seabed could indicate further leakage between the URU and the seabed

via vertical fluid flow structures underlying the pockmarks (Fig. 4; see also Geological models report MS12).

The modeling and fluid flow simulation activities within the ECO2 project focused on the following leakage scenarios that include possible leakage through i) faults, ii) gas chimneys that are realistic scenarios meaning that they resemble realistic geological features. For the realistic scenarios we used the following two realizations, with different permeability and porosity ranges (for the method used in the determination and population of the geomodels with properties see the Geological models report MS 12).

6.1 Faults

One potential scenario is related to the leaking of CO2 from the Tubåen Formation (Fm) and its partial migration upwards to the Hekkingen Fm or less deep formations via the faults (all Jurassic faults, via the NW/SE trending Jurassic faults only or via the tertiary faults also). CO2 is injected in the Tubaen and Stø formations (fig. 8a); The CO2 plume grows and reaches the areas affected by the faults (fig. 8b) If leaking reaches the tertiary faults, CO2 can migrate through the Top Kvitting Fm and may continue via pipe structures, smaller shallower faults or the clinoforms of the Torsk Fm and accumulate under the URU horizon (fig. 8c). The presence of pockmarks at the seabed could indicate further leakage between the URU and the seabed via vertical fluid flow structures underlying the pockmarks (fig. 8c). From the possible leakage pathways mentioned above, a single pathway or a combination of multiple pathways can represent a potential leakage scenario.

Models that include faults needed fault interpretations as initial input. The faults were able to be modeled in a stair-stepped form and include just one fault or several. The geomodels were then used for running CO2 flow simulations using a parameter set as detailed in fig. 9. Here, we refer further to part 3 of this report, where initial simulation results of this scenario are presented.

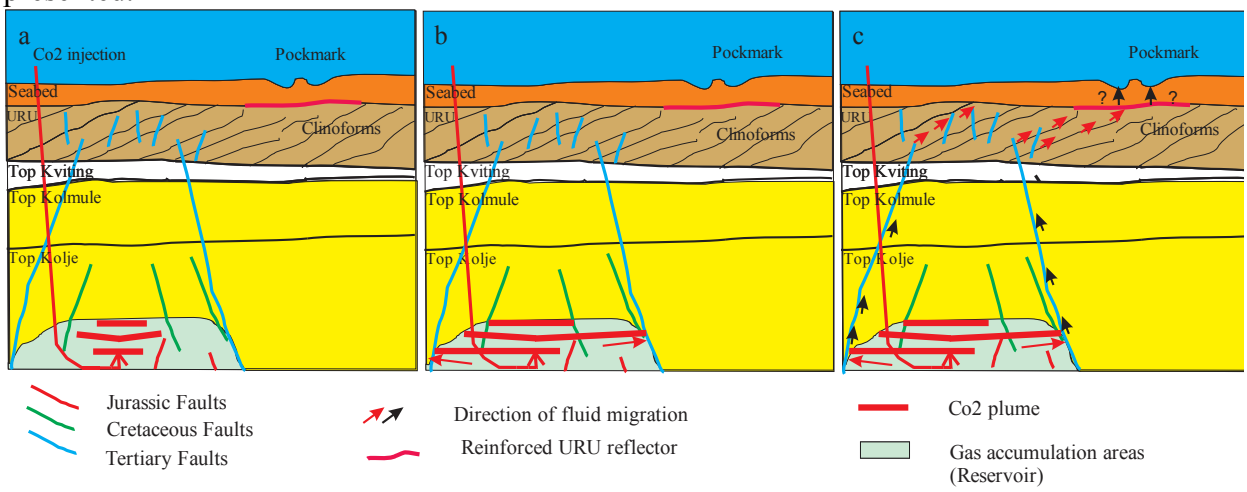

Figure 8: a) CO2 is injected in the Tubaen and Stø formations, b) CO2 plume grows and reaches fault affected areas, c) CO2 travels up the faults through the overburden to the reach near seafloor locations.

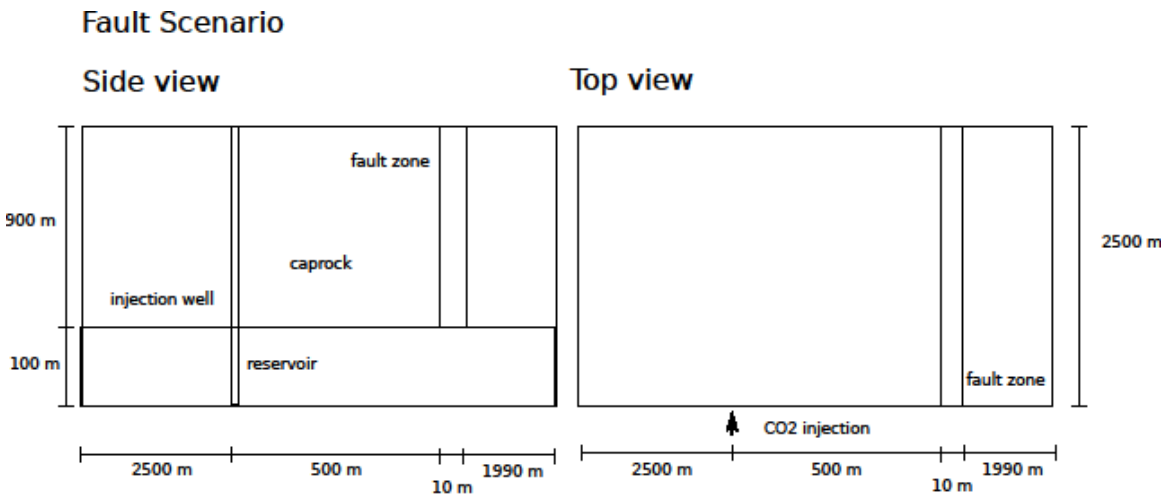

The CO2 is injected over the whole reservoir height of 100 m through
a Neumann boundary condition.
Injection well at y = 0 boundary for fault scenario: 2499 m < x < 2508 m, z < 100 m
IInjection rate: 1Mt/y
Injection period: 40 years
Simulation end: 200 years
The grid is refined around the injection region and around the fault zone.
The fault zone has a width of 10 m.

Figure 9: Fault scenario description

6.2 Chimneys

In this gas chimney potential leakage scenario, CO2 is injected in the Tubåen/Stø formations initially (fig 10a). Tubåen/Stø formations are leaking and CO2 reaches areas affected by the gas chimneys (fig 10b). CO2 leaks into the chimneys and continues by vertical migration upwards via the gas chimneys (mainly vertical fluid conduits) (fig. 10c). CO2 can in this way also reach the Torsk Fm clinoforms above the top Kviting and accumulate beneath the URU (fig. 10c), from where it might leak through e.g. pockmarks similarly to the fault leakage scenario.

To build gas chimney models we needed input such as top and bottom surfaces characterizing the chimney and a 2D boundary polygon of its areal extent was also necessary. It was possible to attribute varying values for horizontal and vertical permeability within the chimney and the rest of the model outside remaining unchanged. The geomodels containing gas chimneys were then used for CO2 simulations using a parameter set as detailed in fig. 11. Here, we refer further to part 3 of this report, where initial simulation results of this scenario are presented.

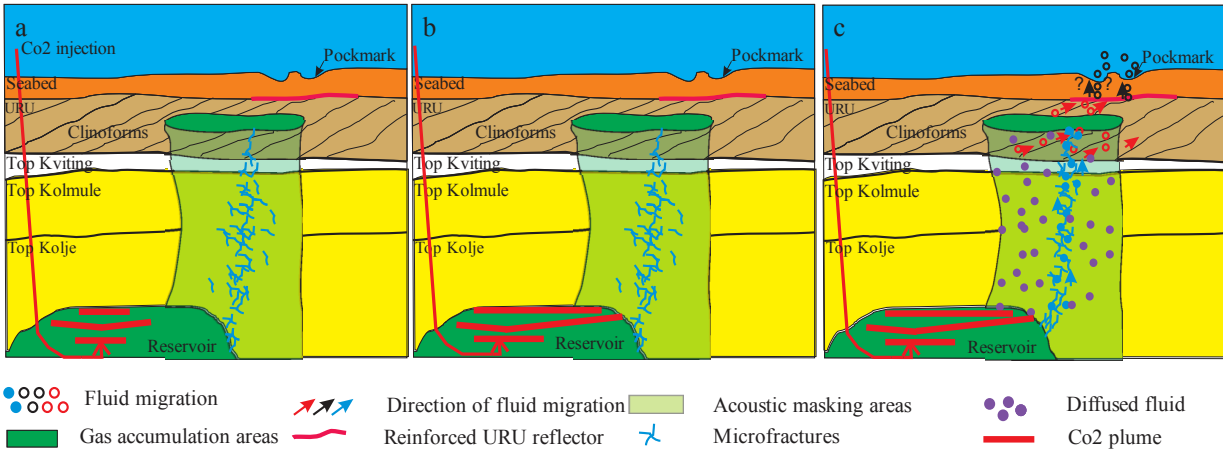

Figure 10: a) CO2 is injected in the Tubaen and Stø formations, b) CO2 plume grows and reaches areas affected by gas chimneys, c) CO2 travels up the gas chimney via the microfractures and as diffused fluid through the overburden to the seafloor.

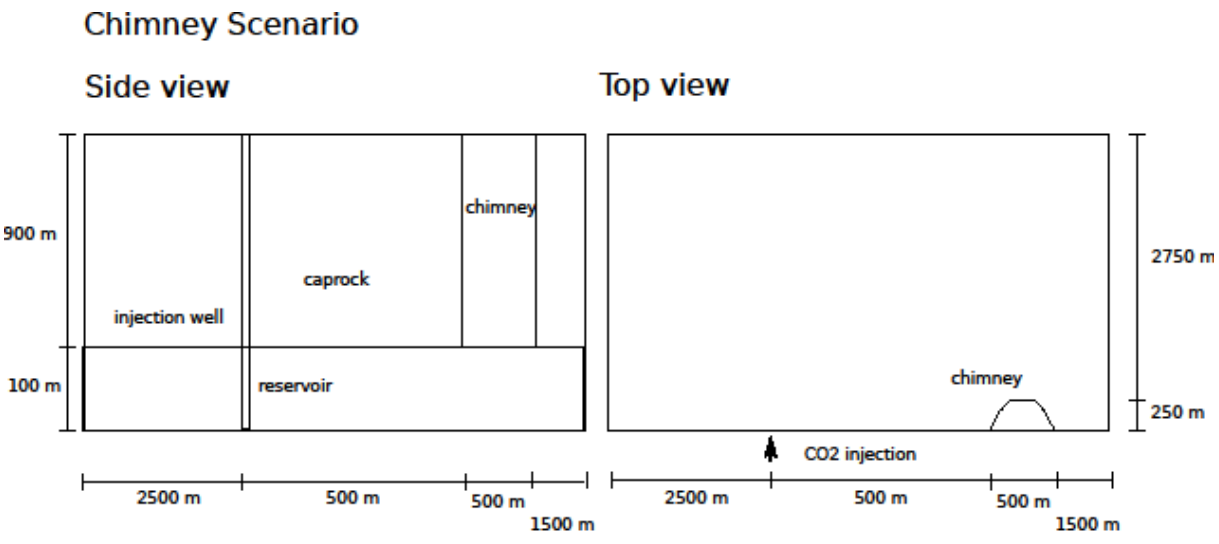

The CO2 is injected over the whole reservoir height of 100 m through
a Neumann boundary condition.
Injection well at y = 0 boundary for chimney scenario Nr. 1: 2499 m < x < 2501 m, z < 100 m
Injection well at y = 0 boundary for chimney scenario Nr. 2: 2485 m < x < 2501 m, z < 100 m
Injection rate: 1Mt/y
Injection period: 40 years
Simulation end: 200 years
The grid is refined around the injection region and around the chimney zone.

Figure 11: Gas chimney scenario description

7 Summary

Fluid leakage in the area can have its roots in major faults cutting through Paleozoic formations with fluid reaching the URU and potentially the seafloor. However, from the seismic data there are few indications that fluid flow reaches the URU and presumably the seafloor.

The most likely sites for leakage, when the crust is subject to erosion-related compressive stresses, would be the faults. Also the fact that we don't expect any major stress changes in the next few million years in the study area signifies that faults should remain sealing and altogether prevent any fluid or CO2 stored in the reservoir at Snøhvit from leaking.

Gas accumulations above gas chimneys may also be trapped by gas hydrates which could provide an additional sealing effect. This might reduce the risk of any plume reaching the seabed. Finally the presence of dense and less permeable glacigenic sediments above the URU can also act as an efficient trap preventing any fluid loss.

There is ample seismic evidence of a pre-existing fluid flow system related to glaciations and deglaciations. The model for both leakage along chimneys and leakage along faults in the area in the past is the same, and it is linked to an underlying mechanism of erosion and uplift. We can conclude that it would probably need another glaciation, and consequent erosion and uplift and other ensuing effects, to stimulate another period of fluid leakage.

8 References

Arntsen, B., Wensaas, L., Lseth, H., and Hermanrud, C. Seismic modeling of gas chimneys. Geophysics, 2007.

Estublier, A., Lackner, A.S. Long-term simulation of the Snøhvit CO2 storage. Energy Procedia 1, 3221-3228., 2009.

Fjaer, E., Holt, R., Horsrud, P., Raaen, A., and Risnes, R. Petroleum Related Rock Mechanics. Developments in Petroleum Science. Elsevier, second edition, 2008.

Gabrielsen, R.H., Færseth, R.B., Jensen, L.N., Kalheim, J.E., Riis, F. Structural elements of the Norwegian Continental Shelf. Part 1: The Barents Sea region. Norwegian Petroleum Directorate, Bulletin 6, 33p, 1990.

Kjemperud, A., Fjeldskaar, W., 1992. Pleistocene glacial isostasy; implications for petroleum geology. In: Norwegian Petroleum Society (NPF) Special Publication. Larsen, E., Brekke, H., Larsen, B.T. and Talleraas, E. 1, 187-195.

Kopp M. Numerical simuklations of CO2 leakage scenarios on a large scale under realistic geologic conditions, 2012.

Landvik, J.Y., Bondevik, S., Elverhøi, A., Fjeldskaar, W., Mangerud, J., Salvigsen, O., Siegert, M.J., Svendsen, J.I., Vorren, T.O. The last glacial maximum of Svalbard and the Barents sea area: Ice sheet extent and configuration. Quaternary Sci Rev 17, 43-75, 1998.

Ligtenberg, J. H. Detection of fluid migration pathways in seismic data implications for fault seal analysis. Basin Research, 2005.

Linjordet, A. og R. G. Olsen. The Jurassic Snøhvit gas field, Hammerfest Basin, offshore northern Norway. Tulsa, Oklahoma, The American Association of Petroleum Geologists, 1992.

Løtveit, F.I., Gudmundsson, A., Sydnes, M. How the stress changes due to glacial erosion may have caused leakage of hydrocarbons in the SW Barents Sea. Arctic Frontiers Conference Presentation, 2012.

Maldal, T. and Tappel, I.M.. CO2 underground storage for Snøhvit gas field development. Energy, 29 (2004), pp 1403-1411, 2004.

Meldahl, P. e. Identifying faults and gas chimneys using multiattributes and neural networks. The Leading Edge, 2001.

Nyland, B., Jensen, L.N., Skagen, J., O., S., O., V.T., 1992. Tertiary uplift and erosion in the Barents Sea; magnitude, timing and consequences. Norwegian Petroleum Society (NPF) 1, 153-162.

Nøttvedt, A., Berglund, T., Rasmussen, E., Steel, R., 1988. Some aspects of Tertiary tectonics and sediments along the western Barents shelf. In: A.C. Morton, L.M. Parson (Eds.), Early Tertiary volcanism and the opening of the NE Atlantic, Geological Society of London, Special publication, 39 (1988), 421–425.

Riis, F., Fjeldskaar, W. On the magnitude of the late Tertiary and Quaternary erosion and its significance for the uplift of Scandinavia and the Barents Sea. Structural and tectonic modelling and its application to petroleum geology, 163-185, 1992.

Sibson, R.H., 2000. Fluid involvement in normal faulting. J Geodyn 29, 469-499.

Vadakkepuliyambatta, S., Bünz, S., Mienert, J., Chand, S., Distribution of subsurface fluid-flow systems in the SW Barents Sea, Marine and Petroleum Geology, Volume 43, 208-221, ISSN 0264-8172, 10.1016/j.marpetgeo.2013.02.007, 2013

Worsley, R.J., Edrich, S.P., Hutchison, I. The Mesozoic and Cenozoic succession of Tromsøflaket In: A Lithostratigraphic Scheme for the Mesozoic and Cenozoic Succession Offshore Mid- and Northern Norway. Norwegian Petroleum Directorate 97 Bulletin No. 4, 42-65, 1988.

PART III

Implementation of leakage scenarios into the geological models (USTUTT)

Implementation of leakage scenarios into the geological models (USTUTT)

Content

1 Introduction

The aim of this subproject is to develop models to simulate the migration of CO_2 throughout the subsurface from the storage formation to the seabed and to describe the effects of injection and accumulation of CO_2 on the integrity of caprock and overburden structures. Multiphase-multicomponent flow and transport processes are modeled using the numerical simulator DuMuX. In this brief report, we aim to show that the proposed leakage scenarios (see Part I and II of this report) can be successfully implemented into the fluid flow simulations. For a better understanding of the more complex scenarios at the storage sites, generic leakage scenarios have been developed that include a simple background model with one leaking structure. Subsequent to that, the generic structures have been adapted into the geological models for both Sleipner and Snøhvit.

2 Generic Leakage Scenarios

Apart from the work with realistic field data of the Snøhvit and the Sleipner study areas, several generic leakage scenarios have been developed. The development of generic leakage scenarios was decided during a WP12 breakout session at the May 2012 Annual Meeting. Since in the ECO2 project a large suite of different models is involved, each looking at a different part of the system, the identification of a small number of generic leakage scenarios allows a coherent model development.

As outlined in the deliverable of the ECO2 Work Package 12 the generic leakage scenarios comprise a wellbore leakage, a fracture/fault leakage, and a chimney or catastrophic blowout scenario. The model domain, the reservoir and caprock layers, and the different leakage features are shown in Figure 1. It is assumed that the vertical plane which connects the injection well and the leakage features is a plane of symmetry. Thus only half of the model domain needs to be simulated (Fig. 1, right). Except for the 550 m high caprock fracture (grey area in Fig. 1) all leakage features penetrate the whole caprock layer up to the seafloor.

The leaky well in the wellbore leakage scenario is approximated as a porous medium with a large permeability value. The fracture/fault leakage scenario includes a 10 m wide fault which spans across the whole model domain in y-direction. The chimney scenario comprises a high permeable chimney, which has a diameter of 500 m. All three leakage features are located in 500 m distance from the injection well. The caprock-fracture scenario is a combination of the chimney scenario and a high permeable caprock fracture (grey area in Fig. 1) which extends 550 m upwards and connects the CO_2 injection well and the chimney.

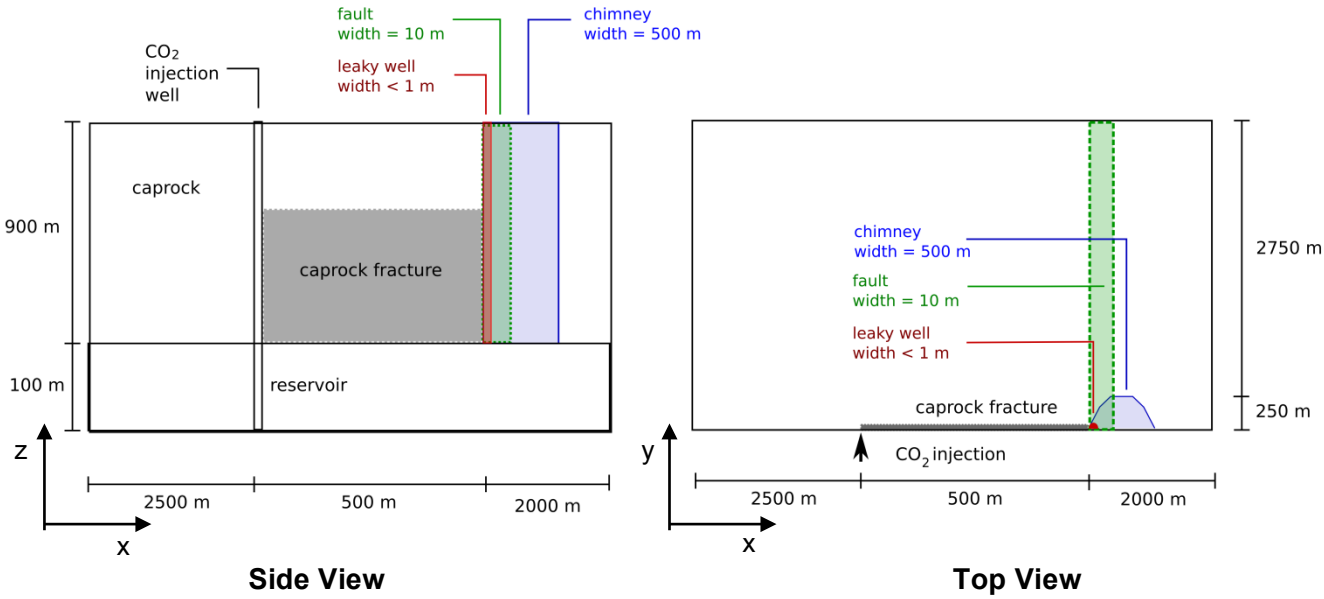

Figure 1: Side view (left) and top view (right) of the model domain and the leakage features applied for the generic leakage scenarios.

In a first step, grids for these generic scenarios have been generated. Figure 2 shows the grids applied for the chimney, the fracture/fault and the leaky well scenarios (from top to bottom).

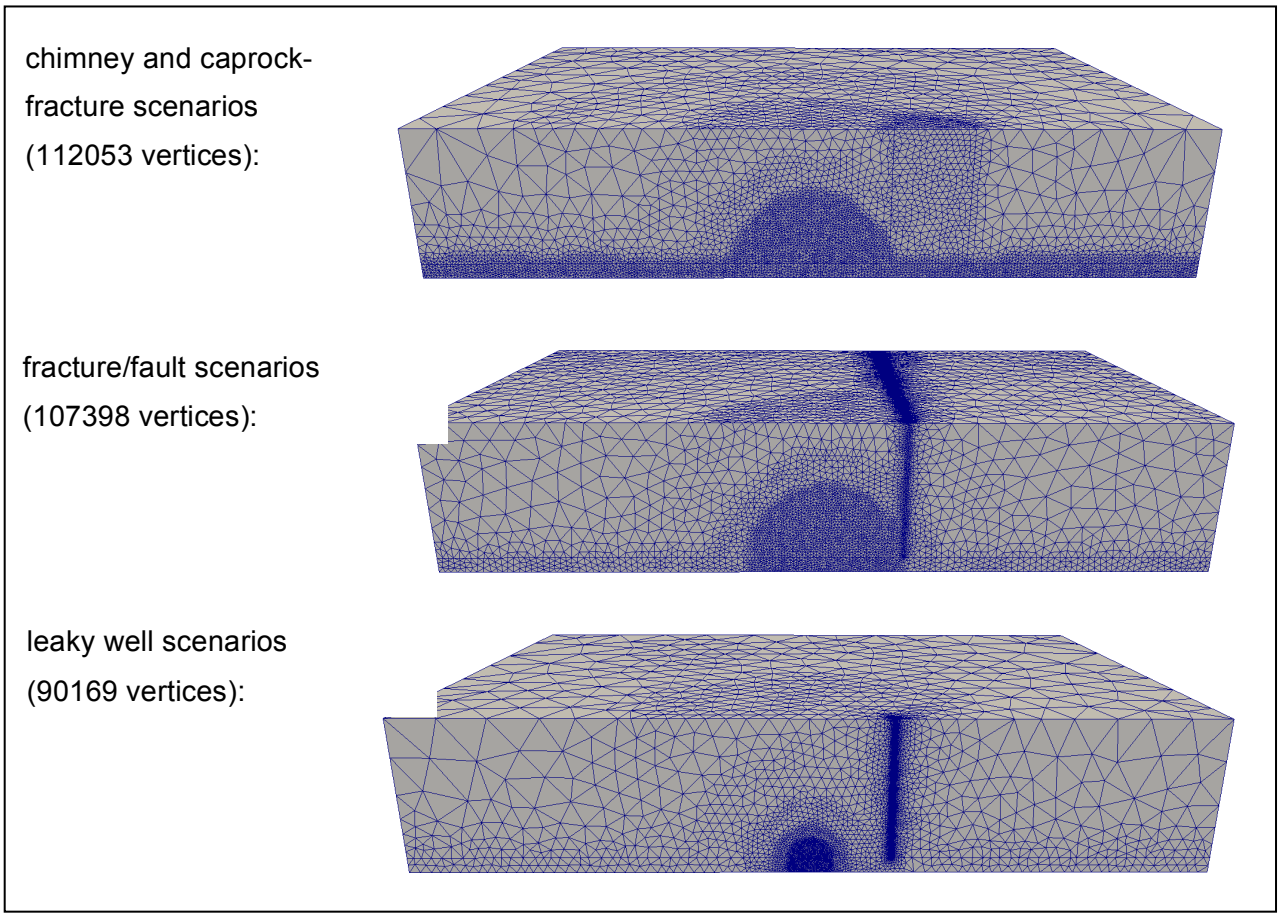

Figure 2: Grids applied for the generic leakage scenarios.

2.1 Boundary Conditions and Parameters for the Generic Leakage Scenarios

In Table 1, the hydraulic parameters which have been applied for the first tests with the generic leakage scenario models are given. For the fluid density and viscosity calculations, a constant temperature profile is assigned with a seafloor temperature of 277.15 K and a geothermal gradient of 0.03 K/m. The capillary pressure and the relative permeabilities are calculated with the Brooks & Corey relations. The fluid properties of the brine phase and of the CO_2-rich phase as well as the mutual solubility relations are determined through the relations given in Darcis (2012). For the brine phase a salinity of 0.1 kg/kg is assumed.

On the left, right, back and top boundaries a hydrostatic pressure and a CO_2 mass fraction of 0.0 are assigned. CO_2 is injected over the bottom 100 m of the injection well at the front boundary. The injection rate is 1 Mt/y and the injection period is set to 40 years. Except for the injection well, the boundary conditions at the front boundary (plane of symmetry) are set to Neumann no flow for both fluid phases. The same holds for the bottom boundary.

Table 1: Hydraulic parameters applied for the first simulations with the generic leakage scenarios. K is the permeability and Φ is the porosity. P_e, λ, S_{wr}, and S_{nr} are the entry pressure, the Brooks & Corey parameter and the residual saturations of the brine and the CO_2-rich phases, respectively.

scenario	domain	K [m^2]	Φ [-]	P_e [Pa]	λ [-]	S_{wr} [-]	S_{nr} [-]
chimney 1	reservoir	10^{-13}	0.3	10^4	2	0.2	0.0
	caprock	10^{-19}	0.1	10^5	2	0.2	0.0
	chimney	10^{-13}	0.3	10^4	2	0.2	0.0
chimney 2	reservoir	10^{-14}	0.2	10^4	2	0.2	0.0
	caprock	10^{-19}	0.1	10^5	2	0.2	0.0
	chimney	10^{-14}	0.2	10^4	2	0.2	0.0
chimney 3	reservoir	10^{-14}	0.2	10^4	2	0.2	0.02
	caprock	10^{-19}	0.1	10^5	2	0.2	0.02
	chimney	10^{-14}	0.2	10^4	2	0.2	0.02
chimney 4	reservoir	10^{-14}	0.2	10^4	2	0.2	0.02
	caprock	10^{-19}	0.1	10^5	2	0.2	0.02
	chimney	10^{-14}	0.3	10^4	2	0.2	0.02
fault 1	reservoir	10^{-14}	0.2	10^4	2	0.2	0.0
	caprock	10^{-19}	0.1	10^5	2	0.2	0.0
	fault	10^{-14}	0.2	10^4	2	0.2	0.0
fault 2	reservoir	10^{-14}	0.2	10^4	2	0.2	0.0
	caprock	10^{-19}	0.1	10^5	2	0.2	0.0
	fault	10^{-14}	0.3	10^4	2	0.2	0.0
fault 3	reservoir	10^{-14}	0.2	10^4	2	0.2	0.02
	caprock	10^{-19}	0.1	10^5	2	0.2	0.02
	fault	10^{-14}	0.3	10^4	2	0.2	0.02
caprock-	reservoir	10^{-14}	0.2	10^4	2	0.2	0.0
fracture 1	caprock	10^{-19}	0.1	10^5	2	0.2	0.0
	fracture	10^{-13}	0.4	10^4	2	0.2	0.0
	chimney	10^{-14}	0.2	10^4	2	0.2	0.0
leaky well 1	reservoir	10^{-14}	0.2	10^4	2	0.2	0.0
	caprock	10^{-19}	0.1	10^5	2	0.2	0.0
	leaky well	10^{-14}	0.2	10^4	2	0.2	0.0

2.2 Models

The models for the generic leakage scenarios have been set up in DuMu^x in a generic way. It is possible to choose between a two-phase (2p) and a more complex two-phase two-component (2p2c) formulation which accounts for the mutual dissolution of CO_2 and H_2O and for the transport of the dissolved components. Whereas the 2p2c model allows a more detailed investigation of the long-term trapping behaviour and also provides information about the migration of dissolved CO_2, the 2p model leads to a more conservative leakage evaluation since the total injected CO_2 mass remains in the buoyant CO_2 phase which tends to migrate upwards (no solubility trapping). For both model formulations, the scenario type and the parameters listed in Table 1 can be changed easily via an input file. Further, all models export time series of the pressure and saturation distributions which are used for geomechanical analyses by the TNO group. For the first test cases with the generic leakage scenarios the 2p2c formulation has been applied. Only the leaky well scenario simulation which exhibits the largest computational cost due to the strong contrast in grid resolution is performed with the less complex 2p model.

2.3 Resulting CO_2 Saturation Distribution at Different Times

The screenshots shown below give an impression of the CO_2 saturation distributions obtained for the first test cases with the generic leakage scenarios. In Figure 3 the CO_2 saturation distributions obtained after 10 years of injection are plotted in a vertical cross-section at y=0 m. At this time, the upward migration of the injected CO_2 is driven both by buoyant forces and by the injection-induced overpressure in the reservoir.

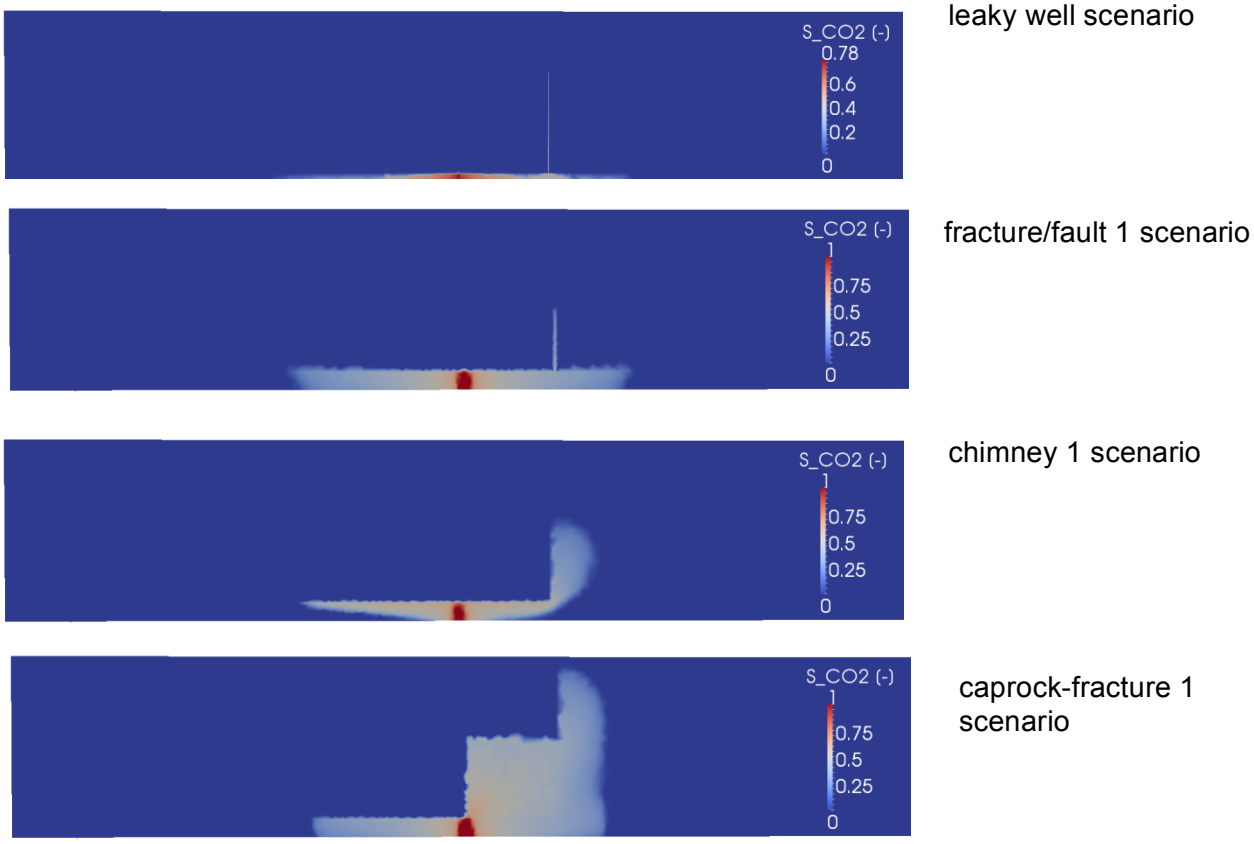

Figure 3: CO_2 saturation distribution after 10 years of injection (vertical cross-section at y=0 m)

In Figure 4, the CO_2 saturation distributions obtained for the fault, the chimney and the caprock-fracture scenarios after 200 years are plotted in a vertical cross-section at y=0 m. The chimney 1 scenario exhibits the largest leakage-feature permeability and thus all CO_2 reaching the chimney migrates upwards. In the caprock-fracture and in the fault scenarios the permeability of the reservoir and the chimney and fault are one order of magnitude smaller than in the chimney 1 scenario. Thus, horizontal CO_2 migration past the leakage feature can be observed and a larger amount of CO_2 can be trapped in the reservoir. The leaky well scenario is currently still running and therefore not shown here.

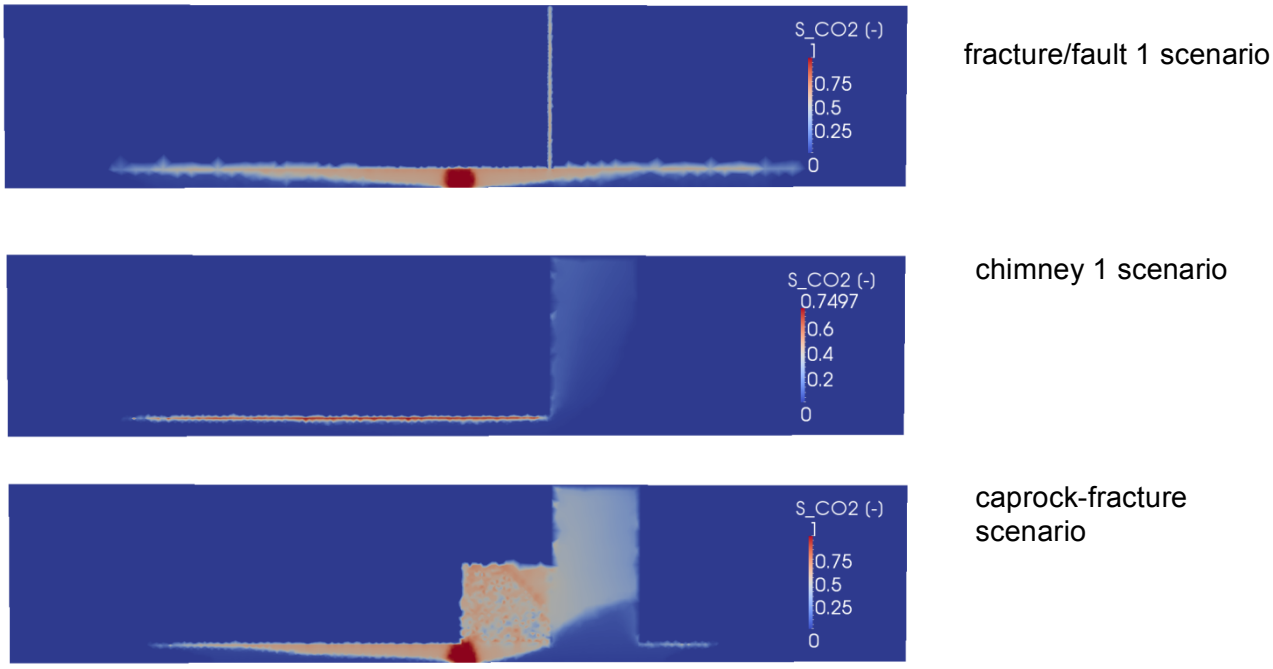

Figure 4: CO_2 saturation distribution after 200 years (vertical cross-section at y=0)

2.4 CO_2 Leakage over Time for Different Generic Scenarios

The CO_2 leakage flux is measured across a horizontal plane, which is located 1 m below the seafloor in all leakage scenarios. The plots shown in Figure 5 and 6 represent the CO_2 leakage flux in t/d (left) and the total CO_2 mass in t (right) stored in the model domain over time.

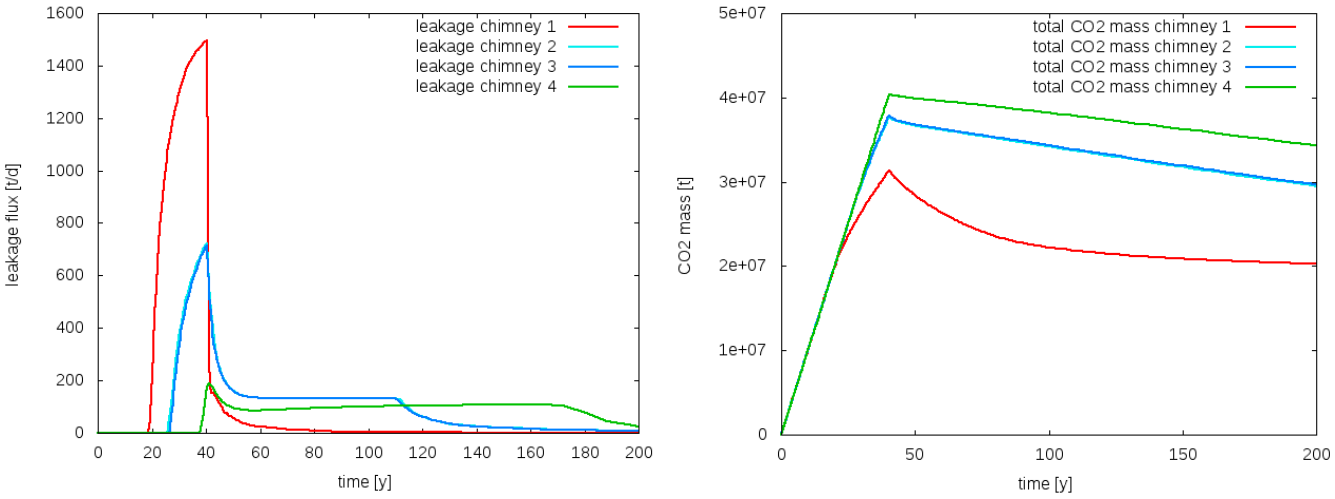

Figure 5: CO_2 leakage over time (left) and total CO_2 mass over time (right) for the chimney scenarios.

Figure 5 shows the leakage rates, which result for the different chimney scenarios. In all chimney scenarios leaking CO_2 reaches the seafloor before CO_2 injection stops (i.e. within 40 years). With a leakage rate of more than 1000 t/d the chimney 1 scenario represents a "catastrophic blowout scenario" (flux range 1000 - 10000 t/d) as it is defined in the WP12 report. As expected, both the chimney permeability and porosity have a large influence on the resulting CO_2 leakage whereas an increase in the residual saturation of the CO_2 phase shows almost no effect.

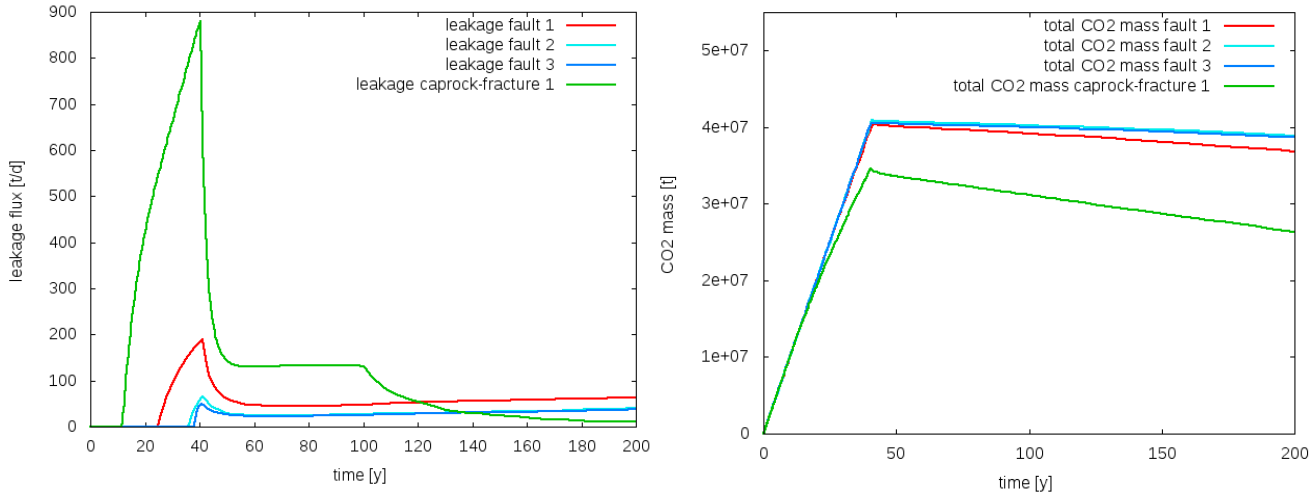

Figure 6: CO_2 leakage over time (left) and amount of stored CO_2 over time (right) for the fault and the caprock-fracture scenarios.

In Figure 6 (left) the leakage rates of the fault and the caprock-fracture scenarios are shown. The high fault and reservoir permeabilities in the fault 1 scenario lead to leakage rates of approximately 200 t/d whereas the leakage rates of the fault 2 and fault 3 scenarios are approximately 60 t/d thus representing a "geological fracture scenario" (flux range 10 - 100 t/d) as it is defined in the WP12 report. The caprock-fracture scenario leads to similar leakage rates as the chimney scenarios. However, through the caprock fracture, the CO_2 migrates much faster to the chimney and leads to CO_2 leakage at the seafloor already after 10 years of injection.

As shown in Figure 5 and 6 on the right, the CO_2 mass in the system shows the strongest decrease for the chimney 1 scenario. After 200 years only 50% of the injected CO_2 mass remains in the system (reservoir and overburden) for this scenario. The smallest loss in CO_2 mass is observed for the fault scenarios 2 and 3 where less than 3% of the injected CO_2 has leaked after 200 years.

In summary, the first test case simulations with the generic leakage models have shown that the developed leakage scenarios are able to reproduce the leakage behaviour upon which the modeling groups in WP12 have agreed. They can now be used to provide input data for geomechanical analyses (TNO) and for the simulation of the processes in shallower sediment layers (HWU).

3 Snøhvit and Sleipner Leakage Scenarios

With respect to the leakage scenario simulations for the Snøhvit site, updated geological models with more realistic values for the reservoir caprock layers have been applied to continue the work described in Kopp (2012).

In order to take into account the uncertainty in the permeability and porosity values assigned to the different geological layers, the new geological models provided by UiT comprise three different realizations i.e. a *HIGH*, a *MEDIUM* and a *LOW* case which are characterized by permeability and porosity values in the high, the medium and the low range of available data. Apart from the variation in hydraulic parameters leakage scenarios with different degrees of model complexity have been simulated. The first test cases have all been modeled with a two-phase (2p) model which neglects the mutual solubility of CO_2 and H_2O and the transport of the dissolved components in the fluid phases. In order to take these effects into account two-phase two-component (2p2c) models have been set up.

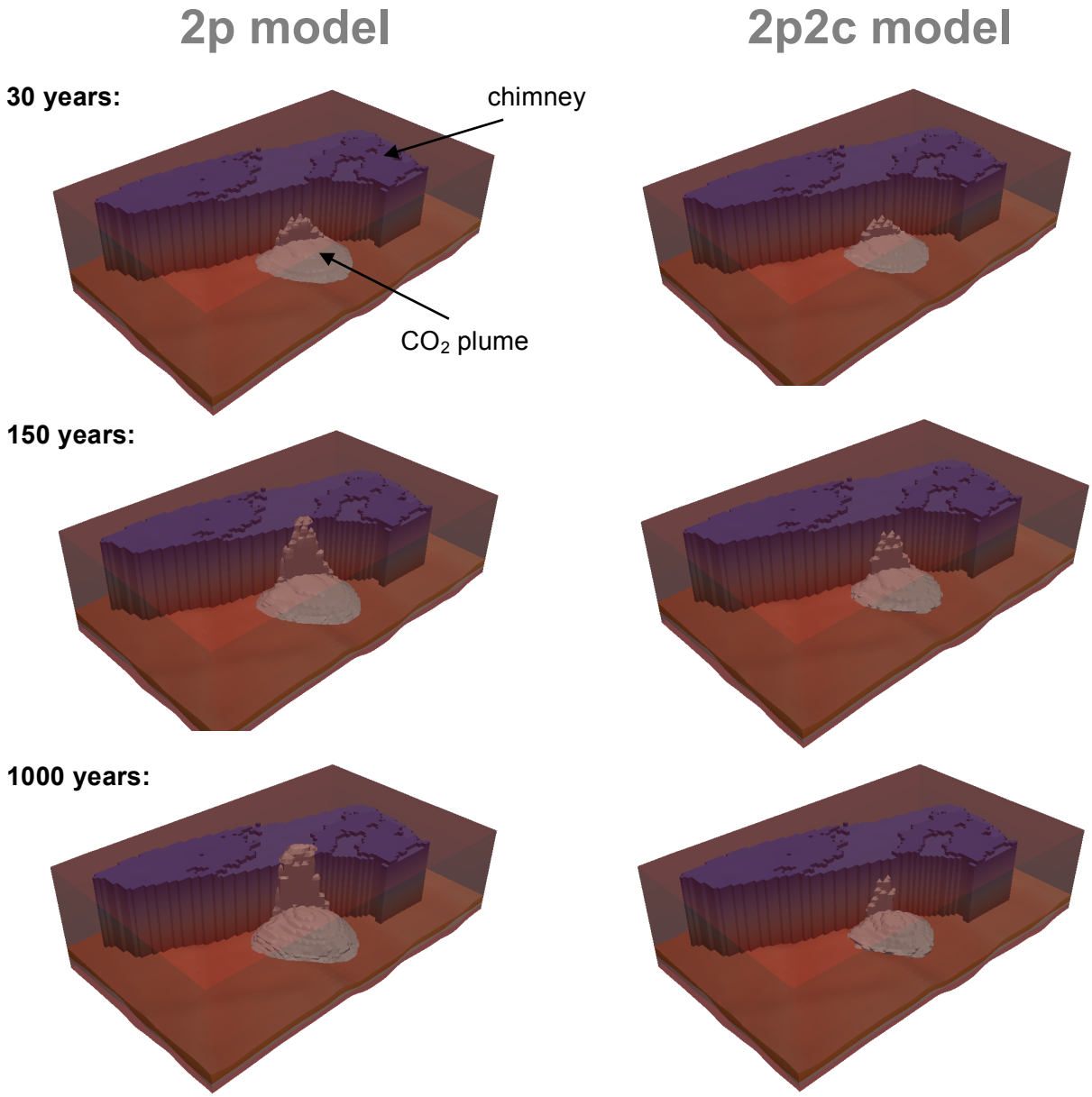

Figure 7: Model domain of the chimney model (HIGH case) with a chimney permeability of 765 mD and CO_2 plumes simulated with the 2p model (left) and with the 2p2c model (right) after 30, 150 and 1000 years.

Figure 7 shows the CO_2 plume extent in the chimney scenario (*HIGH*) with a chimney permeability of 765 mD after 30 and after 1000 years for the 2p and the 2p2c models. The model domain extent is 5.9 km x 9.4 km x 3 km with a horizontal grid resolution of 90 m and a varying grid resolution in vertical direction. CO_2 is injected with a rate of 0.7 Mt/y for 30 years at a virtual location nearby the chimney structure. In the 2p2c model the injected CO_2 can dissolve in the brine phase. Since CO_2-rich brine is heavier than pure brine the dissolved CO_2 sinks down and spreads across the reservoir bottom. Through this dissolution process, the CO_2 mass in the CO_2-rich phase is continuously reduced after injection stop. This results in a reduction of CO_2 leakage in the 2p2c model. However, the coarse grid resolution of the given test case leads to a strong overestimation of the CO_2 dissolution (see also Bergmo et al. 2009, Darcis 2012). Thus,

for a conservative assessment of CO_2 leakage in combination with coarse grid resolution the chosen 2p approach is better suited. For a detailed evaluation of the effects of CO_2 dissolution, e.g. long-term solubility trapping, higher grid resolutions should be applied in future studies.

Apart from the geological model with the high permeable chimney which was investigated in Kopp (2012) a large geological model (15 km x 30 km x 3 km) with 39 impermeable and 15 permeable faults was modelled. The faults which are close to the injection well and which are reached by the CO_2 plume are sealing impermeable faults. Thus, a leakage through permeable faults could not be observed.

Since faults represent areas of weakness with respect to geomechanical processes the simulations for the faulted model domain concentrated on a description of the injection pressure. The horizontal model domain extension was reduced for these short-term simulations to 7 km x 4 km and the grid resolution was refined from 300 m to 50 m in horizontal direction. As for the chimney models, scenarios with different permeability and porosity ranges (HIGH, MEDIUM and LOW) and with varying caprock permeabilities have been modelled. The pressure and saturation data was exported and is currently evaluated within the geomechanical simulator of the TNO group.

For the Sleipner site various realizations of the small-scale features in the overburden which have been observed in the seismic data have been simulated. The permeability of the small-scale features was varied by three orders of magnitude in order to get an impression of their effect on CO_2 leakage. The model domain shown in Figure 8 is 3.9 km x 6.4 km x 1 km large with a horizontal grid resolution of 50 m and a vertical resolution varying from 10 m to 100 m for the different geological layers. CO_2 is injected with a rate of 1 Mt/y for 30 years at a virtual location into the Utsira formation. In Figure 8 the permeability field of the HIGH case with leakage feature permeabilities in the range of 10^{-12} m^2 is shown. For the MEDIUM and the LOW cases the leakage feature permeabilities are reduced by a factor of 10 and 100, respectively.

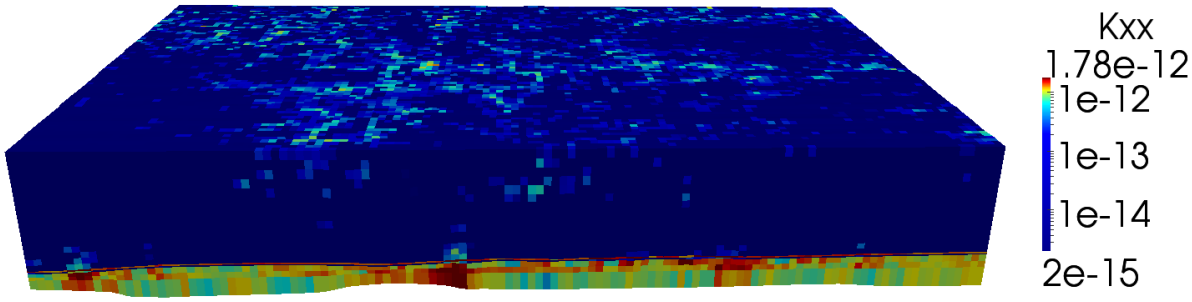

Figure 8: Permeability field of the Utsira formation and the overburden in a 3.9km x 6.4 km subdomain at the Sleipner site with high permeability values assigned to the small-scale features in the overburden.

In Figure 9, the CO_2 plumes after 30 years and after 100 years simulated with the 2p model are shown for the scenario and the three different leakage feature permeabilities. Further investigations aim on determining the most realistic parameters for the leakage features and the overburden.

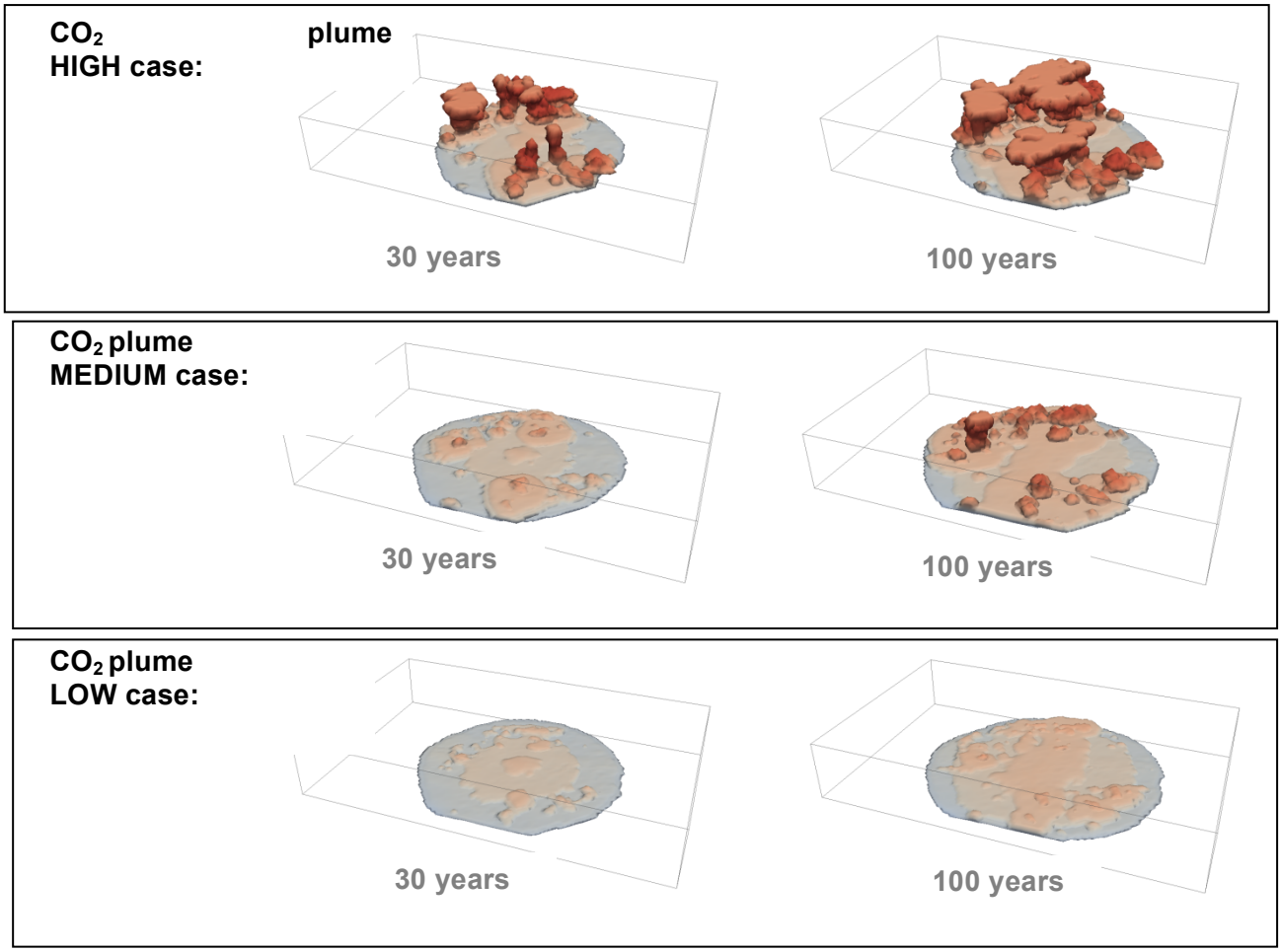

Figure 9: CO_2 plumes after 30 years (left) and after 100 years (right) for a virtual injection scenario into a subdomain of the Sleipner site with small-scale leakage features. For the HIGH and the MEDIUM cases the leakage feature permeabilities are is increased by a factor of 100 and 10 compared to the LOW case, respectively.

Both the Snøhvit and the Sleipner models have been set up in DuMu^x in a generic way. Either 2p or 2p2c formulations can be applied. Pressure and saturation data is exported for geomechanical analyses and leakage flux rates are exported for predefined horizontal planes in the model domain.

4 References

Kopp, M., Numerical simulation of CO_2-leakage scenarios on a large scale under realistic geologic conditions (Diplomarbeit). Institut für Wasser- und Umweltsystemmodellierung, Universität Stuttgart. 2012.

Darcis, M., Coupling models of different complexity for the simulation of CO_2 storage in deep saline aquifers, Mitteilungsheft Nr. 218 (Promotionsschrift), Institut für Wasser- und Umweltsystemmodellierung, Universität Stuttgart. 2012.

Bergmo, P., Grimstad, A., Lindeberg, E., Riis, F., and Johansen, W. Exploring geological storage sites for CO2 from Norwegian gas power plants: Utsira south. Energy Procedia, 1: 2953–2959, 2009.

PART IV

Repeatability of the time lapse seismic data and the detection thresholds for leaking CO_2 in the overburden at Snøhvit (BGS)

Repeatability of the time lapse seismic data and the detection thresholds for leaking CO_2 in the overburden at Snøhvit (BGS)

Content

1 Introduction

This report details a synthetic data study which attempts to answer the question how much CO_2 would need to accumulate at different depths, and at what saturation levels, in order to be identifiable in the seismic data. The primary data sources for this work are well logs from the Snøhvit region which are utilised to build a simple velocity model of the overburden at the CO_2 injection site at Snøhvit. Using typical Vp-Vs relationships an elastic model from the seabed to the base of the injection reservoir is created. 1D seismic traces are computed and realistic noise profiles are added to the data. 3D time-lapse seismic data acquired over the CO_2 injection site is used to assess the noise content and the repeatability and predictability of the synthetic surveys has been assessed against this data.

There is currently no evidence of leakage through the caprock at Snøhvit, but these studies that aim to simulate gas migration into the overburden and are useful for quantifying detection thresholds so early remediation may be applied if problems were to arise. Here we add a small leak at a range of depths and saturations and assess the amplitude effects this generates in the seismic difference data.

2 Snøhvit

The availability of CO_2 at Snøhvit relies upon its separation from hydrocarbon gas extracted from the overlying Snøhvit gas field. The hydrocarbon gas, which contains ~6 % CO_2, is piped to shore 150 km away for processing before CO_2 is returned by pipeline. Analysis of the Snøhvit CO_2 injection program relates to the period prior to the 2009 3D seismic monitoring survey following injection of 0.5 mtons of CO_2 over 16 months. During this period, the injection at Snøhvit was at the base of the Tubaen Formation, a fluvial to tidal sandstone deposit of approximately 100 m thickness, at 2565-2665 m depth below sea surface. The injection infrastructure sits at the sea-bed in ~300 m water depth.

Seismic surveys utilised in this study were collected in 2003 and 2009 and are both orientated North-South. A shared lateral extent of 8.25 km x 9.65 km is analysed in this study. Source steering ensured an excellent match of source and receiver locations between the 2003 and 2009 surveys and repeatability metrics are high.

Seismic cross-sections from the data are displayed in Figure 1 and intersect the injection point. The top Tubaen reflection is poorly imaged on the seismic with the overlying top Fugeln acting as a regional indicator. The base Tubaen is imaged across the survey area but reflection amplitudes significantly reduce to the east - possibly as a consequence of an overlying gas accumulation. Facies and porosity changes in the Tubaen are thought to account for variable amplitudes in the baseline survey at this level. In this region the overburden in predominantly composed of shales and the hypothesis for this work requires migration pathways through the shale and accumulation in sandier parts of the stratigraphy.

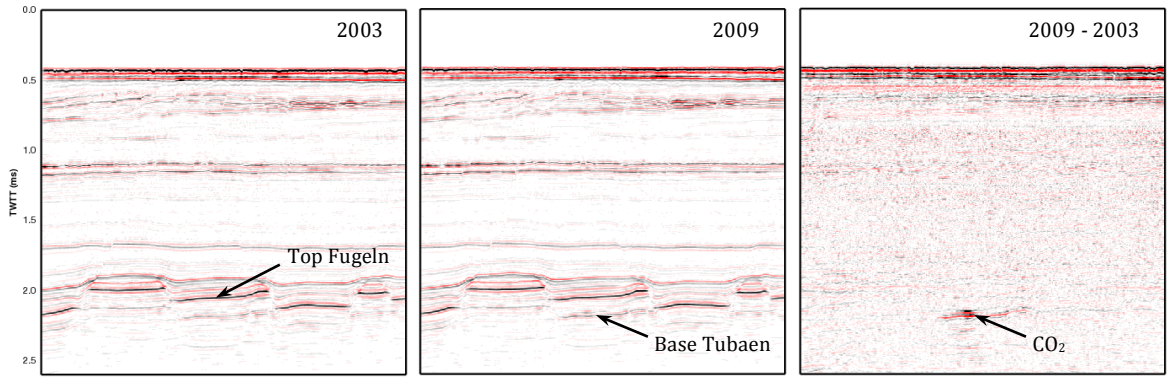

Figure 1: Seismic sections from baseline (left), repeat (middle) and difference (right) data cubes. The fault blocks that dominate the region at depth are clearly visible whilst some structure remains in the difference data.

The seismic data is sampled at 4 ms with a useable frequency content of 10-70 Hz and a peak frequency of 32 Hz for the data imaging the overburden, see Figure 2.

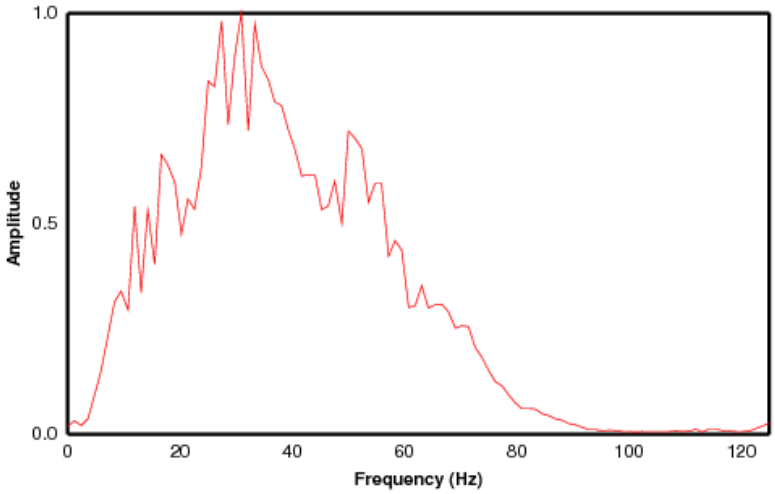

Figure 2: Frequency content of data in baseline survey. Trace data extracted between 0.6 and 1.7 seconds.

2.1 Repeatability of Snøhvit data

Due to the pre-defined acquisition and processing of the repeat survey, and the high data quality, the normalised RMS (NRMS) difference between the two surveys is small. However in order to ensure the correct level of repeatability in the synthetic data repeatability metrics are derived for the time lapse seismic.

The seismic predictability and the NRMS are common measures of repeatability utilised in repeat seismic data (Kragh & Christie, 2002). The NRMS is the difference between two traces (a_t and b_t), in a specified time window, divided by the average RMS amplitude of the two input traces:

$$NRMS = \frac{200 \times RMS(a_t - b_t)}{RMS(a_t) + RMS(b_t)}$$

where the RMS summation is over time window t. As such an NRMS value of zero means there is no difference in amplitude between the two traces.

Predictability is a better constraint for time stretches and shifts in data, and perfectly correlated events will produce a predictability of 100%. It is determined from the summed squared cross-correlation of two traces (φ_{ab}) in a time window, divided by the summed product of the trace auto-correlations (φ_{aa} & φ_{bb}).

$$PRED = \frac{100 \times \sum \emptyset_{ab}(\tau) \times \sum \emptyset_{ab}(\tau)}{\sum \emptyset_{aa}(\tau) \times \sum \emptyset_{bb}(\tau)}$$

Previous WP1 periodic reports have included studies of repeatability and predictability on synthetic data to justify the use of these metrics described here.
Figure 3 shows an analysis panel (for IL 3110) from the Snøhvit time-lapse data with a 128 ms moving window applied down the traces. The data is seen to display a high predictability (just over 90% on average) and low NRMS values suggesting amplitudes are well matched. However, in the regions between significant reflections it is apparent that the metrics show less repeatability due to the uncorrelated noise.

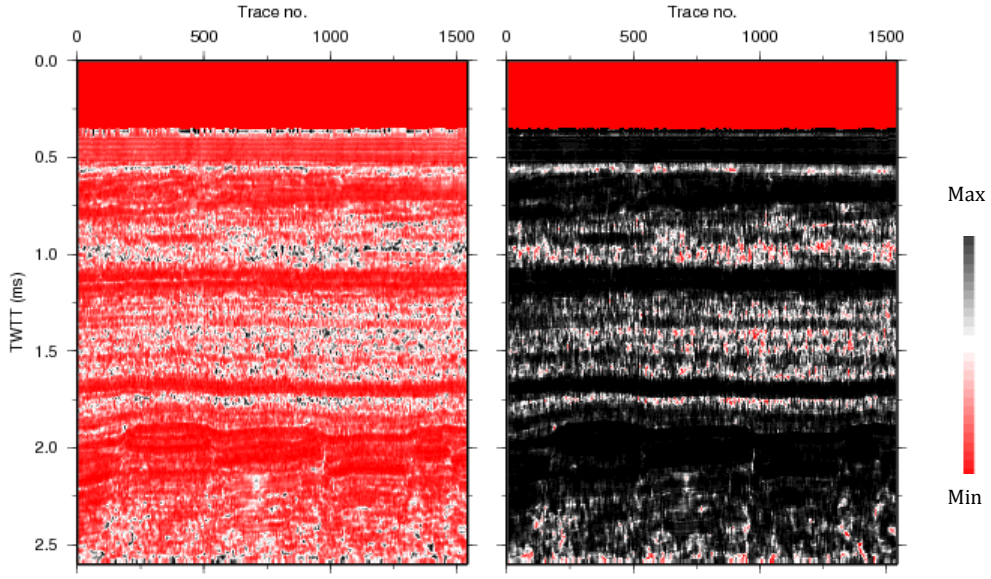

Figure 3: NRMS (left) and predictability (right) for a in line 3110 at Snøhvit. The min=0 in each case whilst NRMS max=200 and predictability max=100.

2.2 Noise extraction at Snøhvit

The difference between time lapse surveys is notoriously difficult to quantify. This is due to the combination of systematic and random noise, and the time window on which the repeatability is to be determined. Generally the repeatability is expressed with a small time window at the target reservoir but since this study aims to assess the detectability of leaking CO_2 in the overburden a more comprehensive approach is required. The random component of the noise is assessed with the following scheme, which is highlighted in:

1. The auto-correlation of each trace in the 3D cube was computed, summed and average over the entire data set.

2. The cross-correlation between adjacent traces was computed using a 1 trace step out, summed and averaged over the entire data set.
3. Power spectra of the mean correlations were obtained from a Fourier transform. The auto-correlation amplitude spectrum contains both a signal and noise component, whereas it is assumed that the power spectrum of the cross-correlation term contains signal only (the earth's reflectivity series convolved with a wavelet).
4. In this case, the noise spectrum can be derived by subtracting the cross-correlation spectrum from the auto-correlation spectrum.

Utilising this approach in 3D it is possible to add noise to synthetic data sets by assigning a random phase to each frequency component and transforming back to the time domain.

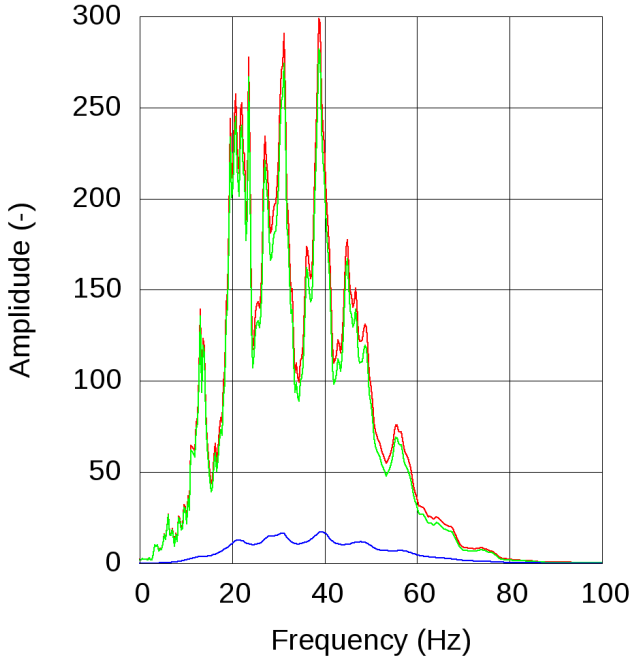

Figure 4: The mean auto-correlation (red) containing noise and signal; the mean cross-correlation (green containing just signal; and the difference (blue) containing the noise.

The systematic noise is assessed in a different way and relies upon the calculation of the total windowed RMS amplitude along each trace.

1. The absolute amplitude along each trace in baseline and repeat survey is determined
2. A smoothing filter is applied to the absolute trace data
3. The difference between spatially equivalent filtered traces in baseline and repeat surveys is calculated
4. From these, the absolute value of the difference traces is derived
5. Next, the mean absolute difference trace and the mean absolute (smoothed) baseline trace are calculated
6. The mean absolute (smoothed) difference trace is divided by the mean absolute (smoothed) baseline trace to give amplitude scaling factor as a function of time, shown in Figure 6.

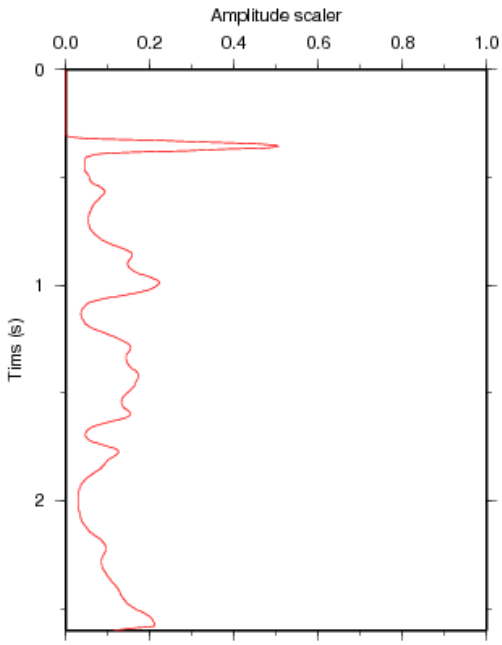

Figure 5: Amplitude scaling factor used to create a systematic noise signature in the repeat synthetic surveys.

2.3 Log data at Snøhvit

A baseline 2D synthetic seismic survey was constructed from the log data from well 71206-1. The sea-floor was aligned with the time domain 3D seismic and the sonic and bulk density curves were used to generate a vertical profile. The reservoir overburden is primarily mudstone; a typical Vp-Vs relationship was employed during this preliminary study. The Vp distribution is shown in Figure 7a.

2.4 Adding leaking CO_2

Having generated a baseline velocity structure for the overburden at Snøhvit whilst also gaining a reasonable approximation of the noise profile within the timelapse seismic data, this study aims to add small amounts of CO_2 to the overburden to investigate the detectability at different depths.

Existing rock physics models for shale-rich rocks require complete suite of V_P, V_S and Density logs + laboratory analyses of matrix mineralogy and porosity and these are only available for a limited section of caprock immediately above reservoir. It is known that the primary effect of clay minerals is to prevent fluid pressures equilibrating at seismic frequencies. This tends to impart increased stiffness to the rock, resulting in higher velocities than those predicted by Gassmann theory. This study uses traditional Gassmann fluid substitution coupled with Voigt patchy mixing model. Previous studies have tested this approach against the soft porosity model of Ruiz & Cheng (2010), which accounts for variable pore geometries and shale effects in shale-rich sandstone sequences with success.

Good mineral content control is available for the immediate overburden of the injection reservoir. CO_2 is placed in the Hekkingen, and Kolje formations at 2300 m and 1900 m depth. Porosity data for these units was also available (Tasianas, pers comm.). This allowed an accurate

fluid substitution scheme to be employed. Additionally leaks are added at 1500 m, 1100 m and 700 m using generic shale parameters from our analysis of the Sleipner overburden. Span and Wagner's equation of state for CO_2 is used to derive the correct gas properties as a function of pressure and temperature.

In these tests a small volume of CO_2 is added. A cone of height 4 m and radius 112 m gives a total rock volume ~50000 m^3 which is then filled with a partial saturation of CO_2. Saturations of 0.02, 0.06, 0.1, 0.15, 0.25, 0.4, 0.55 and 0.8 are used in all the depth scenarios.

Seismic modelling with a 1D finite difference code was undertaken and the noise profiles derived previously were added to the data. Figure 6 – Figure 13 shows the synthetic seismic response at a range of saturations at two depths alongside the difference data (between this result and the baseline response) plotted as a function of in-line number, where spacing is 12.5 m.

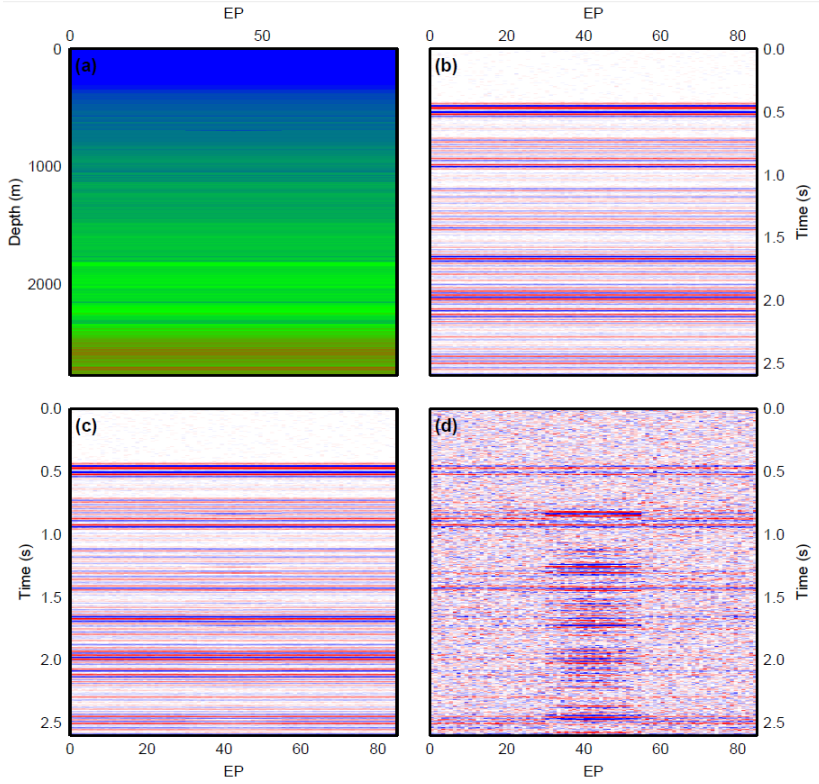

Figure 6: CO2 leak at 700 m, saturation=0.8. (a) Velocity model; (b) baseline survey; (c) repeat survey; and (d) difference section.

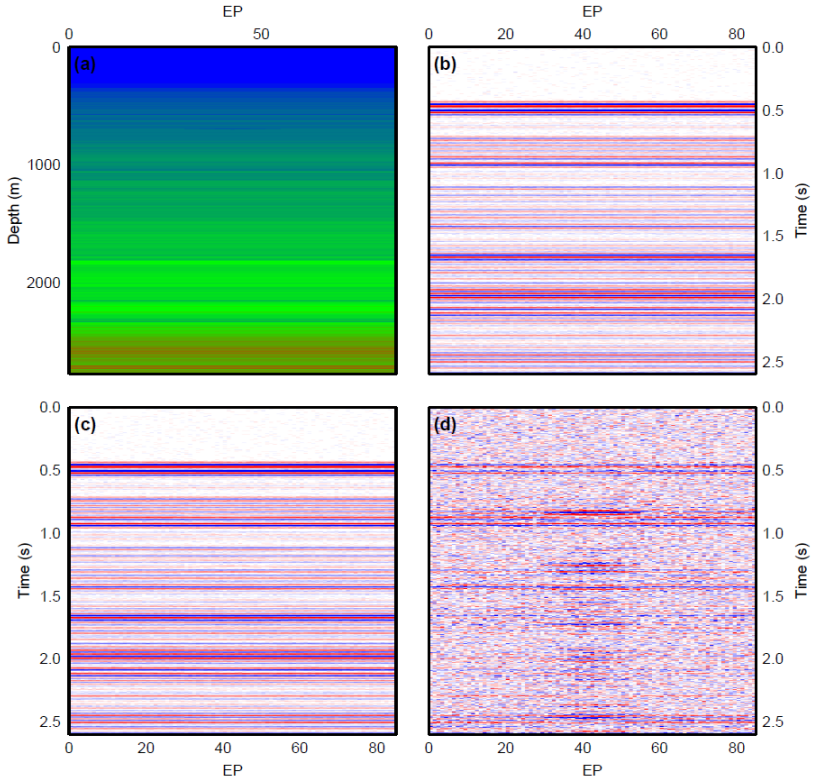

Figure7: CO2 leak at 700 m, saturation=0.55. (a) Velocity model; (b) baseline survey; (c) repeat survey; and (d) difference section.

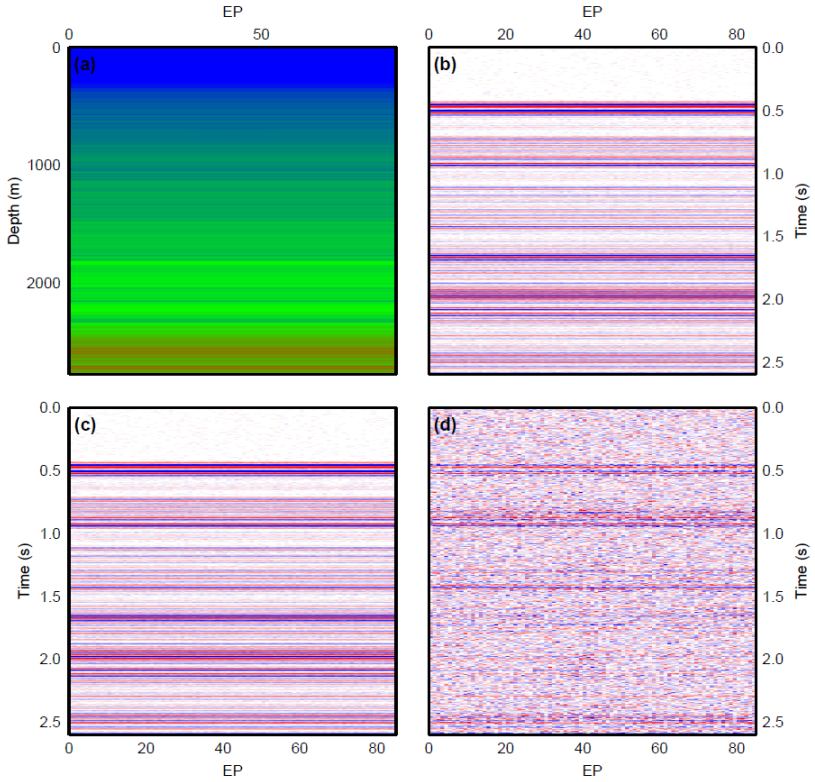

Figure 8: CO2 leak at 700 m, saturation=0.25. (a) Velocity model; (b) baseline survey; (c) repeat survey; and (d) difference section.

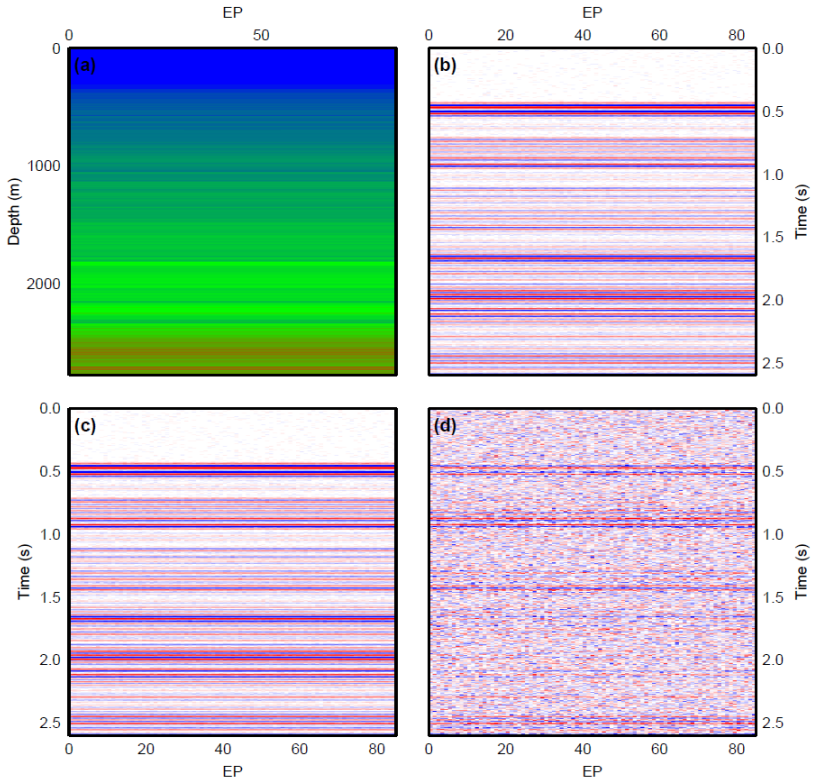

Figure 9: CO2 leak at 700 m, saturation=0.06. (a) Velocity model; (b) baseline survey; (c) repeat survey; and (d) difference section.

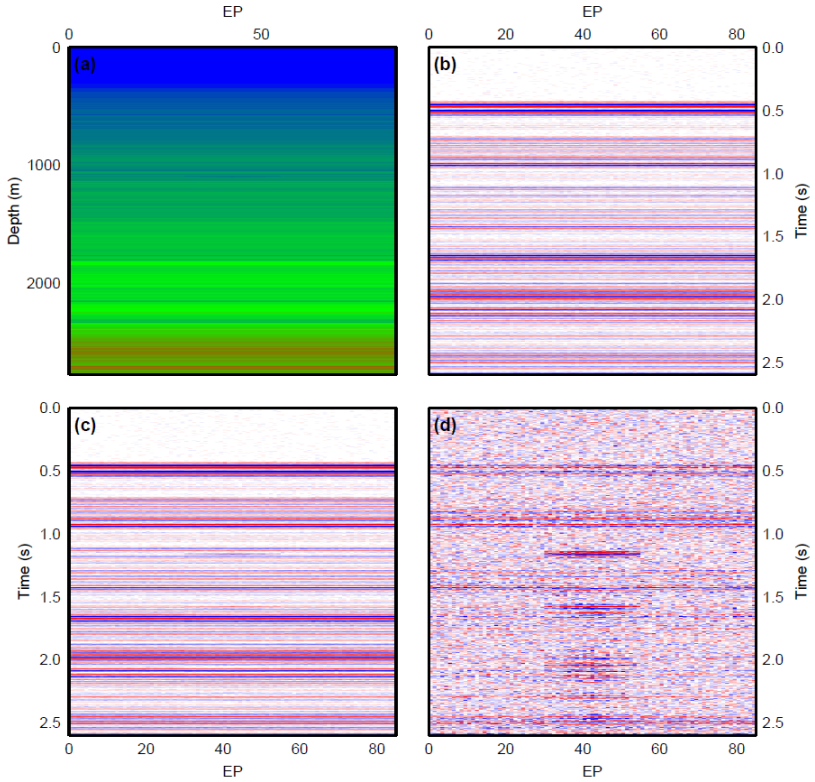

Figure 10: CO_2 leak at 1100 m, saturation=0.8. (a) Velocity model; (b) baseline survey; (c) repeat survey; and (d) difference section.

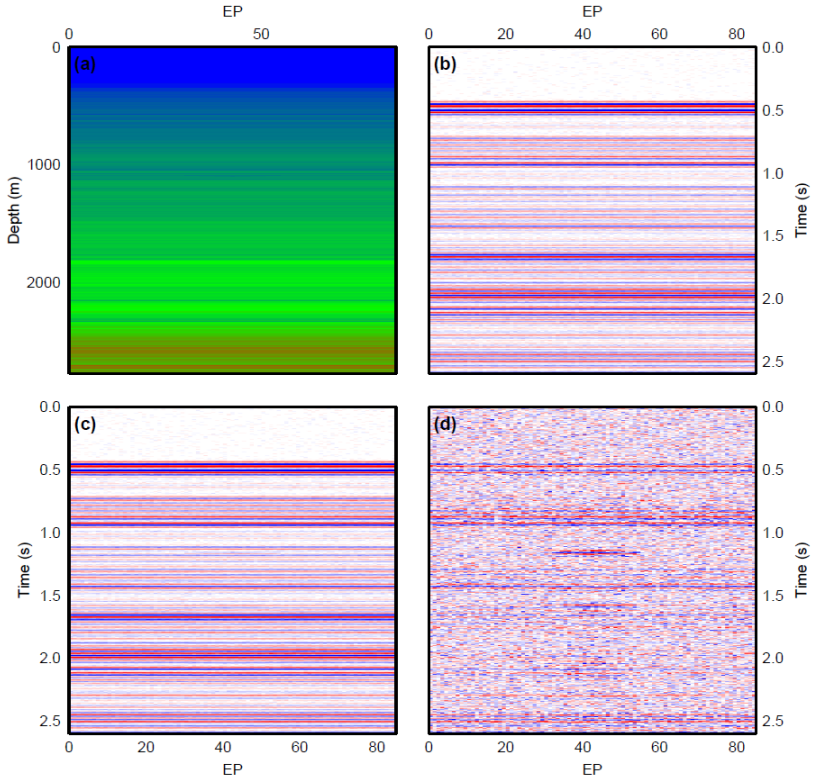

Figure 11: CO2 leak at 1100 m, saturation=0.55. (a) Velocity model; (b) baseline survey; (c) repeat survey; and (d) difference section.

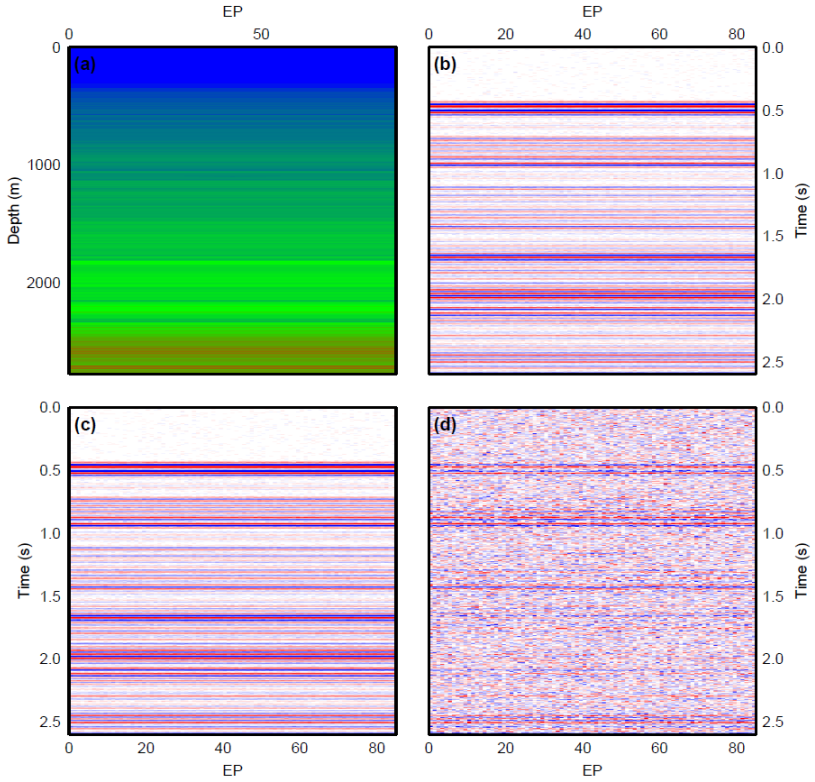

Figure 12: CO2 leak at 1100 m, saturation=0.25. (a) Velocity model; (b) baseline survey; (c) repeat survey; and (d) difference section.

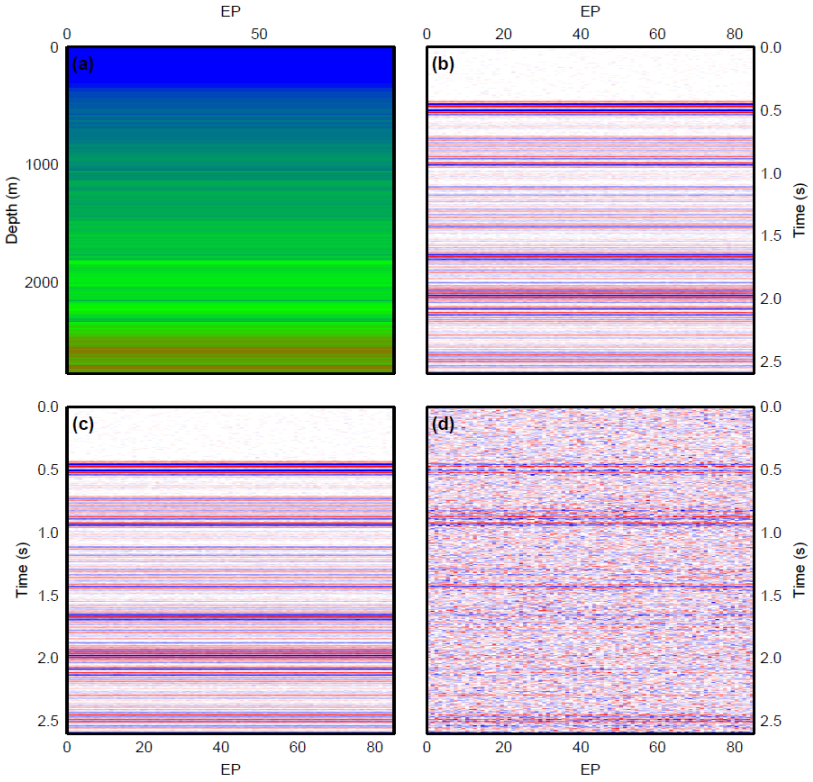

Figure 13: CO2 leak at 1100 m, saturation=0.06. (a) Velocity model; (b) baseline survey; (c) repeat survey; and (d) difference section.

It is apparent that the CO_2 has a slight effect on the velocity profile, causing a reduction in p-wave velocity. Pushdown effects can be seen in the seismic record. The amplitude response of CO_2 for a small accumulation is not always obvious on the repeat data but is clearly imaged on the difference data at moderate to high saturations.

The effect of depth and saturation is reasonably clear but a more quantitative approach is required to assess detection. As such, the amplitude of the reflection caused by the injected CO_2 is summed over a 40 ms window around the arrival time and plotted as a function of in-line number, where spacing is 12.5 m.

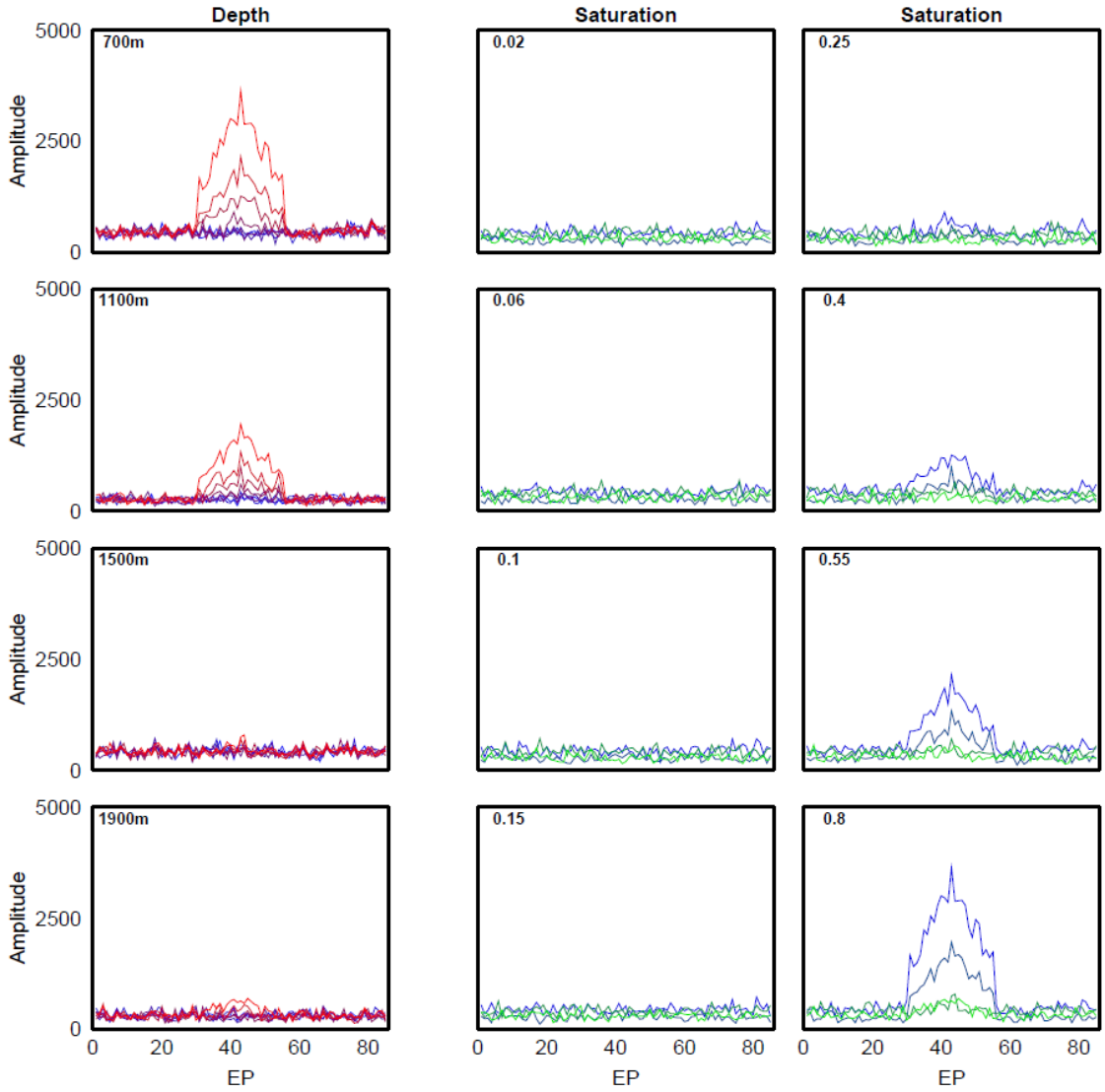

Figure 14: Plots showing the absolute amplitudes of reflections using a patchy mixing model in a 40 ms window around the seismic arrival corresponding to the leaking CO2. Left: As depth increases detection becomes difficult above the noise with increasing saturation expressed as a move from blue to red in the plots. Centre and right:

3 Conclusions

This report has reported on the accumulation of CO_2 leaks added as a cone of varying saturation at increasing depth to the overburden at Snøhvit. A volume of rock is partially saturated with CO_2 but concurrent studies are underway at a range of volumes and shapes in an attempt to study this trade-off. Results are summarised in a series of RMS amplitude curves highlighting the relationships between different parameters. Pushdown effects can be seen in the seismic data as a consequence of leaking CO_2. The amplitude response of CO_2 for a small accumulation is not always obvious on the repeat data but is clearly imaged on the difference data at moderate to high saturations.

We are currently running the seismic modelling with 2D and 3D finite difference codes to quantify the difference seen from varying the modelling strategy.

Suitable trade-off relationships are currently being analysed and it is hopeful that the work will progress into a publishable study. Current work to replicate a leaking chimney structure is underway

This study has so far assumed leakage comparable to a thin spreading CO_2 layer but current and future work relates the leakage, at low saturations through chimney structures.